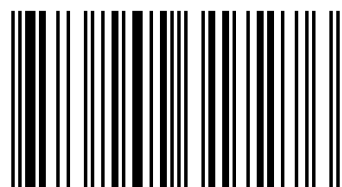


Innovative and Useful Laboratory Experiments of Electrical Machines

This work consists of simple and innovative experiments at the beginning and, as work advances, the experiments become themselves bigger and with more details. The last topics show the analysis of induction and synchronous generators in parallel operation mode and their transients. This work intends to present some innovative and relevant experiments and concepts to electrical machines applications. All chapters show innovations and they are interconnected so that the readers have a wide understanding about these new ways of electrical machines control and operation.



Vinicius Zimmermann Silva graduated in Electrical Engineering at EFEI, Brazil, in 1998. He obtained MSc degree at UNIFEI in 2004 and MBA degree at FGV in 2011. He worked at ALSTOM for six years and at FURNAS for almost one year. Zimmermann who has been working at PETROBRAS since 2005 is in the final stage of his doctorate degree at UNIFEI.



978-620-2-31727-6

Electrical Machines Controls

Silva, Rezek, Camacho

Scholars'
Press

Vinicius Silva
Angelo Rezek
Carlos Camacho

Innovative and Useful Laboratory Experiments of Electrical Machines

Electrical Machines Controls and Operations

**Vinicius Silva
Angelo Rezek
Carlos Camacho**

**Innovative and Useful Laboratory Experiments of Electrical
Machines**

**Vinicius Silva
Angelo Rezek
Carlos Camacho**

Innovative and Useful Laboratory Experiments of Electrical Machines

Electrical Machines Controls and Operations

Scholars' Press

Imprint

Any brand names and product names mentioned in this book are subject to trademark, brand or patent protection and are trademarks or registered trademarks of their respective holders. The use of brand names, product names, common names, trade names, product descriptions etc. even without a particular marking in this work is in no way to be construed to mean that such names may be regarded as unrestricted in respect of trademark and brand protection legislation and could thus be used by anyone.

Cover image: www.ingimage.com

Publisher:

Scholars' Press

is a trademark of

International Book Market Service Ltd., member of OmniScriptum Publishing Group

17 Meldrum Street, Beau Bassin 71504, Mauritius

Printed at: see last page

ISBN: 978-620-2-31727-6

Copyright © Vinicius Silva, Angelo Rezek, Carlos Camacho

Copyright © 2018 International Book Market Service Ltd., member of OmniScriptum Publishing Group

Innovative and Useful Laboratory Experiments of Electrical Machines

Vinicius Zimmermann Silva
Angelo José Junqueira Rezek
Carlos Alexandre Pereira Camacho

Acknowledgements

I owe my most sincere and deepest thanks to God due to the grace of our lives, to my professor adviser and friend Angelo José Junqueira Rezek who always motivated and helped me as well as to my parents Maria das Graças Zimmermann Silva and Jose Carlos Ferreira da Silva who have always been on my side.

I also thank my friend and university co-worker Christel Enock Ghislain Ogoulola for assistance in conversion to LATEX of this work.

Finally, I thank the UNIFEI technicians José Airton de Freitas, Adair Salvado Junior and Jorge Wilson Rosa for assistance in my workbench at laboratory of research development of electrical didactic laboratory of Federal University of Itajubá.

"You don't start out writing good stuff. You start out writing crap and thinking it is good stuff, and then gradually you get better at it. That's why I say one of the most valuable traits is persistence."
(Octavia E. Butler)

Abstract

This work aims to present new contributions for electrical machines application studies, mainly about analysis of induction and synchronous generators in parallel operation mode. Then, in summary, the main topics presented in this work are: an analysis of induction and synchronous generators in parallel operation mode and studies of load and generation transients. All of this main subject are supported by appendixes that contributes with practical and original studies related to each subsystem that is part of main experiments such as: (i) voltage and current regulators for DC machines, (ii) firing circuit, (iii) voltage regulators to synchronous generators, (iv) four-quadrant Driven System for DC Machine and (v) analogical and digital control boards.

Key-words: Asynchronous Generator, Closed loop Control, Induction Generator, Isolated Electric System, Generators in Parallel, Synchronous Generator.

List of Figures

Figure 1.1 – Electric Scheme	24
Figure 1.2 – MP 410T in Speed Control loop	25
Figure 1.3 – MP 410T in Voltage Control loop	25
Figure 1.4 – Speed Control Loop	28
Figure 1.5 – Field Voltage Control Loop	28
Figure 1.6 – Converter Configuration used for control Operational Scenarios	28
Figure 1.7 – Electronic Board MP410T and Connections	29
Figure 1.8 – Circuit boards MP410T used to implement the Control Loops	29
Figure 1.9 – Laboratory assembly in the laboratory of research development of electrical didactic laboratory of Federal University of Itajubá	35
Figure 1.10–Synchronous and Induction Generators in parallel Operation Mode with Steady Armature Voltage for DCM_{IG} (Variation of DCM_{IG} field flux by field Rheostat)	36
Figure 1.11–Synchronous and Induction Generators in Parallel Operation mode with Variable Armature Voltage for DCM_{IG} (DCM_{IG} Steady field flux)	36
Figure 1.12–Synchronous and Induction Generators in Parallel Operation mode with Variable Armature Voltage for DCM_{IG} and an Induction Motor as Load (DCM_{IG} Steady field flux)	37
Figure 1.13–Conjugate vs rpm - Induction Motor and Generator	37
Figure 1.14– PIG vs PSG with DCM_{IG} Field Variation and V_{aDCMIG} kept Constant	42
Figure 1.15– PIG vs PSG with V_{aDCMIG} Variation and Field flux kept Constant (Only resistive load)	43
Figure 1.16– PIG vs PSG with V_{aDCMIG} Variation and Field Flux kept Constant (Resistive load & IM)	43
Figure 1.17– P_{DCMIG} vs P_{DCMSG} with DCM_{IG} Field Flux Variation and V_{aDCMIG} Kept Constant	44
Figure 1.18– V_{SG} (Synchronous generator voltage) x f_{SG} (Synchronous generator frequency) x I_{load} (Load current)	44
Figure 1.19– P_{DCMIG} vs P_{DCMSG} with V_{aDCMIG} Variation and Field Flux Kept Constant (Only resistive load)	45
Figure 1.20– P_{DCMIG} vs P_{DCMSG} with V_{aDCMIG} Variation and Field Flux Kept Constant (Resistive load plus IM)	45
Figure 1.21– n_{IG} vs n_{SG} with DCM_{IG} Field Flux Variation and V_{aDCMIG} Kept Constant	46
Figure 1.22– n_{IG} vs n_{SG} with V_{aDCMIG} Variation and Field Flux kept Constant (Only resistive load)	46

Figure 1.23– n_{IG} vs n_{SG} with $V_{a_{DCMIG}}$ Variation and Field Flux kept Constant (Resistive load plus IM)	47
Figure 2.1 – Laboratory Assembly	52
Figure 2.2 – Connections Arrangement of MP410T and Devices	52
Figure 2.3 – Synchronous and Induction Generators in Parallel Operation Mode	53
Figure 2.4 – Speed Control Loop	53
Figure 2.5 – Field Voltage Control Loop	53
Figure 2.6 – I_{IG} and V_{pn} (Scenario 1)	55
Figure 2.7 – I_{SG} and V_{pn} (Scenario 1)	55
Figure 2.8 – I_{IG} and V_{pn} (Scenario 2)	55
Figure 2.9 – I_{SG} and V_{pn} (Scenario 2)	55
Figure 2.10–Channel 1- I_{SG} , Channel 2- V_{pn} . (2/3 kW is removed and then inserted) (Scenario 2)	56
Figure 2.11–Channel 1- I_{IG} , Channel 2- V_{pn} . (2/3 kW is removed and then inserted) (Scenario 2)	56
Figure 2.12–Channel 1- n_{SG} , Channel 2- I_{IG} . (2/3 kW is removed and then inserted.) (Scenario 2)	56
Figure 2.13–Channel 1- n_{SG} , Channel 2- I_{SG} . (2/3 kW is removed and then inserted.) (Scenario 2)	56
Figure 2.14– V_{pn} , SG is removed and then inserted. Scenarios 4 & 5	57
Figure 2.15– V_{pn} in load. IG is removed and then inserted. Scenarios 4 & 5	57
Figure 2.16– SG speed. IG is removed and then inserted. Scenarios 6 & 7	57
Figure 2.17– I_{SG} , IG is removed and then inserted. Scenarios 6 & 7	57
Figure 2.18– I_{SG} . SG smallest contribution = 0.4A. Scenario 3	58
Figure 2.19– I_{IG} , IG biggest contribution =6.9A. Scenario 3	58
Figure 2.20–Transition between Scenarios 4 and 5	58
Figure 2.21–Transition between Scenarios 6 and 7	58
Figure A.1–Ramp Type Firing Circuit	64
Figure A.2–Waveforms and Firing Angle	64
Figure A.3–Synchronism Transformer	65
Figure A.4–General view of Synchronism Transformer	65
Figure A.5–Motor Armature Circuit and Diagram of the Drive System Mechanical Part	66
Figure A.6–Block diagram of the drive mechanical part	67
Figure A.7–Representation of the Motor Mechanical Part in pu	68
Figure A.8–Block Diagram of the DC Motor Armature Circuit	70
Figure A.9–Reduced Voltage step Applied to the Armature Circuit	70
Figure A.10–Current Response for a Voltage step Applied to the Armature Circuit	70
Figure A.11–Schematic Block Diagram of the Independent Excitation DC Motor	71

Figure A.12–Complete Block Diagram of Controlled Drive	72
Figure A.13–Current Regulation Loop	73
Figure A.14–Current Transducer	74
Figure A.15–Implementation of Current Regulator	78
Figure A.16–Speed Regulation Loop	80
Figure A.17–Implementation of Speed Regulator	82
Figure A.18–General Diagram	85
Figure A.19–Speed and Current Waveforms	86
Figure A.20– <i>DCM</i> coupled with <i>SG</i> and a Resistive Load	87
Figure B.1–Basic Organization of Control Circuit.	91
Figure B.2–Blocks Diagram of Control Circuit using the TCA 785 and 555.	92
Figure B.3–Internal Diagram of TCA 785.	94
Figure B.4–Waveforms Diagram for TCA 785. [1]	95
Figure B.5–TCA 785 Wrapping and Pins	95
Figure B.6–CI 555 as Monostable	98
Figure B.7–Monostable with Adjustable output Pulse Width.	99
Figure B.8–Internal Diagram of TIL111.	99
Figure B.9–Attack stage circuit.	100
Figure B.10–Control Voltage Circuit.	101
Figure B.11–Block Diagram of Complete Control Circuit	101
Figure B.12–Firing Circuit Diagram	102
Figure B.13–Voltage Sources for Firing Circuit Diagram	102
Figure C.1–Auxiliary Circuit Mounted in the Laboratory	105
Figure C.2–Generator Time Constant Determination	106
Figure C.3–Simplified Block Diagram of Voltage Regulation	107
Figure C.4–Full Wave Three-phase Rectifier with thyristor [2]	107
Figure C.5–Full Blocks Diagram of Voltage Regulation System	108
Figure C.6–Value of τ_{gs} and Relation between the large and the Small Time Constants	110
Figure C.7–Graetz Bridge with Thyristor and 220 V Grid Voltage	112
Figure C.8–Voltage regulator	114
Figure C.9–Voltage Regulator Topology with “T” Filter in the Reference Channel	114
Figure C.10–Voltage Regulator Topology	117
Figure C.11–Voltage Regulator System for Synchronous Machine	117
Figure D.1–Full Blocks Diagram of DC Machine	120
Figure D.2–Implemented Drive System	121
Figure D.3–Control Circuit	122
Figure D.4–Conjugate (t) versus Speed (n) Diagram	122
Figure D.5–Closing of Converters I and II	123

Figure D.6–Commutation Switch S1	123
Figure D.7–Control Circuit	124
Figure D.8–Resistance to Energy Dissipation in Machine Field Circuit	125
Figure D.9–Rotation Inversion using the Armature Current Inversion	126
Figure D.10–Rotation Inversion using the Field Current Inversion	126
Figure E.1–No load test and locked rotor test circuit	127
Figure E.2–Induction Motor Equivalent Circuit	127
Figure E.3–Results of no-Load Test: W1+W2 vs Voltage Applied	128
Figure E.4–Equivalent Circuit – No-Load Test	129
Figure E.5–Equivalent Circuit Locked Rotor Test	130
Figure E.6–IM Winding Connection	130
Figure E.7–Magnetization branch power factor	134
Figure E.8–Parameters of Induction Motor	135
Figure E.9–Resistors bank and IM currents in scenarios C as Table 1.10	139
Figure F.1–Scenario 1B	142
Figure F.2–Scenario 2B	142
Figure F.3–Scenario 3B	143
Figure F.4–Scenario 1C	143
Figure F.5–Scenario 2C	143
Figure F.6–Scenario 3C	144
Figure G.1–Proportional device with adjustable gain	145
Figure G.2–Circuit to determination of variable a	146
Figure G.3–Simplified circuit	147

List of Tables

Table 1.1 – Terminal Descriptions of SEMIKRON MP410T Electronic Board	26
Table 1.2 – Electronic Control Board Configuration	27
Table 1.3 – DCM_{IG} (<i>Direct Current Motor coupled with induction generator</i>) Data plate	29
Table 1.4 – DCM_{SG} (<i>Direct current motor coupled with synchronous generator</i>) Data plate	30
Table 1.5 – IG (<i>Induction Generator</i>) Data plate	30
Table 1.6 – SG (<i>Synchronous Generator</i>) Data plate	30
Table 1.7 – Load Data plate	30
Table 1.8 – Load Data plate	30
Table 1.9 – Operational scenarios in controlled mode and three resistors bank as load	39
Table 1.10–Operational scenarios in controlled mode and three resistors bank and induction motor as load	40
Table 1.11–Operational scenarios in controlled mode and a resistor bank	41
Table 2.1 – Scenarios and Transitions	54
Table A.1–DC Motor Data	73
Table A.2–Current Regulator Parameters	77
Table A.3–Complementary Current Regulator Data	79
Table A.4–Speed Regulator Parameters	82
Table A.5–Speed Regulator Parameters	84
Table B.1–Pulse width from pins 14 and 15 related to capacitor C12 values, [3]	97
Table C.1–Excitation Parameters of Salient Poles Synchronous Generator	106
Table C.2–Excitation Parameters of Salient Poles Synchronous Generator	109
Table C.3–Excitation Parameters of Salient Poles Synchronous Generator	109
Table C.4–Regulator Parameters Adjustments and Optimization [4].	112
Table C.5–Optimized Voltage Regulator Parameters	113
Table C.6–Voltage Regulator Adjustments	117
Table D.1–Motor Data	121
Table D.2–Speed Regulator Parameters	121
Table D.3–Current Regulator Parameters	121
Table D.4–Cause and Effect Matrix	124
Table E.1–No load Test	128
Table E.2–Current Regulator Parameters	129
Table E.3–Average Resistance	130

List of abbreviations and acronyms

BL	<i>Ballast load</i>	59
CT	<i>Current transformer</i>	73
DCG_{SG}	<i>Direct current generator coupled with synchronous generator</i>	59
DCM	<i>Direct Current Motor</i>	20
DCM	<i>Direct current motor</i>	44
DCM_{IG}	<i>Direct Current Motor coupled with induction generator</i>	9
DCM_{SG}	<i>Direct current motor coupled with synchronous generator</i>	9
E	<i>DC supply voltage</i>	75
E_{DCM}	<i>Direct current motor voltage</i>	66
E_N	<i>Rated voltage</i>	69
E_{SGf}	<i>Synchronous generator field terminal voltage</i>	107
E_{pp}	<i>Phase-phase voltage</i>	111
$FPSO$	<i>Floating production storage and offloading</i>	21
IG	<i>Induction Generator</i>	9
IG	<i>Gate current</i>	92
IM	<i>Induction motor</i>	34
I_{AK}	<i>Locked rotor current</i>	71
I_C	<i>Capacitor current</i>	33
I_{IG}	<i>Induction generator current</i>	33
I_N	<i>Rated Current</i>	69
I_{SG}	<i>Synchronous generator current</i>	33
I_a	<i>Armature current</i>	66
I_{cc}	<i>Generator field circuit current</i>	104
I_{exc}	<i>excitation current</i>	111
I_{fDCMIG}	<i>Field current of direct current motor coupled with induction generator</i>	21
I_{load}	<i>Load current</i>	5
I_m	<i>Magnetization Current</i>	128
I_{rm}	<i>Magnetization branch current across resistance</i>	134
I_{xm}	<i>Magnetization branch current across inductor</i>	134
I_{aDCMIG}	<i>Direct current motor induction generator armature current</i>	42
I_{c1}	<i>Capacitor current 1</i>	33
I_{c2}	<i>Capacitor current 2</i>	33
I_{dWMT}	<i>Induction motor reactive current</i>	33
I_N	<i>Rated Current</i>	86
I_{WIG}	<i>Induction generator active current</i>	33

$I_{W_{MT}}$	Induction motor active current	33
$I_{W_{SG}}$	Synchronous generator active current	33
$I_{W_{loadR}}$	R Load Active current	33
K_{P_o}	Voltage regulator original gain	149
K_{p_e}	Accurate voltage regulator gain	149
$K_{p_{max}}$	maximum regulator gain	116
$K_{p_{min}}$	minimum regulator gain	116
K_p	regulator gain	117
K'_p	Voltage regulator gain	110
K_t	Temperature correction factor for 40 degree C	136
L_a	Armature circuit inductance	66
L_d	Smoothing reactor inductance	73
L_{fd}	Field inductor	108
L_s	Separated field inductance	73
PI	Proportional-integral regulator	110
PIG	Induction generator power	21
PSG	Synchronous generator power	33
P_{DCMIG}	Power of direct current motor coupled with induction generator	33
P_{DCMSG}	Power of direct current motor coupled with synchronous generator	33
P_{av}	attrition and ventilation losses	128
P_{hf}	hysteresis and Foucault losses	133
P_{in}	Motor input power	137
$P_{jstator}$	No load stator Joules Losses	132
P_{mec}	Mechanical power	87
P_{nl}	No load losses	132
P_{out}	Motor output power	137
P_{tl}	Total losses	137
P_{tl}	Total losses	135
P_{win}	Winding losses	135
P_{win40C}	Corrected winding losses for 40 degree C	136
Q	Reactive power	131
Q_m	No load Reactive Power in Magnetization Branch	133
R''_{eq}	Speed regulator equivalent resistance for $Rq2'=646.25 \Omega$	152
R'_{eq}	Current regulator equivalent resistance	150
R'_e	Speed regulator equivalent resistance	150
RM1	integral branch steady resistor of voltage regulator	116
RM2	Integral branch adjustment resistor of voltage regulator	113
R_{SH}	Shunt resistor	70
R_{adj}	adjustment resistance of regulator	146

R_{aj}	<i>adjustment resistance of voltage regulator</i>	115
R_a	<i>Armature circuit resistance</i>	66
R_{equ}	<i>Equivalent resistance</i>	146
R_{eq}	<i>Voltage regulator equivalent resistance</i>	150
R_{fd}	<i>Field resistor</i>	107
R_{fdmed}	<i>Measured field electrical resistance</i>	104
R_{q1}	<i>Proportional branch adjustment resistor of voltage regulator</i>	113
R_{ti}	<i>total resistor value of integral branch</i>	116
R_{tot}	<i>Total resistance</i>	146
R_{tp}	<i>total resistor value of proportional branch</i>	115
R_d	<i>Phase resistance in delta connection</i>	129
R_m	<i>Motor Average Measured Resistance</i>	129
R_y	<i>Phase resistance in star connection</i>	129
SG	<i>Synchronous Generator</i>	9
SM	<i>Synchronous machine</i>	65
SV	<i>Synchronous voltage</i>	92
SW	<i>Interconnection switch</i>	37
T_c	<i>Load torque</i>	66
T_{fr}	<i>Friction torque</i>	66
T_m	<i>Motor torque</i>	86
T_n	<i>Motor rated torque</i>	86
U_2	<i>AC supply voltage</i>	75
V''_{Ro}	<i>Current regulator original gain</i>	147
V'_Ro	<i>Speed regulator original gain</i>	148
$V1$	<i>Sawtooth voltage</i>	92
$V2$	<i>Rectangular pulse</i>	92
$V3$	<i>Rectangular wave</i>	92
$V4$	<i>Rectangular pulses train</i>	92
$V5$	<i>Amplified rectangular pulses train</i>	92
VC	<i>Control voltage</i>	92
VL	<i>Load voltage</i>	92
V_{IG}	<i>Induction generator voltage</i>	55
V_{Ra}	<i>Total regulator gain</i>	147
V_{Rie}	<i>Accurate current regulator gain</i>	150
V_{Ri}	<i>Gain of the current regulator</i>	72
V_{Rne2}	<i>Accurate speed regulator gain for $Rq2'=646.25 \Omega$</i>	153
V_{Rne}	<i>Accurate speed regulator gain</i>	150
V_{Rn}	<i>Gain of the speed regulator</i>	71
V_{Ro}	<i>Regulator original gain</i>	146

V_{SG}	<i>Synchronous generator voltage</i>	5
V_{cc}	<i>Control voltage of thyristor firing system</i>	64
V_{dc}	<i>Direct current voltage</i>	42
V_{fd}	<i>Generator field terminal voltage</i>	104
V_i	<i>Motor current amplification factor</i>	69
V_i	<i>Gain of machine electric part</i>	72
V_{pn}	<i>Phase neutral voltage</i>	55
V_{pp}	<i>Phase-phase voltage</i>	55
V_{ref}	<i>Reference Voltage</i>	106
V_{sa}	<i>Generator output voltage</i>	107
V_s	<i>Gain of the static converter</i>	72
V_t	<i>Transducer output voltage</i>	107
V_{ADCMIG}	<i>DCM armature voltage coupled with IG</i>	21
Θ_0	<i>Magnetization Branch Power Factor Angle</i>	134
β_{RM2}	<i>adjustable resistor of integral branch</i>	114
η_{IG}	<i>IG efficiency</i>	33
η_{SG}	<i>SG efficiency</i>	33
η_{group}	<i>Group efficiency</i>	33
τ_H	<i>Accelerating time constant</i>	67
τ_a	<i>Inductor circuit or armature time constant</i>	68
τ_e	<i>Equivalent time constant</i>	80
τ_{gi}	<i>Filter time constant of the current transducer</i>	72
τ_{gn}	<i>Filter time constant of the speed transducer</i>	72
τ_{gs1}	<i>Filter time constant of the reference channel of the speed loop</i>	71
τ_{gs2}	<i>Filter time constant of the reference channel of the current loop</i>	71
τ_{gs}	<i>Smoothing time constant</i>	108
τ_i	<i>Current regulator time constant</i>	72
τ_n	<i>Time constant of the speed regulator</i>	72
τ_{ss}	<i>Firing circuit time constant</i>	72
f_{SG}	<i>Synchronous generator frequency</i>	5
i_a	<i>Armature current in pu</i>	68
m	<i>Motor torque in pu</i>	68
$n.a.$	<i>Not applicable</i>	38
n_{IG}	<i>Induction generator speed</i>	34
n_{REF}	<i>Reference speed</i>	72
n_{SG}	<i>Synchronous generator speed</i>	55
n_u	<i>Speed in pu</i>	72
r_1	<i>Stator winding resistance</i>	130
r_{140C}	<i>Corrected stator winding resistance for 40 degree C</i>	136

r_2'	<i>Rotor winding resistance referred to stator winding</i>	131
$r_2'40C$	<i>Corrected rotor winding resistance referred to stator for 40 degree C</i>	136
rm	<i>Magnetization branch resistance</i>	134
t_c	<i>Load torque in pu</i>	72
v_i	<i>Signal from the current transducer</i>	73
x_1	<i>Stator winding reactance</i>	131
x_2'	<i>Rotor winding reactance referred to stator winding</i>	131
xm	<i>Magnetization branch reactance</i>	135
R''_{aje}	<i>Accurate adjustment resistance of Appendix D speed regulator</i>	152
R'_{aje}	<i>Accurate adjustment resistance of speed regulator</i>	148
RM_2''	<i>Integral branch adjustment resistor of current regulator</i>	78
RM_2'	<i>Integral branch adjustment resistor of speed regulator</i>	82
R''_{aje}	<i>Accurate adjustment resistance of current regulator</i>	147
R_{aje}	<i>Accurate adjustment resistance of voltage regulator</i>	148
R''_{aj}	<i>adjustment resistance of current regulator</i>	78
R'_{aj}	<i>adjustment resistance of speed regulator</i>	83
R''_{q1}	<i>Proportional branch adjustment resistor of current regulator</i>	78
R'_{q1}	<i>Proportional branch adjustment resistor of speed regulator</i>	82
R''_{q2}	<i>Proportional branch steady resistor of current regulator</i>	79
R'_{q2}	<i>Proportional branch steady resistor of speed regulator</i>	83
$V1'$	<i>Rectangular pulse</i>	93
$V2'$	<i>Wider Rectangular pulse</i>	93
$V3'$	<i>Wider Rectangular pulse</i>	93
$V4'$	<i>Wider Rectangular pulse</i>	93
τ'	<i>Generator field time constant</i>	104
τ'_i	<i>Regulator time constant</i>	108
MHPP	<i>Micro-Hydro Power Plants</i>	20

List of symbols

B	Resultant torque	66
$F(s)$	Transfer function	110
J	Inertia moment, motor plus load	66
M	Torque	66
M_n	Rated torque	67
N_n	Rated speed	86
U	Counter electromotive force	66
ΔV	Voltage error signal	107
Θ_{med}	Measured winding temperature	105
Θ_{ref}	Reference temperature resistance	105
α	thyristor firing angle	74
α_u	Value in pu of the thyristor firing angle	75
η	motor efficiency	87
μ	Overlap angle	75
ϕ	Machine flux	42
σ	Sum of small time constant	109
k	Proportionality constant 0	87
n_0	No load speed	66
t	Time	86
w	Rotation $\frac{rad}{s}$	66
σ'	Sum of small time constant of speed regulator	80
k''''	Proportionality constant 4	88
k'''	Proportionality constant 3	87
k''	Proportionality constant 2	87
k'	Proportionality constant 1	87
n	Speed	66

Contents

1	ANALYSIS OF SYNCHRONOUS AND INDUCTION GENERATORS IN PARALLEL OPERATION MODE IN AN ISOLATED ELECTRIC SYSTEM	23
1.1	Introduction	23
1.2	Isolated Electric System	24
1.3	Digital Control Board	25
1.3.1	MP410T Electronic Board Parameterization	26
1.3.2	Voltage and Speed Control Loops	27
1.3.3	Arrangement	28
1.4	Data Plate	29
1.5	Equations - Part I	30
1.5.1	Capacitor Bank Sizing	31
1.5.2	Resistive Divider Sizing	31
1.6	Equations - Part II	32
1.7	Equations - Part III	34
1.8	The Experiment and Schemes	34
1.8.1	Methods of IG Connection into the Electric System	35
1.8.2	Experiment Data	38
1.9	Results	42
1.10	Conclusion	47
2	LOAD AND GENERATION TRANSIENTS OF SYNCHRONOUS AND INDUCTION GENERATORS IN PARALLEL OPERATION MODE IN AN ISOLATED ELECTRIC SYSTEM	49
2.1	Introduction	49
2.2	Isolated Electric System	50
2.3	Data Plate	50
2.4	Equation - Part I	50
2.5	Equation - Part II	50
2.6	Experiment and Schemes	51
2.7	Voltage and Speed Control Loops	52
2.8	Experimental Data	53
2.9	Results	55
2.10	Conclusion	59

APPENDIX	62
APPENDIX A – FILTERS AND REGULATORS PROJECT	63
A.1 Introduction	63
A.2 Ramp Firing Circuit	63
A.3 Synchronism Transformer	64
A.4 Current and Speed Regulators of DC machine project	65
A.4.1 Introduction	65
A.4.2 Motor Block Diagram	65
A.4.3 Armature Circuit Equations	68
A.4.4 Complete Block Diagram with Regulators, Filters and Transducers	71
A.5 Current Regulator and Filters Project of DC Machine (practical case) 72	72
A.5.1 Current Regulator Parameters	77
A.5.2 Current Regulator Arrangement	77
A.5.2.1 Calculus of RM'_2 and Rq'_1	78
A.6 Speed Regulators and Filters Project of DC machine (practical case) Project	80
A.6.1 Capacitors calculus	81
A.6.2 Speed Regulator Parameters	82
A.6.2.1 Calculus of RM'_2 and Rq'_1	82
A.6.3 General Arrangement	84
A.7 Results	84
APPENDIX B – ANALOGICAL CONTROL BOARD (FIRING CIRCUIT)	91
B.1 Introduction	91
B.2 Stage Descriptions	93
B.2.1 Pulse generation by TCA 785	93
B.2.2 Integrated Circuit Characteristics	93
B.3 Operation of TCA 785	96
B.4 Equations	97
B.5 The Pulse Enlargement Stage using the Integrated Circuit 555	98
B.6 Coupling Stage with TIL111	99
B.7 Attack Stage	100
B.8 Control Voltage	100
B.9 General Overview	101
B.10 Conclusion	103
APPENDIX C – VOLTAGE REGULATORS AND FILTERS PROJECT TO SYNCHRONOUS MACHINE	104

C.1	Introduction	104
C.2	Calculus of Generator Field Resistance and Inductance	104
C.3	Voltage Regulators and Filters Project	106
C.3.1	Introduction	106
C.3.2	Voltage Regulator Optimization	107
C.3.3	Practical Implementation of Voltage Regulator	114
C.4	Results	116
C.5	Conclusion	118

**APPENDIX D – FOUR-QUADRANT REGENERATIVE DRIVEN
SYSTEM FOR DC MACHINE APPLYING SPEED
REVERSION USING EITHER ARMATURE CUR-
RENT REVERSION OR FIELD CURRENT RE-
VERSION** **119**

D.1	Introduction	119
D.2	Block Diagram of Controlled Drive System for use in DC Machine	119
D.3	Laboratory Implementation	120
D.4	Full Hardware of Implemented Drive System	121
D.5	Speed Inversion by Armature Current Inversion	122
D.6	Rotation Inversion using the Field Current Inversion	124
D.7	Results	125
D.8	Conclusion	125

APPENDIX E – INDUCTION MOTOR PARAMETERS **127**

E.1	No Load and Locked Rotor Tests	127
E.1.1	No Load Test	127
E.1.2	Locked Rotor Test	129
E.2	Stator and Rotor Parameters	129
E.3	Power and Losses Calculus	132
E.3.1	No Load Reactive Power	133
E.3.2	Magnetization Branch	133
E.4	Parameters of Induction Motor	135
E.5	Induction Motor Efficiency	135
E.5.1	Temperature Correction Factor and Resistance Correction	136
E.6	Corrected Winding Losses for 40 °C and Total Losses	136
E.7	Motor Efficiency Estimate	137
E.8	Induction Motor Currents	138

APPENDIX F – SOLVING EQUATIONS WITH MATLAB **140**

F.1	Introduction	140
------------	---------------------	------------

F.2	Equations	140
F.2.1	Electrical system feeding three resistor banks	140
F.2.2	Electrical system feeding three resistor banks and an induction motor	140
F.2.3	Power and Efficiencies	141
F.3	Matlab Code	141
F.3.1	Electrical system feeding three resistor banks	141
F.3.2	Electrical system feeding three resistor banks and an induction motor	142
	APPENDIX G – PI REGULATOR GAIN CORRECTION	145
G.1	Introduction	145
G.2	Calculations	145
G.3	Current regulator adjustment resistance calculation	147
G.4	Speed regulator adjustment resistance calculation	148
G.5	Voltage regulator adjustment resistance calculation	149
G.6	Gain Calculations	149
G.6.1	Current Regulator Gain	149
G.6.2	Speed Regulator Gain	150
G.6.3	Voltage Regulator Gain	150
G.7	Key Topics	151
G.8	Speed Regulator with Gain 4.0	151
G.8.1	Calculation of Division Constant "a"	152
G.8.2	Adjustment Resistance Calculation	152
G.8.3	Rough Calculation for Gain 4.0	152
	BIBLIOGRAPHY	154

Introduction

In recent years, self-excited induction generators have been employed as suitable isolated power sources in MHPP (*Micro-Hydro Power Plants*) and wind energy applications [5, 6, 7, 8, 9, 10, 11]. In wind power generating systems, the physical size of the individual machines operating at maximum efficiency and dealing with regular routine maintenance related to necessary interruptions, future growth and reliability are reasons for them to be operated in parallel [12, 13, 14].

The studies related to *IG* and *SG* in parallel operation mode [15, 16, 17, 18, 19, 20, 21, 22] show a newer knowledge border, that show the results and behavior of this kind of generation topology, including simulation results for an MHPP. Overall, one of the main contributions of this work is the use of actual control loops in practical experiments involving *SG* and *IG* in parallel operation and their optimization and adjustments [4]. These control loops and experiments were mounted in the Laboratory of research development of electrical didactic laboratory of Federal University of Itajubá.

This work is focused on the operational behavior of two different kinds of generators operating in parallel mode, their roles within the electric system, their controls and characteristics of each generator, some transients and their effects, as well as studies and implementations of control alternatives in order to avoid the undesirable transient effects.

As basis of the target study, this work presents various experiments accomplished in this cited laboratory, which are related to *DCM* (*Direct Current Motor*) and their speed and current control loops. The *DCM* are used as primary machine to *SG* and *IG*. Then, it is essential that DCM_{SG} has speed control loop and DCM_{IG} can be driven manually due to their functional characteristics.

The *SG* requires synchronous speed rotation in its shaft regardless to load transients or any other disturbs on going in the electric system. On the contrary, the *SG* does not operate. The *SG* shaft speed is sensible to disturbs and any other changes on going in the electric system. It means that, speed regulation or speed control loop is required for the *SG* primary machine or DCM_{SG} in order to keep its shaft synchronous speed.

On the other hand, *IG* has different functional characteristics that make it able to supply active power taking only into account its shaft speed be higher than synchronous speed. As *IG* shaft speed increases above the synchronous speed, the supply power is higher. The other characteristic is that, regardless of load changes or disturbs on going in the electric system, its shaft speed and power supply is the same for the *IG*. Then, these functional characteristics do not require any *IG* shaft automatic speed regulation. It means that its primary machine or DCM_{IG} , in the case of these experiments studied in

this work, do not need automatic speed regulation or any speed control loop. From these cited reasons, the DCM_{IG} speed is not automatically controlled, differently of the DCM_{SG} speed that is automatically controlled. The control of DCM_{IG} speed is done manually by open control loop. The two methods used to change the DCM_{IG} speed are: the $V_{aDCM_{IG}}$ (*DCM armature voltage coupled with IG*) method and the field flux or $I_{fDCM_{IG}}$ (*Field current of direct current motor coupled with induction generator*) method.

In general, the generators used in the industry are driven by gas or steam turbines. One of the main characteristics of these turbines is the availability of keeping the machine shaft speed even in adverse conditions as in load transients. The cited turbine speed variation does not overcome ten percent independently of electrical system transients, [23]. Then, in order to do the DCM_{IG} closer to turbine behavior in the experiment implemented in laboratory, two methods of DCM_{IG} speed elevation were studied in order to rise the PIG (*Induction generator power*) supplied. First, the machine field flux is decreased and, the second, the DCM_{IG} armature voltage $V_{aDCM_{IG}}$ is increased. The increase of $V_{aDCM_{IG}}$ has better results than decrease of machine field flux.

In the experiments of this work, the wound rotor machine was used instead of squirrel cage rotor machine. The wound rotor machine can have an extra advantage that is the high startup torque due to resistors that can be connected at the induction machine rotor circuit [24]. In this way, the induction machine can start directly as motor and it can turn a IG by increase of speed up to this speed exceeds the synchronous speed as detailed in chapter 1. Besides of likely higher wound rotor machine cost, the unique technical considerable difference between the two machines considered in this work is that the wound rotor machine can have a higher startup torque and then it permits an additional option of synchronism between the IG and SG , that is the method of direct startup as mentioned in chapter 1. Then, except that mentioned difference, the results obtained with wound rotor machine can be also considered identical to results with squirrel cage rotor machine. Considering that explanation, the results of this work are valid to as wound rotor machine as squirrel cage rotor machine.

One of the potential motivations for this study is to identify a potential alternative capable of optimizing the main electric system currently adopted in oil platforms or $FPSO$ (*Floating production storage and offloading*), making them cheaper, simpler, lighter and more efficient. The oil platforms use traditionally three of four SGs in parallel operation mode.

Analysis of a generator's power balance and its interactions is presented in this work in various operational scenarios. The results enable comparisons of the two methods of induction generator speed control, by either the autotransformer method or the field flux variation method. The former results in a larger range of speed and power from the induction generator. Therefore, it has more desirable features for actual operational

conditions.

In addition, this work is based on thesis [25] and shows six appendixes to the chapters 1 and 2, as follow: the appendix A says about Filter and Regulator Project for direct current motor, DC motor, appendix B says about Analogical Control Board for current and voltage control loops, appendix C says about Voltage Regulators Project to Synchronous Machine, appendix D shows studies about a practical case using *DCM* controls for driving in four quadrants [26], appendix E calculates the induction motor parameters used in one of the experiments of chapter 1, appendix F shows the Matlab codes used to solve the equation system indicated in chapters 1 and 2 and appendix G shows the more accurate method for the regulator parameter adjustments. Thus, these additional studies provide the basis of knowledge [27] for the analysis of synchronous and induction generators in parallel operation mode in an isolated electric system. These generators feed either a resistive load or a resistive load and an induction motor together.

1 Analysis of Synchronous and Induction Generators in Parallel Operation Mode in an Isolated Electric System

1.1 Introduction

This work is composed of analysis over an electric system that includes an induction motor, a resistive load and an autotransformer connected to a diodes bridge to feed the DCM_{IG} armature, what permits to increase manually the IG electric power limits, [28], [29] with better efficiency [30]. Therefore, this work shows the IG supplying more active power than it was shown in [28] and an induction motor inserted in experiment what enables an wider analysis of the system behavior.

Two methods of DCM_{IG} speed elevation were studied in order to rise the PIG supplied. First, the machine field flux is decreased and, the second, the DCM_{IG} armature voltage V_{aDCMIG} is increased. The increase of V_{aDCMIG} has better results than decrease of machine field flux.

This work presents results that show additional remarkable characteristics by operation in parallel mode between one SG and one IG . Some characteristics, such as reduced weight and size, easier maintenance, and shorter manufacturing and delivery time are more associated with induction generators and are relevant to $MHPP$ as demonstrated in general introduction and they could also be to oil platforms. Besides, it has absence of dc supply for excitation and better transient performances [20], [8].

In this chapter, the three different methods of IG connection into the electric system were studied as follow: (i) direct startup as a motor and rising the induction motor speed up to induction motor turns IG , (ii) synchronism of self-excited IG with the electric system and (iii) adjustment of IG speed at synchronous speed and IG connection into the system;

In the experiments of this chapter, the wound rotor machine was used instead of squirrel cage rotor machine. The wound rotor machine can have an extra advantage that is the high startup torque due to resistors that can be connected at the induction machine rotor circuit [24]. For this work, the unique differential advantage by the use of this kind of machine is making the first method of IG connection into the electric system available, (i) direct startup as a motor and rising the induction motor speed up to it turns IG .

A potential application of this cited generator topology is in $MHPP$, which has

already been partially tested as cited in general introduction.

Therefore, the study target is concerned for analysing various aspects of generators topology and operating, involving an induction generator in parallel with a synchronous generator for application in an isolated electric system, and establish the operational viability aspects, advantages and challenges.

1.2 Isolated Electric System

The isolated electric system was mounted in laboratory as Figure 1.1 and sized as shown in sections 1.5 and 1.6. The automatic controls of the system consist of a voltage control loop and a speed control loop as shown in Figure 1.1. In this chapter, the three electric system settings are shown in Figure 1.10, Figure 1.11 and Figure 1.12 will be studied. The data plates of the principal equipment are shown from Table 1.3 to Table 1.6.

The electronic control boards shown in Figure 1.1 are indicated in 1.1. The parametrizations used in both are shown in Table 1.2, except for the references of voltage and speed for each one of control loops which are respectively 65.5 and 65.2 as shown in Table 1.2.

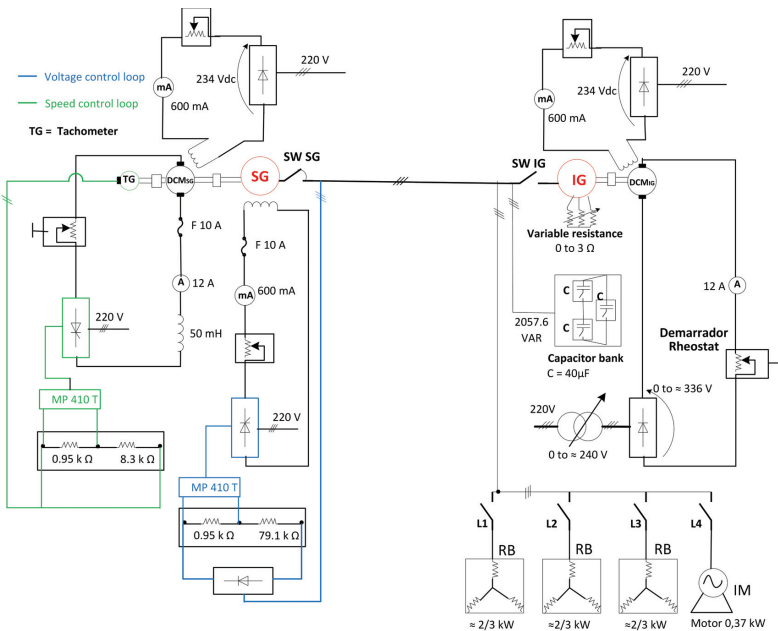


Figure 1.1 – Electric Scheme

1.3 Digital Control Board

The digital control board MP 410T aims to control the three-phase thyristor bridge firing angle. After the correct connections between the thyristors bridge and the electronic board, the MP 410T board can be set as shown in Table 1.1, so that all firing gates from thyristors bridge operate properly. It means that all firing angle turn itself controlled by the MP 410T electronic board. All reference signals from control loops are connected to MP 410T such as speed and field voltage references. This kind of electronic board are inserted in the circuit as part of speed and voltage control loops as shown in Figures 1.2 and 1.3. The correct connections and electronic board configuration are necessary to proper operation of MP 410T. The terminal descriptions of electronic boards MP 410T follow in the Table 1.1.

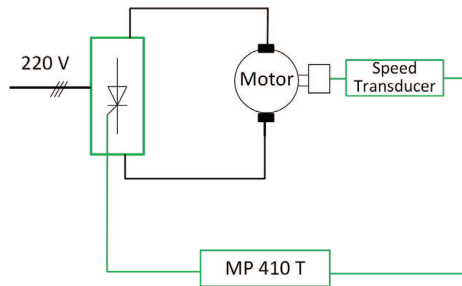


Figure 1.2 – MP 410T in Speed Control loop

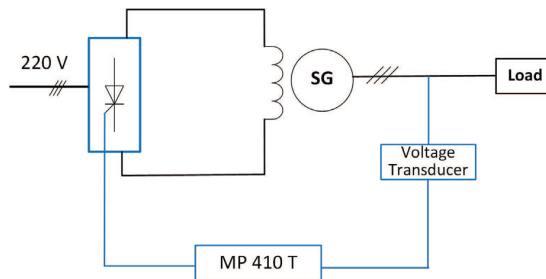


Figure 1.3 – MP 410T in Voltage Control loop

Table 1.1 – Terminal Descriptions of SEMIKRON MP410T Electronic Board

Terminal	Name	Description
1	10	10 V voltage source to 3 and 5 outputs
2	VCC	5 V voltage source to 3 and 5 outputs
3	LIM	Limitation display
4	F_RAMP	Running display
5	INHI_OUT	Inhibition display
6	GND	Earth to 3 and 5 outputs
7	INHI_IN	inhibitory input
8	TERMO	Thermostate input
9	START_STOP	Start stop input
10	POT_KEY	The reference value is put in through by potentiometer or keyboard. Once set STARTER the energy save mode is disabled.
11	GND	Earth to 1 and 4 inputs
12	RS485+	Positive terminal to RS485 bar
13	RS485-	Negative terminal o RS485 bar
14	5	Voltage source of 5 V
15	-5	Voltage source of -5 V
16	CON_IN_TEMPE	Temperature sensor input
17	AGND	Temperature sensor earth
18	IN_0_5	Reference value input to the range 0V to 5V
19	IN_0_10	Reference value input to the range 0V to 10V
20	AGND	Reference value earth
21	INTI+	Pos ¹ terminal of analog ² differential current input
22	INTI-	Neg. ³ terminal of analog. differential current input
23	START_STOP	START_STOP input
24	AGND	Voltage analogical input Earth
25	L1	Analogical current input for current transformer
26	L2	Analogical current input for current transformer
27	COM	Common to current analog. input to current transformer

¹ positive

² negative

³ analogical

1.3.1 MP410T Electronic Board Parameterization

The MP 410T board was parametrized as shown in Table 1.2.

Table 1.2 – Electronic Control Board Configuration

Memory Position	Name (abbreviation at display)	Value (unit)
0	Local Remote (LR)	0(0=local)
1	Adres (Ad)	1(default)
2	Configuration 9 (CF)	1B6C
3	Phase Difference (DY)	0°
4	Auto Manual (Am)	0(0=auto)
5	Peak (P)	66.0%
6	Time Peak (PS)	0s(default)
7	Pedestal (D)	66.0%
8	Ramp Up (RU)	0s
9	Ramp Down (Rd)	0s
10	Lim Intensity (CL)	0
11	Max Intensity (Cm)	0
12	AL Temperature (HL)	0=non(default)
13	Com Temperature (Hm)	0
14	AL_ Failure Phase (PA)	0=non(default)
15	AL_ Failure Thiristor (SA)	0=non(default)
16	Energy Saving (ES)	0
17	Regulation Mode (Rm)	1(1=voltage)
18	Linear (LI)	1(1=yes)
19	Reference Value (E)	65.2%(speed) or 65.5%(voltage)
20	KP_ Intensity (PC)	non used
21	TI_ Intensity (IC)	non used
22	TD_ Intensity (DC)	non used
23	LIM_ Voltage (VL)	1(1=sim)
24	MAX_ Voltage (Vm)	99.9%
25	KP_ Voltage (PV)	0.10 both controller
26	TI_ Voltage (IV)	0.04s both controller
27	TD_ Voltage (DV)	0.0
28	Input_ Intensity (CI)	0 (default)

1.3.2 Voltage and Speed Control Loops

The Figure 1.4 and Figure 1.5 show the close control loop used to control the *SG* voltage and frequency via electronic boards which are shown in Figure 1.10, Figure 1.11 and Figure 1.12.

Note: In Appendix C, an analogical control board was used in the generator field voltage control loop instead of digital control board as this one described here. In addition, that regulator was parametrized by symmetrical optimization technique. The information contained in Appendix C adds this issue.

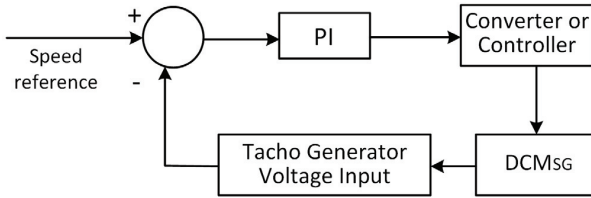


Figure 1.4 – Speed Control Loop

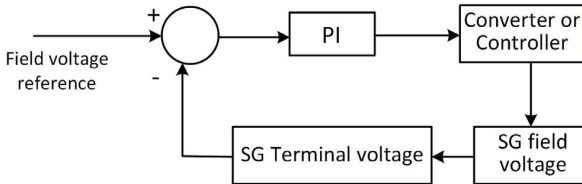


Figure 1.5 – Field Voltage Control Loop

The figure 1.6 shows the configuration 1B6C used for the two thyristor-converter bridges which were used in these control loops.

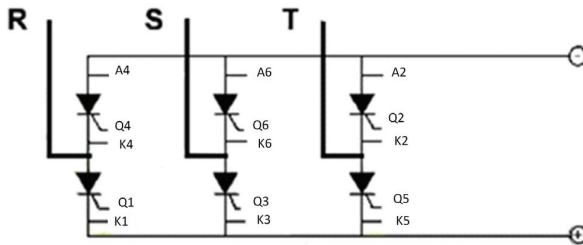


Figure 1.6 – Converter Configuration used for control Operational Scenarios

1.3.3 Arrangement

The figure 1.7 shows the connections arrangement of MP410T electronic board.

Figure 1.8 show the circuit boards with the respective working point or reference points defined during parameterization for the speed control loop, 65.2, and the voltage control loop, 65.5.

The master and slave behavior between generators were realized, considering that the *SG* is the master for the system frequency and voltage. The *IG* is master for the active power and the slave for the system frequency and voltage. *SG* determines the frequency and voltage, while *IG* controls active power supplied to load.

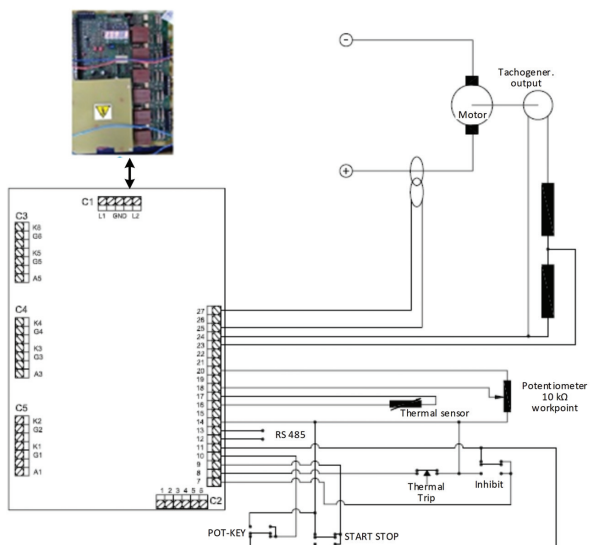
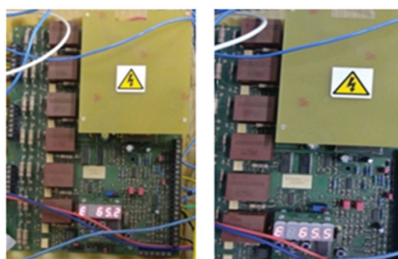


Figure 1.7 – Electronic Board MP410T and Connections



(a) Speed Control Loop (b) Voltage Control Loop

Figure 1.8 – Circuit boards MP410T used to implement the Control Loops

1.4 Data Plate

In tables 1.3 to 1.8 are shown the main equipment's data plates. The tables 1.7 and 1.8 show the loads data plates that are used in the experiments along this work.

Table 1.3 – DCM_{IG} Data plate

Direct Current Motor IG				
220 V	7.72 A	1500 rpm	1.7kW	600 mA

Table 1.4 – DCM_{SG} Data plate

Direct Current Motor SG				
220 V	9.1 A	2.0 kW	1800 rpm	600 mA

Table 1.5 – IG Data plate

Induction Generator (IG)					
220 V	7.5 A	1.86 kW	1410 rpm	0.8 PF	50 Hz

Table 1.6 – SG Data plate

Synchronous Generator (SG)					
230 V	5,0 A	2,0 kVA	1800 rpm	0,8 PF	60 Hz
Vfield: 220 V			Ifieldmax: 600 mA		

Table 1.7 – Load Data plate

Resistive Load		
Load 1 (kW)	Load 2 (kW)	Load 3 (kW)
2/3	2/3	2/3

Table 1.8 – Load Data plate

Induction Motor			
0.37 kW	1715 rpm	Cos ϕ 0.71	60 Hz

1.5 Equations - Part I

Follow the main equations:

- Direct Current Motor

$$n = \frac{E}{k \times \phi} \quad (1.1)$$

$$n = \frac{U_a - (\sum R_a) \times I_a}{k \times \phi} \quad (1.2)$$

$$C_{conjugate} = k \times \phi \times I_a \quad (1.3)$$

- Synchronous Generator

$$\dot{E} = \dot{U}_a + (R_a + jX_s) \times \dot{I}_a \quad (1.4)$$

- Induction Generator

$$S_{slip} \% = \frac{n_s - n_{IG}}{n_s} \times 100 \quad (1.5)$$

$$n_s = \frac{120 \times f_{SG}}{P_{\text{number of poles}}} \quad (1.6)$$

1.5.1 Capacitor Bank Sizing

As informed at the *IG* data plate, $\cos\phi=0.8$, then $\sin\phi=0.6$. The reactive power is calculated to attend the reactive demand of the Induction Machine [31].

$$Q = \sqrt{3} \times V \times I \times \sin\Phi \therefore Q = \sqrt{3} \times 220 \times 7.5 \times 0.6 = 1714.7 \text{ Var} \quad (1.7)$$

$$Q_{\text{generated}} = F_c \times Q \therefore F_c = 1.2 \quad (1.8)$$

For the induction machine coupled to a resistive load, it is necessary a reactive power generation to be approximately 2057.6 VAr as demonstrated below. The 50 Hz was used in the calculus because it is one of the frequencies used in the experiments and it is that which results in the biggest capacitance.

$$Q_{\text{generated}} = 1.2 \times 1714.7 = 2057.6 \text{ Var} \quad (1.9)$$

$$Q_{\text{generated}} = \frac{3 \times V^2}{X_c} \quad (1.10)$$

$$X_c = \frac{3 \times 220^2}{2057.6} = 70.6 \Omega \quad (1.11)$$

$$C = \frac{1}{2 \times \pi \times f \times X_c} = \frac{1}{2 \times \pi \times 50 \times X_c} \quad (1.12)$$

$$= \frac{1}{2 \times \pi \times 50 \times 70.6} \cong 40 \mu F \text{ per phase} \quad (1.13)$$

1.5.2 Resistive Divider Sizing

- Field Control Loop Resistive Divider as shown in Figures 1.10, 1.11 and 1.12.

$$(1k\Omega + r_1) - > 300 V_{(\text{output voltage})} \quad (1.14)$$

$$r_2(1k\Omega) - > 4V_{(MP410T-VOLTAGE-LIMIT)} \quad (1.15)$$

$$r_1 = 74k\Omega \text{ and } r_2 = 1k\Omega \quad (1.16)$$

- Resistor Power Sizing:

$$P_{power} = \frac{300^2}{(75 \times 10^3)} = 1.2 \text{ W} \quad (1.17)$$

- The resistors that were selected based on the sized resistor, were:

$$r_1 = 79.1k\Omega \text{ } r_2 = 947\Omega \quad (1.18)$$

- Speed Control Loop Resistive Divisor as shown in Figure 1.10, 1.11 and 1.12.

$$(1k\Omega + r_1) - > 36V_{(tachogeneratoroutputvoltage)} \quad (1.19)$$

$$r_2(1k\Omega) - > 4 V_{(MPT410voltage\ limit)} \quad (1.20)$$

$$r_1 = 8k\Omega \text{ and } r_2 = 1k\Omega \quad (1.21)$$

- Resistor Power sizing:

$$P_{power} = \frac{36^2}{(9 \times 10^3)} = 1.14 \text{ W} \quad (1.22)$$

- Based on the sized resistor, the following resistors were chosen:

$$r_1 = 8.3 \text{ k}\Omega \text{ and } r_2 = 947 \Omega \quad (1.23)$$

1.6 Equations - Part II

Follow the system of equations to calculate the power and efficiencies shown in Tables 1.9, 1.10 and 1.11 for each generator and entire group of machines.

$$I_{SG}^2 = Iw_{SG}^2 + I_{c1}^2 \quad (1.24)$$

$$I_{IG}^2 = Iw_{IG}^2 + I_{c2}^2 \quad (1.25)$$

$$I_c = I_{c1} + I_{c2} \quad (1.26)$$

$$Iw_{loadR} = Iw_{SG} + Iw_{IG} \quad (1.27)$$

$$I_c - Idw_{MT} = Ic_1 + Ic_2 \quad (1.28)$$

$$Iw_{loadR} + Iw_{MT} = Iw_{SG} + Iw_{IG} \quad (1.29)$$

The I_{SG} (*Synchronous generator current*), I_{IG} (*Induction generator current*), I_c (*Capacitor current*) and Iw_{loadR} (*R Load Active current*) are measured values and these are shown in Tables 1.9, 1.10 and 1.11. The Idw_{MT} (*Induction motor reactive current*) and Iw_{MT} (*Induction motor active current*) are values calculated as appendix E and these are also shown in Table 1.11.

Then, the system has 4 four variables and 4-four equations. Then, for each scenario, the four variables, Iw_{SG} (*Synchronous generator active current*), Ic_1 (*Capacitor current 1*), Iw_{IG} (*Induction generator active current*) and Ic_2 (*Capacitor current 2*), were calculated by Matlab software as appendix F and these are shown in Table 1.9, 1.10 and 1.11.

The entire group efficiency η_{group} (*Group efficiency*) and the efficiency of each subgroup, η_{SG} (*SG efficiency*) and η_{IG} (*IG efficiency*), were calculated based on PIG , PSG (*Synchronous generator power*), P_{DCMSG} (*Power of direct current motor coupled with synchronous generator*), and P_{DCMIG} (*Power of direct current motor coupled with induction generator*), as follows.

$$P_{SG} = \sqrt{3} \times V_{SG} \times Iw_{SG} \quad (1.30)$$

$$P_{IG} = \sqrt{3} \times V_{IG} \times Iw_{IG} \quad (1.31)$$

$$P_{DCMSG} = Va_{DCMSG} \times Ia_{DCMSG} \quad (1.32)$$

$$P_{DCMIG} = Va_{DCMIG} \times Ia_{DCMIG} \quad (1.33)$$

$$\eta_{group\%} = \frac{P_{SG} + P_{IG}}{P_{DCMSG} + P_{DCMIG}} \times 100 \quad (1.34)$$

$$\eta_{SG\%} = \frac{P_{SG}}{P_{DCMSG}} \times 100 \quad (1.35)$$

$$\eta_{IG\%} = \frac{P_{IG}}{P_{DCMIG}} \times 100 \quad (1.36)$$

1.7 Equations - Part III

The equations e calculus used to determine the *IM* (*Induction motor*) parameters and *IM* equivalent circuit such as the primary and secondary impedances and also the primary and secondary currents are showed in Appendix E.

1.8 The Experiment and Schemes

The experiment was mounted in the laboratory as shown in Figure 1.9 a) and b). The detailed circuit is shown in Figures 1.10, 1.11 and 1.12.

Figure 1.9 b) shows another experiment view, including the taco generator and its connections. The detailed circuits are shown in Figures 1.10, 1.11 and 1.12.

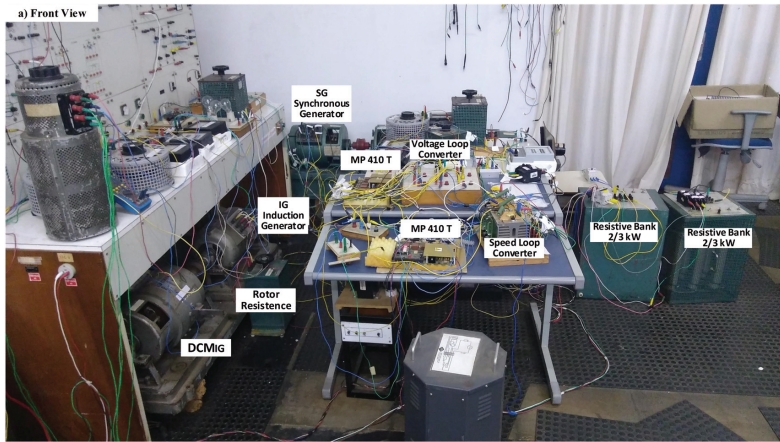
The power from *IG*, *PIG*, was limited because the I_{fDCMIG} reached the maximum value in accordance with DCM_{IG} current specifications. This limited speed from DCM_{IG} was a challenge because the low speed resulted in low contribution from *PIG*. Then, it was necessary to elevate the DCM_{IG} speed, n_{IG} (*Induction generator speed*).

Then, the methodology consists of implementing the comparative analysis of the power and efficiencies, starting with an analysis between the *PIG* from the scheme in Figure 1.10 and *PIG* from the schemes in Figure 1.11 and Figure 1.12, covering the scenarios shown in Table 1.11, Table 1.9 and Table 1.10 respectively.

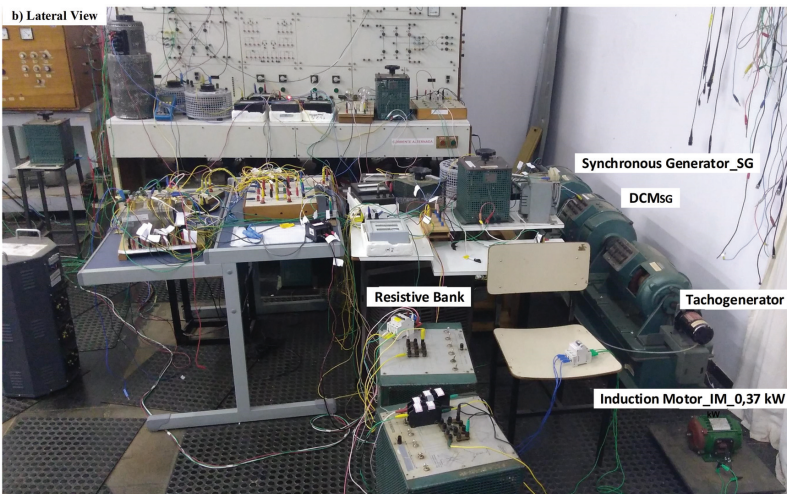
Finally, a comparative efficiency analysis was conducted for two subgroups, one composed of *IG* and a DCM_{IG} and the other composed of *SG* and a DCM_{SG} . These analyses are done over the scenarios related to the scheme in Figure 1.10, the scheme in Figure 1.11 and the scheme in Figure 1.12.

Thus, the increase of DCM_{IG} speed results in increase of the *PIG* contributions and *IG* subgroup efficiencies such as they are shown in the results.

The Figure 1.11 and Figure 1.12 show the schemes implemented in the laboratory to overcome the challenge related to limitation of *IG* speed [28] such as bringing the experiment closer to actual conditions and taking into advantages of *IG* power capacity. It was used as an autotransformer connected to a diodes bridge to vary the voltage applied on the DCM_{IG} armature circuit and obtain a higher speed and *PIG*.



(a) Front View



(b) Lateral View

Figure 1.9 – Laboratory assembly in the laboratory of research development of electrical didactic laboratory of Federal University of Itajubá

1.8.1 Methods of IG Connection into the Electric System

This work studies three different methods of *IG* connection into the electric system such as: (i) direct startup as a motor and rising the *IG* speed, (ii) synchronism of self-excited *IG* with the electric system and (iii) adjustment of *IG* speed at synchronous speed and connect it into the system [28].

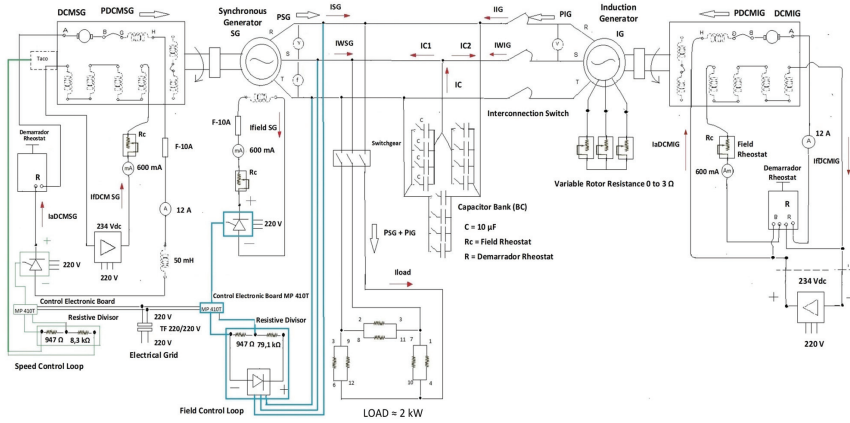


Figure 1.10 – Synchronous and Induction Generators in parallel Operation Mode with Steady Armature Voltage for DCM_{IG} (Variation of DCM_{IG} field flux by field Rheostat)

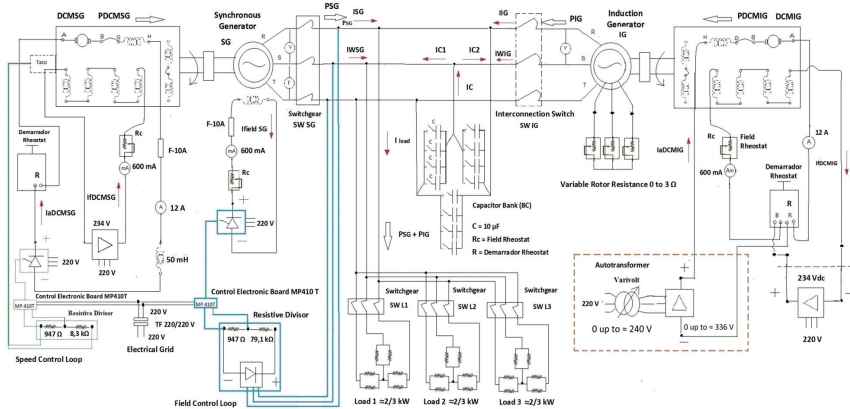


Figure 1.11 – Synchronous and Induction Generators in Parallel Operation mode with Variable Armature Voltage for DCM_{IG} (DCM_{IG} Steady field flux)

- Direct Startup

For this option, the induction machine is started up directly as motor. In this case, rotor resistance was necessary to reach the required torque for start up as shown in Figure 1.12. After start up, the IG speed is raised by manual command up to it overcomes the synchronous speed. In this moment, the induction motor becomes the IG .

- Synchronism of self-excited IG with the Electric System

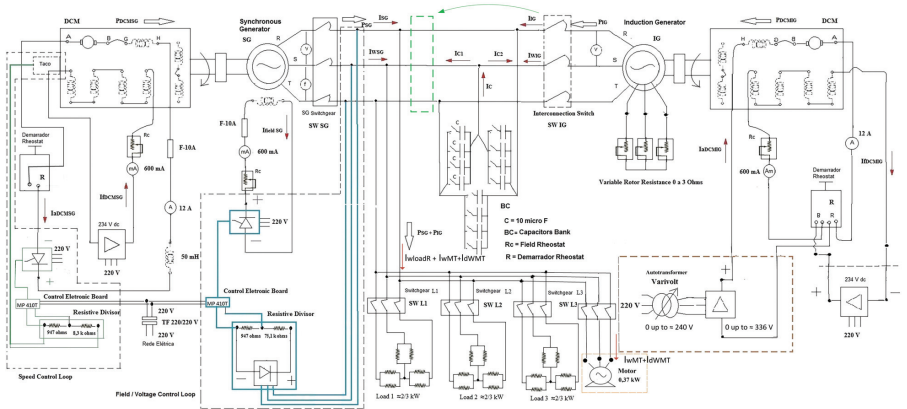


Figure 1.12 – Synchronous and Induction Generators in Parallel Operation mode with Variable Armature Voltage for DCM_{IG} and an Induction Motor as Load (DCM_{IG} Steady field flux)

For this option, the induction generator is auto-excited and the capacitor bank is required and connected in the IG directly as well as the interconnection switch, SW (Interconnection switch), is placed beside of capacitor bank as shown in Figure 1.12 by green arrow. For this option, it was used a synchroscope for closing the interconnection switch.

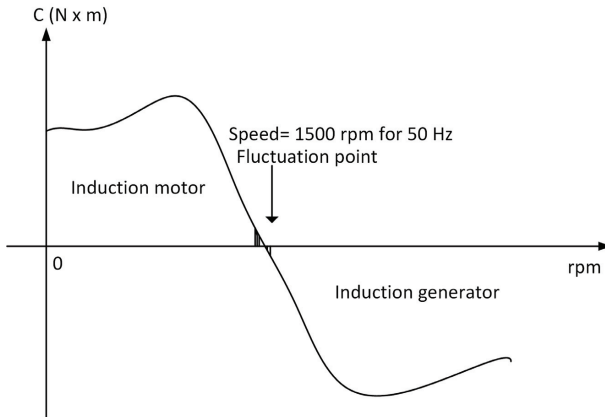


Figure 1.13 – Conjugate vs rpm - Induction Motor and Generator

- Adjustment of IG Speed at Synchronous Speed

Considering the scheme shown in the Figure 1.12, the IG speed was led to close and below the fluctuation point, it means some value close to point where the torque or

conjugate is null as it can be seen in Figure 1.13 below. The fluctuation point is at the intersection with rpm axis. The interconnection switch shown in Figure 1.12 was closed when the Induction motor speed is in the fluctuation area. From this IG speed, the DCM_{IG} speed should be raised up to overcome the fluctuation point to become the induction motor an induction generator.

For this option, the IG is not auto-excited, the reactive is obtained from the grid.

1.8.2 Experiment Data

The experimental data obtained in the laboratory are shown in Table 1.11, Table 1.9 and Table 1.10. The Table 1.9 shows the data obtained from the scheme in Figure 1.11, Table 1.10 shows the data obtained from the scheme in Figure 1.12 and Table 1.11 shows the data obtained from the scheme in Figure 1.10. The unique difference between Figure 1.11 and Figure 1.12 is the presence of IM in Figure 1.12 as additional load. The difference between the Figure 1.10 and the others is basically the presence of an autotransformer in the DCM_{IG} field circuit and an additional motor as load in Figure 1.12.

The autotransformer is responsible for applying a voltage range directly on the DCM_{IG} armature to obtain a larger speed range of the DCM_{IG} and to push more power to the IG , keeping the DCM_{IG} parameters into the rated values. Hence, the elevation of IG speed and power depend on DCM_{IG} armature voltage, V_{aDCMIG} . It means that the DCM_{IG} speed control method used for the scheme in Figure 1.10 is different of the method used in the Figures 1.11 and 1.12. The IG speed of scheme shown in Figure 1.10 depends on just the DCM_{IG} field flux because V_{aDCMIG} is steady. The DCM_{IG} field flux is adjusted manually and V_{aDCMIG} as well.

In summary, the Table 1.11 shows the data obtained from the scheme shown in Figure 1.10 that has the 234 V_{dc} steady source; Table 1.9 and Table 1.10 show respectively the data obtained from the schemes shown in Figure 1.11 and Figure 1.12. These schemes have an autotransformer and a diodes bridge as substitute of the 234 V_{dc} steady source shown in Figure 1.10. The difference between Figures 1.11 and 1.12 is the induction motor that is inserted as additional load in Figure 1.12.

Then, from these three schemes, the data obtained from each operation scenario into a same scheme are analyzed and compared among themselves. The generators performances between different schemes are analyzed and compared considering the similar operational scenarios under tests and the respective schemes' differences. The results are shown along this work.

Note: The abbreviations *n.a.* (*Not applicable*) shown in scenarios 1, 1C and 1B of tables 1.9, 1.10 and 1.11 refer to values not used in SG and IG power graphics. The cited graphics are based on the scenarios 2 onwards.

Table 1.9 – Operational scenarios in controlled mode and three resistors bank as load

Results	Scenario 1B	Scenario 2B	Scenario 3B	Scenario 4B	Scenario 5B	Scenario 6B	Scenario 7B	Scenario 8B	Scenario 9B
V_{SG} (V)	220.0	220.0	220.0	220.0	220.0	220.0	220.0	220.0	220.0
f_{SG} (Hz)	60	60	60	60	60	60	60.0	60.0	60.0
$I_{fieldSC}$ (mA)	190	320	300	300	320	350	370	340	100
V_{DCMSG} (V)	272.9	275.0	276.2	276.8	277.5	278.0	280.7	278.5	270.0
$I_{apDCMSG}$ (A)	2.0	2.5	3.8	4.7	6.2	7.4	9.5	10.6	2.0
I_{FDMSG} (mA)	510.0	530.0	520.0	520.0	515.0	510.0	515.0	515.0	515.0
V_{IG} (V)	220.0	220.0	220.0	220.0	220.0	220.0	220.0	220.0	n.a.
I_{IG} (Hz)	60	60	60	60	60	60	60	60	n.a.
η_{IG} (rpm)	1793	1896	1878	1857	1848	1821	1794	n.a.	n.a.
$V_{apDCMIG}$ (V)	291.3	323.6	316.7	308.3	301.3	293.0	284.1	n.a.	n.a.
$I_{apDCMIG}$ (A)	0.5	8.0	7.0	6.0	4.7	3.5	2.0	n.a.	n.a.
$I_{FD MIG}$ (mA)	330.0	330.0	330.0	330.0	330.0	330.0	330.0	n.a.	n.a.
$I_{\eta_{loadR}}$ (A)	0.0	5.0	5.0	5.0	5.0	5.0	5.0	5.0	0.0
I_{IG} (A)	2.4	5.8	5.1	4.4	3.7	2.9	2.4	0.0	0.0
I_{SG} (A)	2.9	1.5	2.0	2.8	3.6	4.5	5.6	7.4	4.0
IC (A)	5.4	5.4	5.4	5.4	5.4	5.4	5.4	5.4	4.0
I_{wsg} (A)	0.0	1.05	1.48	1.97	2.47	3.32	4.65	5.03	0.0
$IC1$ (A)	2.9	1.13	1.60	2.13	2.66	3.03	3.13	5.40	4.0
$IC2$ (A)	2.4	4.26	3.80	3.27	2.74	2.37	2.27	0.0	0.0
I_{wIG} (A)	0.0	3.95	3.51	3.03	2.53	1.68	0.35	0.0	0.0
PSG (W)	0.0	400.5	565.5	750.0	939.8	1266.6	1770.1	1915.8	0.0
P_{IG} (W)	0.0	1504.8	1335.8	1155.3	965.5	638.67	135.17	0.0	0.0
P_{DCMSG} (W)	545.8	687.5	1049.6	1301.0	1665.0	2057.2	2666.7	2962.7	543.4
P_{DCMIG} (W)	145.7	2588.8	2216.9	1849.8	1416.1	1025.5	568.2	0	0.0
η_{convP} (%)	0.0	58.15	58.33	60.47	61.84	61.80	58.89	64.66	0.0
η_{SG} (%)	0.0	58.25	53.88	57.65	56.44	61.57	66.38	64.66	0.0
η_{IG} (%)	0.0	58.12	60.43	62.45	68.18	62.28	23.79	n.a.	n.a.

¹ 40 μ F / phase
² 30 μ F / phase

Table 1.10 – Operational scenarios in controlled mode and three resistors bank and induction motor as load

Results	Scenario 1C	Scenario 2C	Scenario 3C	Scenario 4C	Scenario 5C	Scenario 6C	Scenario 7C	Scenario 8C	Scenario 9C
	SG and IG in parallel and no R load, ¹	SG and IG in parallel load in, ¹	SG and IG in parallel load in, ¹	SG and IG in parallel mode and load in, ¹	SG and IG in parallel mode and load in, ¹	SG and IG in parallel mode and load in, ¹	SG and IG in parallel mode and load in, ¹	SG alone and load in, ¹	SG alone and no load, ²
V_{SG} (V)	220.0	220.0	220.0	220.0	220.0	220.0	220.0	220	220.0
f_{SG} (Hz)	60	60	60	60	60	60	60	60	60
$I_{fieldSG}$ (mA)	170	420	410	400	400	430	475	390	100
V_{adcmSG} (V)	278.9	277.0	277.5	280.5	281.0	281.1	282.9	279.2	271.7
I_{adcmSG} (A)	2.0	2.9	4.0	5.0	6.3	7.6	9.6	10.5	2.0
I_{adcmSG} (mA)	530.0	530.0	530.0	530.0	530.0	520.0	520.0	520.0	515.0
V_{IG} (V)	220.0	220.0	220.0	220.0	220.0	220.0	220.0	0.0	n.a.
f_{IG} (Hz)	60	60	60	60	60	60	60	0.0	n.a.
n_{IG} (rpm)	1803	1893	1868	1857	1843	1821	1793	0.0	n.a.
V_{adcmIG} (V)	288.9	330.0	318.0	310.0	302.3	295.2	285.9	0.0	n.a.
I_{adcmIG} (A)	1.0	8.0	7.0	6.0	4.7	3.5	2.0	0.0	n.a.
I_{adcmIG} (mA)	330.0	330.0	330.0	330.0	330.0	330.0	330.0	0.0	n.a.
I_{wloadR} (A)	0.0	5.0	5.0	5.0	5.0	5.0	5.0	5.0	0.0
I_{wMT} (A)	0.2	0.2	0.2	0.2	0.2	0.2	0.2	0.2	0.0
I_{dwmT} (A)	1.23	1.23	1.23	1.23	1.23	1.23	1.23	1.23	0.0
I_{IG} (A)	2.3	6.0	5.0	4.4	3.6	2.9	2.3	0.0	0.0
I_{SG} (A)	2.8	0.7	1.6	2.3	3.3	4.1	5.3	6.7	4.0
IC (A)	5.4	5.4	5.4	5.4	5.4	5.4	5.4	5.4	4.0
I_{wSG} (A)	1.55	0.65	1.29	1.99	3.04	3.74	4.95	5.23	0.0
$IC1$ (A)	2.33	0.28	1.03	1.17	1.29	1.66	1.88	4.2	4.0
$IC2$ (A)	1.85	3.91	3.14	3.00	2.88	2.51	2.29	0.0	0.0
I_{wIG} (A)	-1.37	4.55	3.91	3.22	2.16	1.45	0.25	0.0	0.0
PSG (W)	591.2	247.97	490.34	753.80	1156.9	1428.7	1887.8	1993.7	0.0
PIG (W)	-521.1	1733.5	1491.1	1227.7	824.52	552.74	93.68	0.0	0.0
P_{dcmsG} (W)	557.8	803.30	1110.0	1402.5	1770.3	2136.4	2715.8	2931.6	624.5
P_{dcmsG} (W)	288.9	2640.0	2226.0	1860.0	1420.8	1033.2	571.8	0.0	0.0
η_{GROUP} (%)	0.0	57.55	59.40	60.73	62.09	62.52	60.27	67.59	0.0
η_{SG} (%)	0.0	30.87	44.17	53.75	65.35	66.88	69.51	67.59	0.0
η_{IG} (%)	0.0	65.66	66.99	66.00	58.03	53.50	16.38	0.0	n.a.

¹ 40 μ F / phase

² 30 μ F / phase

Table 1.11 – Operational scenarios in controlled mode and a resistor bank

Results	Scenario 1 SG and IG in parallel mode and no load, ¹	Scenario 2 SG in parallel mode $I_{IG} = 5.3 \text{ A}$, ¹	Scenario 3 SG and IG in parallel mode $I_{IG} = 4.5 \text{ A}$, ¹	Scenario 4 SG and IG in parallel mode $I_{IG} = 4.0 \text{ A}$, ¹	Scenario 5 SG and IG in parallel mode $I_{IG} = 3.5 \text{ A}$, ¹	Scenario 6 SG and IG in parallel mode $I_{IG} = 3.2 \text{ A}$, ¹	Scenario 7 SG alone and load in ¹	Scenario 8 SG alone and no load ¹
V_{SG} (V)	228.0	228.0	228.0	228.0	228.0	228.0	228.0	228.0
f_{SG} (Hz)	55	55	55	55	55	55	55	55
$I_{fieldSG}$ (mA)	380	510	500	500	510	580	400	100
V_{apcMSG} (V)	232.1	234.0	237.6	239.5	239.4	243.0	239.0	232.4
I_{apcMSG} (A)	0.0	4.7	6.8	8.0	9.5	12.0	12.0	2.0
I_{fpcMSG} (mA)	450	420	450	440	440	440	420	420
V_{IG} (V)	228.0	228.0	228.0	228.0	228.0	228.0	0.0	0.0
I_{IG} (Hz)	55	55	55	55	55	55	0.0	0.0
η_{IG} (rpm)	1679	1720	1707	1693	1683	1663	0	0
V_{apcMIG} (V)	232.1	225.4	226.8	228.2	229.8	231.2	0.0	0.0
I_{fpcMIG} (A)	0.0	9.8	7.4	6.0	4.2	2.3	0.0	0.0
I_{load} (A)	0.0	100	200	220	245	310	0.0	0.0
I_{IG} (A)	0.0	5.0	5.0	5.0	5.0	5.0	5.0	0.0
I_{SG} (A)	1.9	2.2	3.0	3.5	4.3	5.3	7.3	5.2
IC (A)	5.2	5.2	5.2	5.2	5.2	5.2	5.2	5.2
I_{wSG} (A)	n.a.	2.05	2.68	3.06	3.86	4.91	5.00	0.00
$IC1$ (A)	n.a.	0.79	1.34	1.70	1.89	2.00	5.20	5.2
$IC2$ (A)	n.a.	4.40	3.86	3.50	3.31	3.20	0.00	0.00
I_{wTG} (A)	n.a.	2.94	2.32	1.94	1.14	0.10	0.00	0.00
PSG (W)	n.a.	809.9	1059.5	1207.5	1525.3	1938.1	1998.4	0.0
PIG (W)	n.a.	1.164.7	915.04	767.07	449.27	36.48	0.00	0.0
P_{DCMSG} (W)	n.a.	1099.8	1615.7	1916.0	2274.3	2916.0	2868.0	464.8
P_{DCMIG} (W)	n.a.	2208.9	1678.3	1369.2	965.2	531.8	0.0	0.0
η_{GROUP} (%)	n.a.	59.68	59.94	60.10	60.95	57.27	68.85	n.a.
η_{SG} (%)	n.a.	73.64	65.58	63.02	67.07	66.46	68.85	n.a.
η_{IG} (%)	n.a.	52.73	54.52	56.02	46.55	6.9	n.a.	n.a.

¹ 40 μ F / phase

1.9 Results

The results show graphs, analysis of configurations presented in Figure 1.10, Figure 1.11 and Figure 1.12 and analysis of contribution from each generator for each arrangement of load, that is either a resistive bank or three resistive banks added with an induction motor.

All graphs obtained from scheme in Figure 1.10 [28] are based on a system frequency of 55 Hz. For the others experiments from Figures 1.11 and Figure 1.12, the system frequency is 60 Hz. Then, the synchronous speed for the experiments from Figure 1.10 is 1650 rpm, see the equation 1.6, and 1800 rpm for the other experiments.

In order to highlight the contributions from autotransformer and Diodes Bridge to the experiments, it will be presented some analysis based on graphs and experiment results.

Figure 1.14 shows that the *PIG* was limited to 1164 W in scenario 2 from Table 1.11 because the over current of $I_{a_{DCMIG}}$ (*Direct current motor induction generator armature current*) 9.8 A, that is a value greater than the rated $I_{a_{DCMIG}}$ of 7.72 A as Table 1.3. To overcome this barrier, an autotransformer and a diodes bridge were installed to widen the voltage range applied over the *DCMIG* armature, as shown in Figure 1.11 and Figure 1.12. The armature voltage range with the autotransformer and diodes bridge can vary from 0 to $336 V_{dc}$ (*Direct current voltage*). This range is bigger than the previous case with $V_{a_{DCMIG}}$ of $234 V_{dc}$. As the *DCMIG* speed, n_{IG} , is directly proportional to $V_{a_{DCMIG}}$, 1.2, the n_{IG} is elevated proportionally with the $V_{a_{DCMIG}}$, as shown in scenarios 2 to 8 from Table 1.9 and Table 1.10. Then, in this latter method, $I_{a_{DCMIG}}$ variation depends on the load conjugate variation only, whereas the *DCMIG* flux, ϕ , remains constant as 1.3.

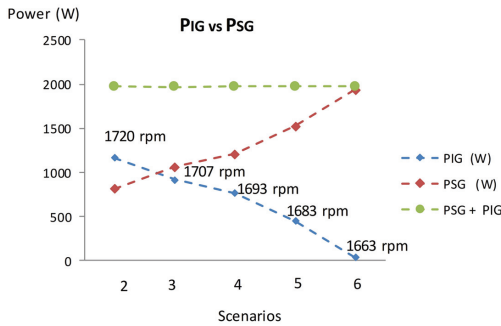


Figure 1.14 – *PIG* vs *PSG* with *DCMIG* Field Variation and $V_{a_{DCMIG}}$ kept Constant

Figure 1.15 and Figure 1.16 shows that the power range supplied from *IG*, *PIG*,

through the autotransformer method, is greater than PIG of $234 V_{dc}$ steady source method. Consequently, the PSG supplied from this autotransformer method is lower than the PSG supplied from $234 V_{dc}$ steady source method. Both methods feed the entire resistive load as shown in Figure 1.14 and Figure 1.15, and the resistive and motor load as shown in Figure 1.16.

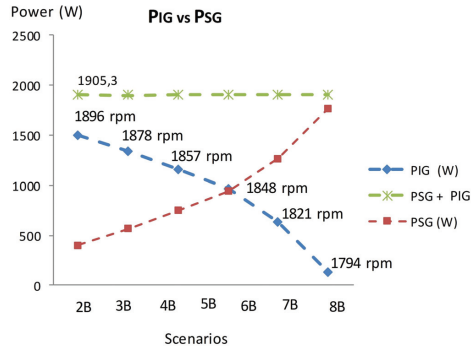


Figure 1.15 – PIG vs PSG with V_{aDCMIG} Variation and Field flux kept Constant (Only resistive load)

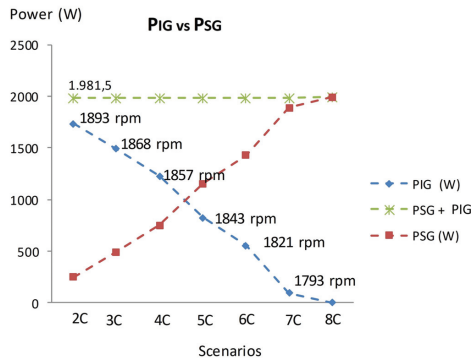


Figure 1.16 – PIG vs PSG with V_{aDCMIG} Variation and Field Flux kept Constant (Resistive load & IM)

In Figure 1.17, Figure 1.19 and Figure 1.20 show the comparative results of IG and SG primary machine output power, P_{DCMIG} vs P_{DCMSG} . These performances are similar to PIG and PSG performances shown in Figure 1.14, Figure 1.15 and Figure 1.16. The P_{DCMIG} in Figure 1.17 elevates because a field flux decreases and V_{aDCMIG} kept constant.

The P_{DCMIG} in Figure 1.19 and Figure 1.20 elevates because of the V_{aDCMIG} increases, which is manually adjusted by the autotransformer shown in Figure 1.11 and Figure 1.12.

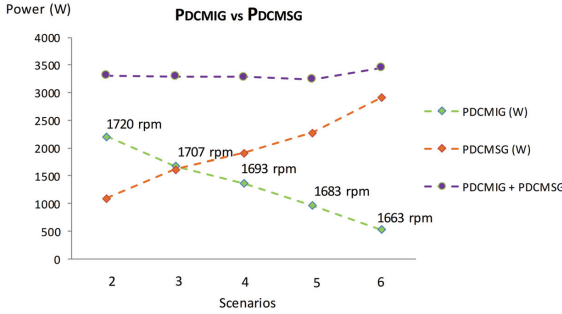


Figure 1.17 – P_{DCMIG} vs P_{DCMSG} with $DCMIG$ Field Flux Variation and V_{aDCMIG} Kept Constant

Figure 1.18 shows that the system voltage and frequency are kept the same even with the resistive load is connected or disconnected, showing a good regulation control in system voltage and frequency [28]. This voltage and frequency performance was realized in all scenarios of load transients with the loads shown in Tables 1.9, 1.10 and 1.11.

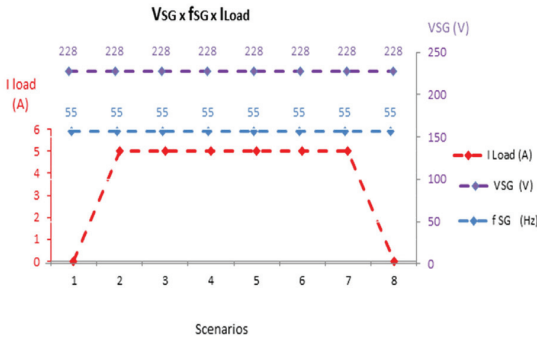


Figure 1.18 – $V_{SG} \times f_{SG} \times I_{load}$

The efficiency results shown in Figure 1.21, Figure 1.22 and Figure 1.23 show each subgroup efficiency for each scenario and load conditions. Each subgroup efficiency is resulted from relation between a generator and its respective *DCM (Direct current motor)* as shown in equations 1.32 and 1.33.

In summary, the following scenarios are shown: scenarios 2 to 7 (without autotransformer), scenarios 2B to 8B (with autotransformer and just resistive load) and scenarios 2C to 8C (with autotransformer, resistive load and induction motor).

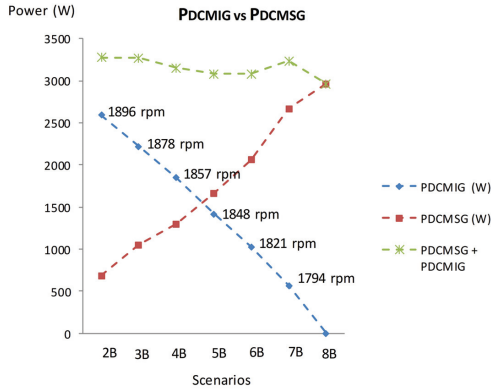


Figure 1.19 – P_{DCMIG} vs P_{PDCMSG} with V_{aDCMIG} Variation and Field Flux Kept Constant (Only resistive load)

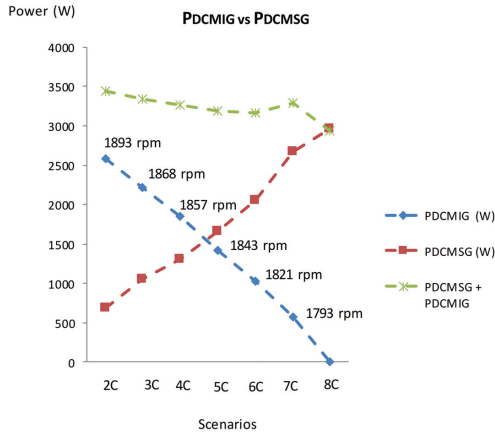


Figure 1.20 – P_{DCMIG} vs P_{PDCMSG} with V_{aDCMIG} Variation and Field Flux Kept Constant (Resistive load plus IM)

The *IG* subgroup efficiencies shown in Figure 1.22 and Figure 1.23 are bigger than *IG* subgroup efficiencies from similar scenarios in Figure 1.21. Moreover, the elevation of power from *IG* due to the increase of *DCMIG* speed, n_{IG} , is more representative of actual conditions. For instance, the turbines can assume whatever speed required from generators in offshore platforms.

The reduction of losses resulted in better *IG* subgroup efficiency as shown in Figure

1.22 and Figure 1.23. Figure 1.21 shows the machine's efficiencies when the I_{fDCMIG} or field flux decreases to elevate the speed. The efficiency improves when the V_{aDCMIG} elevation method is applied as shown in Figure 1.22 and Figure 1.23.

The efficiencies shown in Figure 1.22 and Figure 1.23 are higher than the efficiency presented in Figure 1.21, that indicates the $DCMIG$ speed range is more restricted [28].

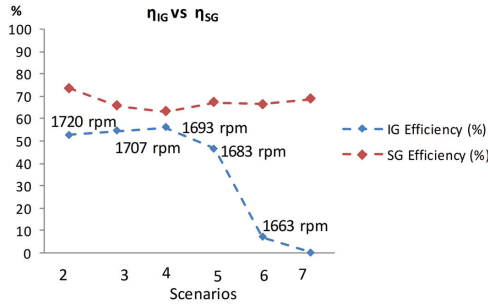


Figure 1.21 – n_{IG} vs n_{SG} with $DCMIG$ Field Flux Variation and V_{aDCMIG} Kept Constant

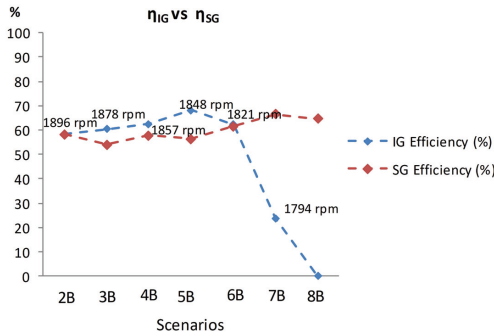


Figure 1.22 – n_{IG} vs n_{SG} with V_{aDCMIG} Variation and Field Flux kept Constant (Only resistive load)

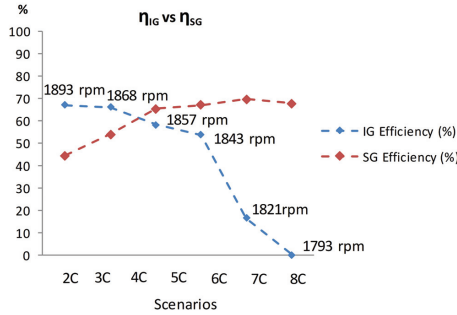


Figure 1.23 – n_{IG} vs n_{SG} with $V_{a_{DCMIG}}$ Variation and Field Flux kept Constant (Resistive load plus IM)

1.10 Conclusion

The cited electric system shows voltage and frequency regulation for each scenario transition as demonstrated in Figure 1.18, tables 1.9, 1.10 and 1.11 and respective analysis.

SG presented the master behavior for the system frequency and voltage as [28]. *IG* did the master behaviour for the active power and slave behavior for the system frequency and voltage. *SG* controls the system voltage and frequency and *IG* follows the voltage and frequency defined by *SG*. The *IG* establishes the active power supplied to the system and the *SG* complements the rest of active power and reactive power required. The *PSG* depends on the *IG* shaft speed imposed by *DCM_{IG}*. The *PSG* and the system voltage and frequency are controlled respectively by field voltage and speed control loops presented in Figure 1.10, Figure 1.11 and Figure 1.12.

It was realized a bigger *PIG* range in the scenarios shown in Table 1.9 and in Table 1.10, than the scenarios shown in Table 1.11 due to $V_{a_{DCMIG}}$ elevation method. The *PSG* fulfilled the load power automatically from the *PIG* manually adjusted by autotransformer.

The field flux variation method of DCM_{IG} , [28], does not result in P_{DCMIG} increase, whereas the $V_{a_{DCMIG}}$ elevation method results in increase of P_{DCMIG} , *PIG* and *IG* subgroup efficiency. The increase of *PIG* is resulted from *IG* speed increase, n_{IG} , that was obtained by elevation of $V_{a_{DCMIG}}$ as shown in Figure 1.15, Figure 1.16, Figure 1.19 and Figure 1.20.

The use of $V_{a_{DCMIG}}$ method, instead of V_{dc} steady source or flux ($I_{f_{DCMIG}}$) reduction method, enables to reach the $I_{a_{DCMIG}}$ limit of 8.0 A and 1893 rpm of DCM_{IG} shaft speed. It is higher than the DCM_{IG} speed from V_{dc} steady source, see Figure 1.21.

The efficiencies from the $V_{a_{DCMIG}}$ elevation method were greater than those from

the scheme with V_{dc} steady source [28], as shown in Figure 1.22 and Figure 1.23. V_{aDCMIG} elevation method does not have the additional current losses that the V_{dc} steady source method have.

The V_{dc} steady source method consist of reduction of field flux ϕ , I_{fDCMIG} , and increasing of I_{aDCMIG} as 1.3. Then, the IG speed, n_{IG} , is increased as equation 1.2.

The main losses for the V_{dc} steady source method are related to higher I_{aDCMIG} elevation, $P_{(w)} = Ra * I_{aDCMIG}^2$, than the I_{aDCMIG} elevation caused by V_{aDCMIG} elevation method. Then, by use of V_{dc} steady source method, the I_{aDCMIG} is elevated due to reduction of I_{fDCMIG} . The higher I_{aDCMIG} is, the higher losses are. Then, as the losses of V_{aDCMIG} elevation method are lower, the efficiencies are higher.

As shown in power performance graphs related to V_{aDCMIG} elevation method, Figure 1.15, Figure 1.16, Figure 1.19 and Figure 1.20, the PIG and P_{DCMIG} are more representative of actual operation conditions.

All of the followings three different methods of IG connection into the electric system were implemented and the results were satisfactory: (i) direct startup as a motor and rising the induction motor speed up to it turns IG , (ii) synchronism of self-excited IG with the electric system and (iii) adjustment of IG speed at synchronous speed and IG connection into the system;

2 Load and Generation Transients of Synchronous and Induction Generators in Parallel Operation Mode in an Isolated Electric System

2.1 Introduction

This section presents an analysis of load and generation transients in an isolated electric system with a parallel connection of one synchronous generator and induction generator, each one coupled to a dc machine or primary machine as well as to a capacitor bank. A resistive load is connected to the system. Changes in the load were intentionally provoked. Then, each generator was removed, one at a time, and reconnected. The results are shown here and the respective curves are analysed.

The results show the performance and responses of the cited system regarded to either transients from load changes or from partial generation withdrawal [32].

Differently of scheme shown in Figure 1.10, the schemes shown in Figures 1.11, 1.12 and in the Figure 2.3 have an autotransformer for actuating directly in V_{aDCMIG} in order to permit a greater speed elevation range and, then, a higher power contribution from the IG . Furthermore, the current resistor bank consists of three individual bank resistors connected in parallel, as presented in Figure 2.3 [28].

In the experiments of this chapter, the first method of IG connection into the electric system was implemented, (i) direct startup as a motor and rising the induction motor speed up to it turns IG . As the wound rotor machine was used instead of squirrel cage rotor machine, that first method can be used to the experiments described here. As already informed in general introduction and in chapter 1, the wound rotor machine can have an extra advantage that is the high startup torque due to resistors that can be connected at the induction machine rotor circuit [24].

One of the motivations of this study is related to the main advantages of induction generators over synchronous generators which are: brushless construction with squirrel-cage rotor, reduced size and weight, absence of DC supply for excitation, reduced maintenance cost, and better transient performance [8]. As previously informed, the use of wound rotor machine does not make invalid the results obtained in this work for squirrel cage rotor machine because the functioning of both machines is the same, except the

possibility of increasing of wound rotor startup torque.

Then, this work presents conclusions about the system performance regarding to load and generation transients.

2.2 Isolated Electric System

The isolated electric system was sized as shown by the equations and data given in the following paragraphs. The equations are based on calculations in [33].

The system automatism consists of a voltage control loop and a speed control loop. Both are inserted in the *SG* scheme, as shown in Figure 2.3.

The data plates of the principal equipment are shown in Tables 1.3 to Table 1.7.

The speed and voltage control loops are presented respectively in Figure 2.4 and Figure 2.5.

The voltage and speed electronic control boards are shown in Figure 2.1, Figure 2.2 and Figure 2.3.

The parametrization used in both electronic control boards was shown in chapter 1, except de reference values of voltage and speed. The references of voltage and speed control loops are respectively 68.6 and 60.1.

2.3 Data Plate

The equipment's data plates are shown in tables 1.3 to 1.8. The tables 1.7 and 1.8 show the loads data plates that are used in the experiments along this work.

2.4 Equation - Part I

The equations of this section are the same used in the previous chapter as shown in section 1.5.

2.5 Equation - Part II

The equations 2.1, 2.2, 2.3 and 2.4 together with the equations 2.5 to 2.11 were employed to calculate the power and efficiencies as shown in the Table 2.1 for each generator and the entire group of machines.

$$I_{SG}^2 = Iw_{SG}^2 + I_{cl}^2 \quad (2.1)$$

$$I_{IG}^2 = Iw_{IG}^2 + I_{c2}^2 \quad (2.2)$$

$$I_c = I_{c1} + I_{c2} \quad (2.3)$$

$$I_{load} = Iw_{loadR} = Iw_{SG} + Iw_{IG} \quad (2.4)$$

As I_{SG} , I_{IG} , I_c and Iw_{loadR} are measured values, (see Table 2.1), the system has four variables and four equations. Then, for each scenario, the four variables Iw_{SG} , I_{c1} , Iw_{IG} and I_{c2} were calculated by Matlab software as appendix F and result in values shown in Table 2.1.

The entire group efficiency and the efficiency of each subgroup were calculated based on PIG , PSG , P_{DCMSG} , and P_{DCMIG} as follows.

$$PSG = \sqrt{3} \times V_{SG} \times Iw_{SG} \quad (2.5)$$

$$PIG = \sqrt{3} \times V_{IG} \times Iw_{IG} \quad (2.6)$$

$$P_{DCMSG} = Va_{DCMSG} \times Ia_{DCMSG} \quad (2.7)$$

$$P_{DCMIG} = Va_{DCMIG} \times Ia_{DCMIG} \quad (2.8)$$

$$\eta_{group\%} = \frac{P_{SG} + P_{IG}}{P_{DCMSG} + P_{DCMIG}} \times 100 \quad (2.9)$$

$$\eta_{SG\%} = \frac{P_{SG}}{P_{DCMSG}} \times 100 \quad (2.10)$$

$$\eta_{IG\%} = \frac{P_{IG}}{P_{DCMIG}} \times 100 \quad (2.11)$$

2.6 Experiment and Schemes

The experiment was mounted in the laboratory as shown in Figures 2.1, 2.2 and 2.3.

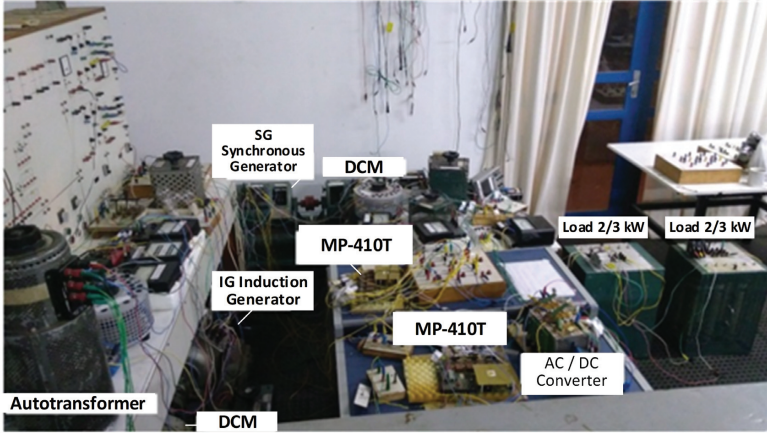


Figure 2.1 – Laboratory Assembly

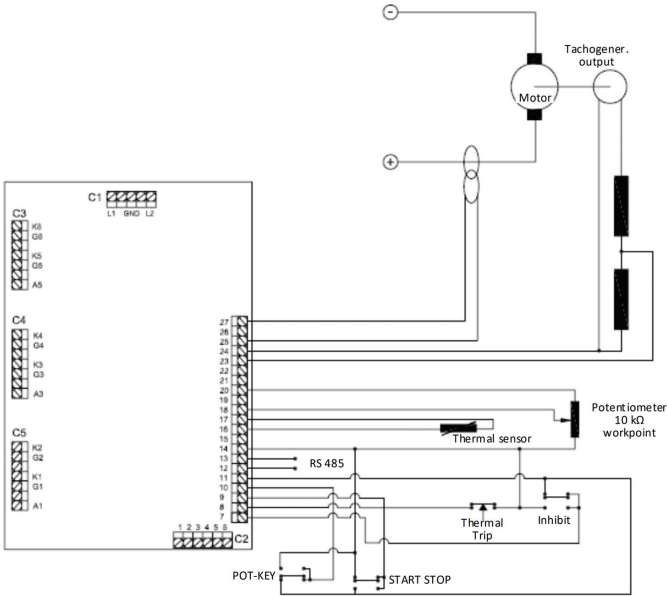


Figure 2.2 – Connections Arrangement of MP410T and Devices

2.7 Voltage and Speed Control Loops

The Figures 2.4 and 2.5 show the close control loop used to control the *SG* speed and voltage via electronic boards.

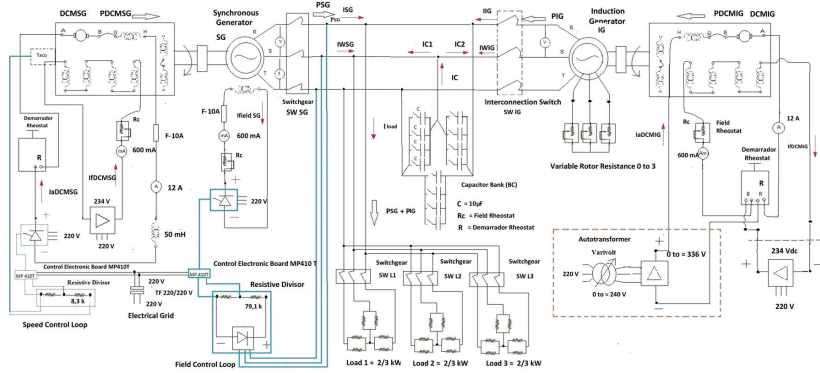


Figure 2.3 – Synchronous and Induction Generators in Parallel Operation Mode

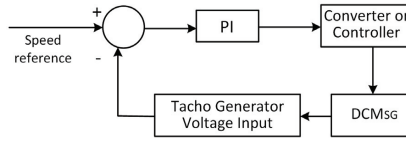


Figure 2.4 – Speed Control Loop

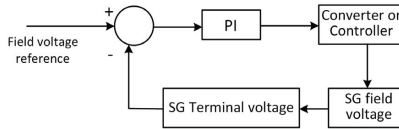


Figure 2.5 – Field Voltage Control Loop

The master and slave behavior of the generators (SG is the master and IG is the slave for the system frequency and voltage) as well as the IG is the master for the active power supply as verified and detailed in chapter 1 of this work. The frequency and voltage are determined by SG , while the active power consumed at load is supplied by the IG and complemented by SG .

2.8 Experimental Data

The laboratorial data are shown in Table 2.1.

Table 2.1 – Scenarios and Transitions

	Scenario 1	Scenario 2	Scenario 3	Scenario 4	Scenario 5	Scenario 6	Scenario 7
Results	Scenario 1	Scenario 2	Scenario 3	Scenario 4	Scenario 5	Scenario 6	Scenario 7
V_{SG} & V_{IG} (V)	228.0	228.0	228.0	228.0	204.0	228.0	228.0
f_{SG} (Hz)	55	55	55	55	53.3	55	55
$I_{fieldSG}$ (mA)	380	500	550	520	600	510	420
V_{aDCMSG} (V)	238.4	240.2	235.3	238.0	234.1	238.3	241.5
I_{aDCMSG} (A)	2.0	4.7	3.0	4.9	0.0	3.6	12.0
I_{fDCMSG} (mA)	450	450	450	450	450	450	450
f_{IG} (Hz)	55	55	55	55	53	55	0.0
n I G (rpm)	1650	1731	1746	1724	1697	1747	1954
V_{aDCMIG} (V)	299.5	323.3	334.4	323.1	322.2	323.5	333.5
I_{aDCMIG} (A)	1.9	7.0	8.6	6.8	8.0	8.2	0.0
I_{fDCMIG} (mA)	400	380	380	380	380	380	370
I_{load} (A)	0.0	5.1	5.1	5.1	4.5	5.1	5.1
I_{IG} (A)	3.1	5.6	6.9	5.6	6.5	6.4	0.0
I_{SG} (A)	1.9	1.7	0.4	1.6	0	0.9	7.3
I_C (A)	5.1	5.1	5.1	5.1	4.4	5.1	5.1
I_{wSG} (A)	n.a.	1.32	0.3967	1.14	0.0	0.8396	5.1
I_{C1} (A)	1.9	1.06	0.0513	1.14	0.0	0.3241	5.1
I_{C2} (A)	3.1	4.14	5.05	3.96	4.4	4.7759	0
I_{wIG} (A)	n.a.	3.77	4.70	3.96	4.65	4.26	0
P_{SG} (W)	n.a.	524.91	156.65	449.50	0.0	331.57	2038.60
P_{IG} (W)	n.a.	1489.10	1857.40	1564.50	1643.0	1682.50	0.0
P_{DCMSG} (W)	n.a.	1128.9	705.90	1166.20	0.0	857.88	2898.0
P_{DCMIG} (W)	n.a.	3168.30	2875.80	2197.10	2577.60	2652.70	0.0
η_{CBOUP} (%)	n.a.	46.87	56.23	59.88	61.70	57.37	69.50
η_{SG} (%)	n.a.	46.50	22.19	38.54	n.a.	38.65	69.50
η_{IG} (%)	n.a.	47.00	64.59	71.21	61.70	63.42	n.a.

¹ 40 μ F / phase

2.9 Results

For each scenario and transition indicated in Table 2.1, the respective voltage and current signal and their transition waveforms are shown below.

The oscilloscope configurations are: I_{IG} , I_{SG} and I_{load} : 100mV/A and 500mV/division. V_{pn} (Phase neutral voltage): 100 V/division or 50V/division. n_{SG} (Synchronous generator speed): 550 rpm/division.

Note: As the generators are in parallel connection, $V_{SG}=V_{IG}$ (Induction generator voltage)= V_{pp} (Phase-phase voltage)= $V_{pn} * \sqrt{3}$

- Load Transients: The load changes consist of removal and insertion of 2/3 kW. The other 4/3 kW remain connected. Figures 2.6, 2.7, 2.8 and 2.9 show I_{IG} , I_{SG} and V_{pn} for scenarios 1 and 2. The figures show the actual state and values of these parameters in accordance with Table 2.1. The I_{IG} is advanced from V_{pn} because the reactive bank supply during these scenarios. In scenarios 1 (no load) and scenario 2 (low resistive load),

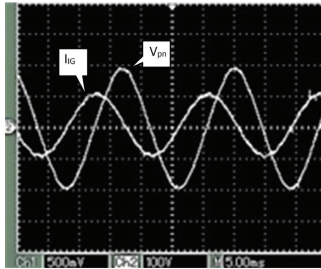


Figure 2.6 – I_{IG} and V_{pn} (Scenario 1)

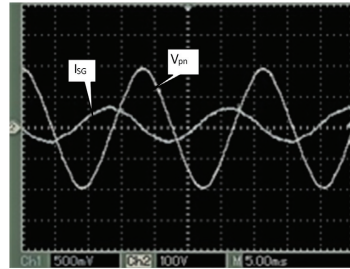


Figure 2.7 – I_{SG} and V_{pn} (Scenario 1)

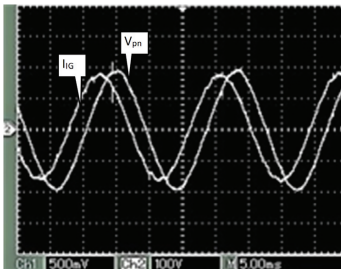


Figure 2.8 – I_{IG} and V_{pn} (Scenario 2)

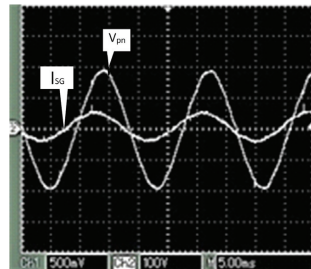


Figure 2.9 – I_{SG} and V_{pn} (Scenario 2)

Figure 2.10 reveals the automatic I_{SG} regulation upon removal and insertion of 2/3 kW from the resistor bank. Figure 2.11 shows that I_{IG} remains the previous values with an identical load change.

Figures 2.10 and 2.11 also show that V_{pn} keeps a constant value. This means that the system regulation for load changes is managed solely by SG . The V_{pn} and V_{IG} remains constant.

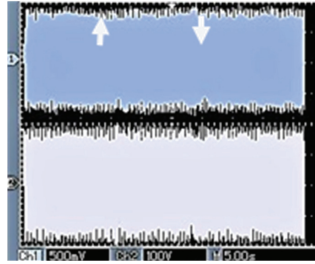
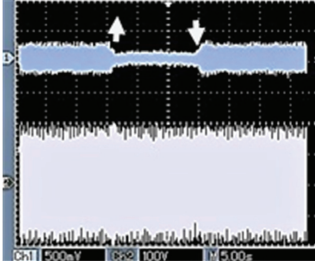


Figure 2.10 – Channel 1- I_{SG} , Channel 2- V_{pn} . (2/3 kW is removed and then inserted) (Scenario 2)

Figure 2.11 – Channel 1- I_{IG} , Channel 2- V_{pn} . (2/3 kW is removed and then inserted) (Scenario 2)

Figure 2.12 shows that I_{IG} does not change with removal and insertion of load. All the PIG that feed the load before the load change, still feeding the load after the load change. The SG just participates this by complementing the load power required.

Figure 2.13 shows that I_{SG} adjustments for the load change in order to provide the increased power required by the load.

Figures 2.12 and 2.13 also show that n_{SG} does not change, and the SG 's controls regulate the speed to synchronous speed for 55 Hz, 1650 rpm, always when the load changes.

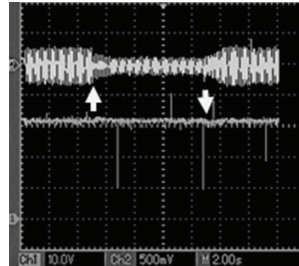
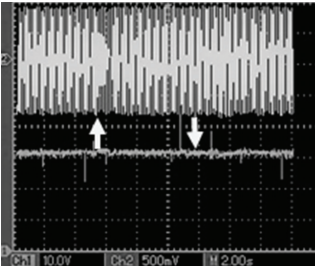


Figure 2.12 – Channel 1- n_{SG} , Channel 2- I_{IG} . (2/3 kW is removed and then inserted.) (Scenario 2)

Figure 2.13 – Channel 1- n_{SG} , Channel 2- I_{SG} . (2/3 kW is removed and then inserted.) (Scenario 2)

- Generation Transients: The changes created in the generation system consist of removal and insertion of each generator.

Figure 2.14 shows that when SG is removed, the voltage system has a small drop and the voltage regulation is lost. This shows that the voltage regulation is the sole responsibility of SG .

Figure 2.15 shows the regulation of V_{pn} from the SG (master) when the IG (slave) is removed.

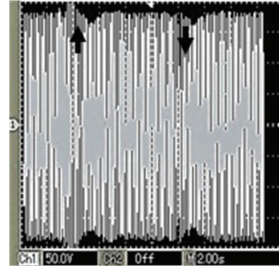
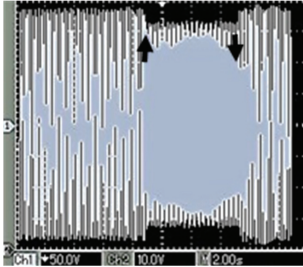


Figure 2.14 – V_{pn} , SG is removed and then Figure 2.15 – V_{pn} in load. IG is removed and then inserted. Scenarios 4 & 5

Figure 2.16 reveals good speed regulation from the SG when the IG is removed and inserted.

Figure 2.17 shows that I_{SC} assumes the IG load when IG is removed. In contrast to IG , SG realizes the IG is out and regulates itself to meet the demand and keeping the previous voltage and speed as shown in Figure 2.17, Figure 2.18 and Table 2.1.

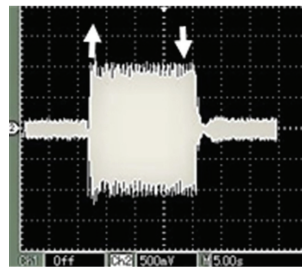
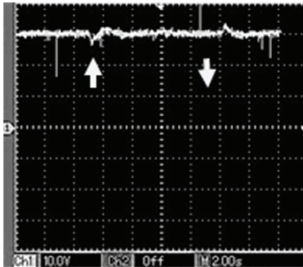


Figure 2.16 – SG speed. IG is removed and Figure 2.17 – I_{SG} , IG is removed and then inserted. Scenarios 6 & 7

Figures 2.18 and 2.19 show I_{SC} and I_{IG} , which are representing respectively, the smallest I_{SC} and the biggest I_{IG} obtained in the experiment.

Note: In the case of Figure 2.18, the oscilloscope scale was set to 1000mV/A.

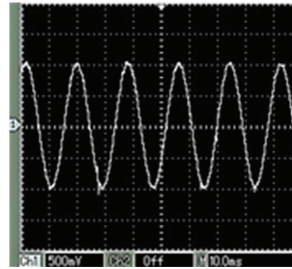
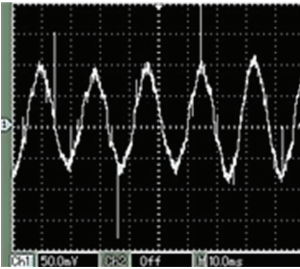


Figure 2.18 – I_{SG} . SG smallest contribution Figure 2.19 – I_{IG} , IG biggest contribution = 0.4A. Scenario 3 = 6.9A. Scenario 3

Figure 2.20 indicates that IG continues supply a steady power to the load, even with the SG removed. As SG is out, the system loses the voltage and frequency regulation. In this condition, the system voltage and frequency are imposed by IG .

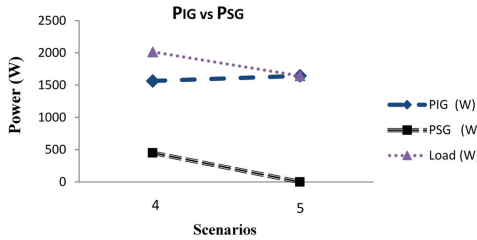


Figure 2.20 – Transition between Scenarios 4 and 5

On the contrary, Figure 2.21 shows the transition between the scenarios 6 and 7, it means when IG is disconnected, SG assumes the full load and still regulates the system voltage and frequency.

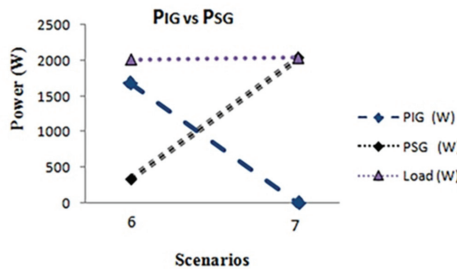


Figure 2.21 – Transition between Scenarios 6 and 7

2.10 Conclusion

Regarding to load changes, with removal and insertion of load, the SG can regulate the system voltage and frequency. The I_{SG} adjustments to the new load demand, while the I_{IG} keeps the previous values during transients. IG continues to supply the same power previously set for.

Regarding to IG transients, IG removed or inserted, SG and its system can regulate the system voltage and frequency. This is running even if the IG is fully loaded or IG is removed abruptly.

Regarding to SG transients, SG removed or inserted, IG is not capable of maintaining the system voltage and frequency, because IG does not have the voltage and frequency controls as the SG has. In this situation, the system frequency falls slightly as well as the system voltage.

In addition, when the system has no load or has only 2/3 kW and the two machines operating in parallel, when P_{DCMIG} is elevated to a value bigger than 600 W, the system frequency exceeds 55 Hz. Then, the IG and DCM_{IG} group motorizes the SG , and the DCM_{SG} operates as a no load DCG_{SG} (*Direct current generator coupled with synchronous generator*). As it is shown in the scheme shown in Figure 2.3, there is not no other way besides the load for receiving the generated power. Moreover, as the converter is operating as rectifier instead of inverter, the generated energy does not have another way to be regenerated or dissipated, then, the system frequency increases. When the system has 2/3 kW or 2kW connected, it is realized that the frequency does not exceed the rated value. In this case, all generated power is being consumed by loads. It consists of scenarios two to seven as shown in Table 2.1. Therefore, when P_{DCMIG} is adjusted to a value bigger than load power, the system frequency exceeds 55 Hz.

In [34] is shown two systems capable to regulate the system frequency in an electric system, the one of them is able to regulate the system frequency in an isolated electric that uses BL (*Ballast load*) (energy dissipation) and the other uses energy regeneration to the grid. It requires interconnected system. This latter serves as a didactic alternative only.

Conclusion

After the studies of DC machines regulators project (appendix A), thyristor firing circuit (appendix B), voltage regulators and filters project to synchronous machine (appendix C) and four-quadrant operations for DC machines (appendix D) was possible implement the target experiment of this work which consist of laboratorial scheme of induction and Synchronous generators in parallel operation mode feeding inductive and resistive loads. This experiment was target of analysis and studies of generation and load transients and specific contingencies for this kind of generators topology.

The main conclusions about the experiments are:

1. The *SG* presents a master behavior for the system frequency and voltage. *IG* does a master behavior for the active power supply and slave behavior for the system frequency and voltage. *SG* controls the system voltage and frequency and *IG* establishes the active power supplied to the system and *SG* complements the rest of active power and reactive power required;
2. The $V_{a_{DCMIG}}$ elevation method resulted in increase of P_{DCMIG} , PIG and higher *IG* subgroup efficiency than the $I_{f_{DCMIG}}$ reduction method [28]. The increase of P_{DCMIG} and PIG are consequences of *IG* speed increase, n_{IG} , that was obtained by elevation of $V_{a_{DCMIG}}$.
3. When the *IG* generates more than the load demand, the system frequency grows up and stays out of rated system frequency. The *IG* motorizes synchronous machine and DCM_{SG} operates as a no load DCG_{SG} ;
4. In the scenario "*IG* out and *IG* in", *SG* and its system can regulate the system voltage and frequency and *SG* keeps running even if the *IG* is fully loaded and is removed abruptly. On the contrary, when the *SG* is disconnected, the system voltage and frequency go out of control.
5. Voltage and speed control loops were implemented in lab to control the parallel operation of synchronous and induction generators.
6. Three different methods of *IG* connection into the electric system were studied as follow: (i) direct startup as a motor and rising the speed up to it turns *IG*, (ii) synchronism of self-excited *IG* with the electric system and (iii) adjustment of *IG* speed at synchronous speed and connection into the system;

7. It was used an original method to find power and efficiencies values of different equipment in different scenarios as demonstrated in chapters 1, 2 and complemented by appendix F;
8. The frequency elevation was checked when load transients happen in specific scenarios or *PIG* is bigger than load demand as indicated in chapter 2;

Based on the results obtained, the operation in parallel of induction and synchronous generators in an isolated electric system is technically viable in *MHPP* and it should be economic advantageous for *MHPP* and other applications due to some reasons such as: the *IG* final price is so lower than *SG* final price even to big machines 25 MW (information has obtained from Brazil traditional machine supplier), *IG* maintenance is simpler and consequently cheaper and *IG* is lighter than *SG*. Beyond, The *IG*'s reply for short circuit events is better than *SG*'s one because the *IG* contributes less than *SG* to short circuit power, [20]. Otherwise, mainly for greater applications as oil platforms and *FPSO*, there are other equipment and accessories that may be required, such as capacitor bank, switches and filters which should be also considered for a more deeper economic and technical evaluation.

Appendix

APPENDIX A – Filters and Regulators Project

A.1 Introduction

In this appendix, two kinds of analogical filters and regulators for a DC motor will be studied, namely a speed regulator that is composed of a speed control loop and current regulators [35]. Both loops, the current control loop and speed control loop aim to control the DC motor speed as shown in [34].

These loops will be used in primary machines that will serve as the primary drives of induction and synchronous generators. The primary machines used in the experiments are independent excitation ones. They are proper to speed control because their speed is basically controlled by armature current or field flux variation.

Initially, in this appendix will be present some devices required in DC motor controllers such as a ramp type firing circuit and synchronism transformer.

And then, it will be followed by practical cases and instructions of how design the analogical speed and current DC machine regulators and how define filters, capacitors, resistors and others necessary devices to implement the regulators. In add, all of the time constants and gains values will be estimated or calculated and the experiments will be didactically presented.

All the issues studied in this appendix are based on original and practical-case projects carried out and tested in the Laboratory of research development of electrical didactic laboratory of Federal University of Itajubá.

The analogical voltage regulator will be shown in appendix C.

The speed and current regulators used in chapters 1 and 2 are digital ones, otherwise, these can be replaced by analogical ones as those described here and in appendixes C and G.

A.2 Ramp Firing Circuit

The ramp-type firing system are used in all the experiments accomplished in this work and its functioning shown in Figure A.1 was implemented either with an analogical circuit detailed in appendix B or inside of the electronic board MP 410T algorithm used in chapters 1 and 2:

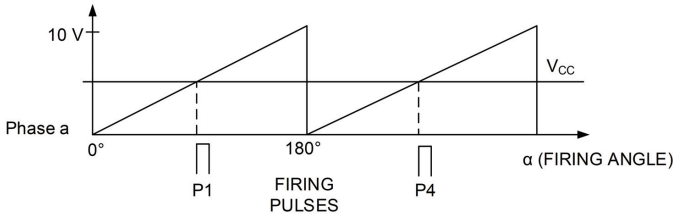


Figure A.1 – Ramp Type Firing Circuit

The intersection of the DC level with a ramp, which is internally generated in the TCA 785 integrated circuit, produces the pulses. The V_{cc} (*Control voltage of thyristor firing system*) is the output of the current regulator. Three TCA 785 integrated circuits should be used to produce six firing pulses for the Graetz converter bridge that is built by thyristors. The pulses generated by TCA 785 are P1 and P4 for the thyristors 1 and 4; P3 and P6 for the thyristors 3 and 6; and P5 and P2 for the thyristors 5 and 2 respectively. This is the explanation of the firing circuit pulse generation stage.

The other additional firing circuit functions such as enlargement of pulses, galvanic isolation of pulses and pulse amplification will be shown in details in appendix B.

A.3 Synchronism Transformer

The synchronism transformer function causes a 30° displacement on the grid voltage signal in order to synchronize this grid voltage and the interested start points with the thyristor firing angle, as demonstrated in Figure A.2. This kind of transformer is shown in Figure A.3 and it will be used in this work as a device necessary in the driven system.

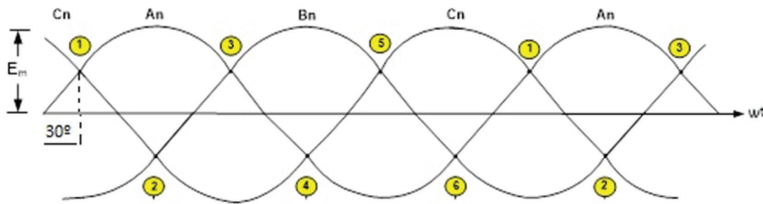


Figure A.2 – Waveforms and Firing Angle

This kind of transformer is used in practically all experiments carried out in this work.

Figure A.4 shows the synchronism transformer in a typical diagram which will be used in the experiments. Each TCA 785 controls the two thyristors connected to its

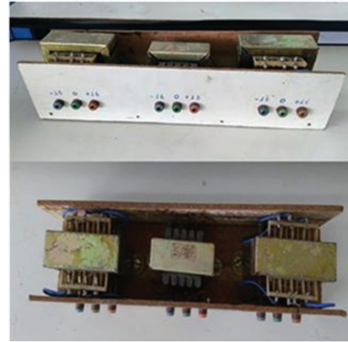
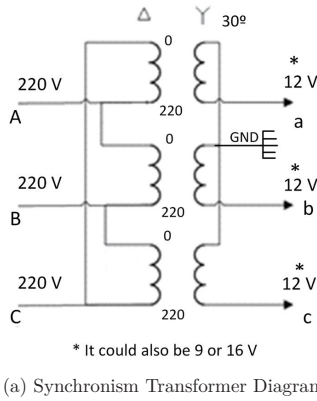


Figure A.3 – Synchronism Transformer

respective phase, e.g., the TCA 785 located in phase a controls the two thyristor firing angles located in phase a, thyristors 1 and 4. For more details, see the Figure B.12 of appendix B.

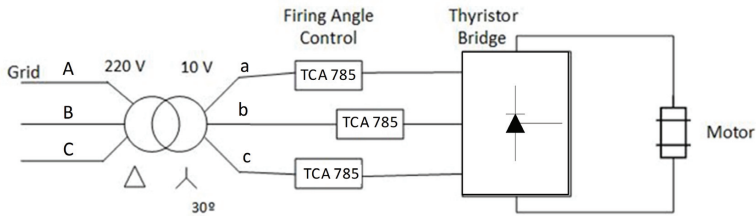


Figure A.4 – General view of Synchronism Transformer

A.4 Current and Speed Regulators of DC machine project

A.4.1 Introduction

The digital regulators were implemented in [36] and in the chapters 1 and 2. The analogical current and speed regulators of DC machine will be described and detailed in this appendix.

A.4.2 Motor Block Diagram

Figure A.5 shows the motor armature circuit and the driven system of *DCM*, *SM* (*Synchronous machine*) and load. The diagram of the driven system mechanical part is also presented in [36, 37].

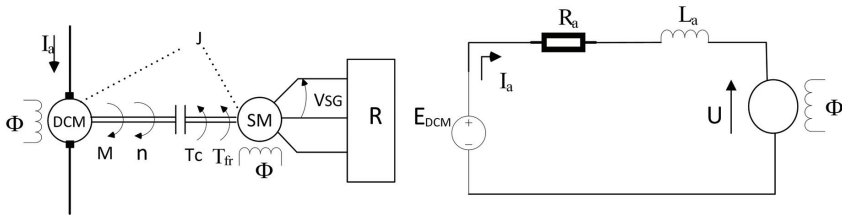


Figure A.5 – Motor Armature Circuit and Diagram of the Drive System Mechanical Part

where:

U Counter electromotive force [V]

E_{DCM} (Direct current motor voltage) [V]

R_a (Armature circuit resistance)

L_a (Armature circuit inductance)

ϕ Motor flux

I_a (Armature current)

M Motor torque

T_c (Load torque)

T_{fr} (Friction torque)

J Moment of inertia (motor + load)

n Speed [rpm]

w Rotation [rad/s]

B Resultant torque

Also:

$$M = k \times \phi \times I_a \quad (\text{A.1})$$

For the accelerating torque:

$$M - T_c = B \quad (\text{A.2})$$

$$B = J \times \frac{dw}{dt} \quad (\text{A.3})$$

$$\omega = \frac{2 \times \pi}{60} \times n_0 \times \frac{n}{n_0} \quad (\text{A.4})$$

where:

n_0 No load speed [rpm]

M_n Rated torque.

$$B = M_n \times \frac{B}{M_n} \tag{A.5}$$

Substituting A.4 and A.5 into A.3 results in:

$$M_n \times \frac{B}{M_n} = J \times \frac{d \frac{2\pi \times n_0 \times \frac{n}{n_0}}{60}}{d_t} \tag{A.6}$$

$$M_n \times \frac{B}{M_n} = J \times \frac{2\pi \times n_0}{60 \times n_0} \times \frac{d_n}{d_t}$$

$$n = \frac{n_0}{M_n} \times \frac{1}{\frac{2\pi J n_0}{60 M_n}} \int B.d_t \tag{A.7}$$

The τ_H (*Accelerating time constant*) is defined as:

$$\tau_H = \frac{2\pi J n_0}{60 M_n} \tag{A.8}$$

This time constant may be interpreted as the time required for the motor to reach no load speed from rest, as it is accelerated by a resultant torque equal to the rated motor torque.

$$n = \frac{n_0}{M_n} \frac{1}{\tau_H} \int B.d_t \tag{A.9}$$

Figure A.6 shows the block diagram related to the motor mechanical part.

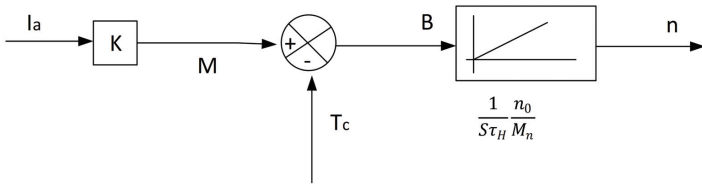


Figure A.6 – Block diagram of the drive mechanical part

Setting the values in pu (per unit) for the current, load torque, speed and motor torque results in:

$$\frac{I_a}{I_N} = i_a(pu)$$

$$\frac{T_c}{M_n} = t_c(pu)$$

$$\frac{B}{M_n} = b(pu)$$

$$\frac{n}{n_0} = n_u(pu)$$

$$\frac{M}{M_n} = m(pu)$$

The mechanical block diagram of Figure A.6 can be represented in pu as shown in Figure A.7.

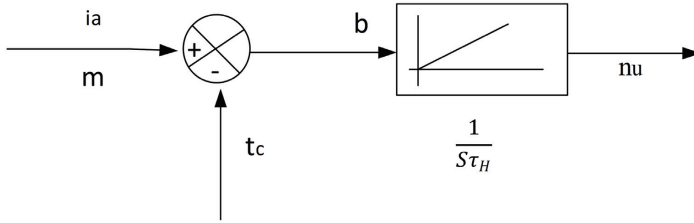


Figure A.7 – Representation of the Motor Mechanical Part in pu

Notes: 1- All variables from Figure A.6 are shown in Figure A.7 in per unit mode and lower-case letters. 2- The variables i_a (*Armature current in pu*) and m (*Motor torque in pu*) are equal.

A.4.3 Armature Circuit Equations

In order to define the τ_a (*Inductor circuit or armature time constant*) and the block diagram, the calculus are shown in the following.

$$E_{DCM} = R_a I_a + L_a \frac{dI_a}{dt} + U \quad (\text{A.10})$$

Applying the Laplace transform results in:

$$E_{DCM} = R_a I_a(S) + S L_a I_a(S) + U(S)$$

$$E_{DCM} = U(S) = I_a(S) [R_a + S L_a]$$

$$i_{a(S)} = \frac{E_{DCM}(S) - U(S)}{R_a + SL_a} \quad (\text{A.11})$$

Defining τ_a :

$$\tau_a = \frac{L_a}{R_a} \quad (\text{A.12})$$

$$I_a(S) = \frac{E_{DCM}(S) - U(S)}{1 + S\tau_a} \times \frac{1}{R_a} \quad (\text{A.13})$$

$$\frac{I_a}{I_N} \times I_N = \frac{E_{DCM} - U}{R_a} \times \frac{E_N}{E_N} \times \frac{1}{1 + S\tau_a}$$

$$\frac{I_a}{I_N} = \frac{E_{DCM} - U}{E_N R_a} \times \frac{E_N}{I_N} \times \frac{1}{1 + S\tau_a}$$

$$\frac{I_a}{I_N} = \frac{E_{DCM} - U}{E_N} \times \frac{E_N}{R_a I_N} \times \frac{1}{1 + S\tau_a}$$

The armature current I_a seems to be normalized by the current I_N (*Rated Current*). Voltages E_{DCM} and U are also normalized by the voltage E_N (*Rated voltage*). The normalized values are set as:

$$I_a = \frac{I_a}{I_N} \quad (\text{A.14})$$

$$e = \frac{E_{DCM}}{E_N} \quad (\text{A.15})$$

$$u = \frac{U}{E_N} \quad (\text{A.16})$$

$$V_i = \frac{E_N}{R_a I_N} \quad (\text{A.17})$$

where V_i (*Motor current amplification factor*).

The block diagram of the DC motor armature circuit is shown in Fig. A.8.

The factor $\frac{V_i}{1+S\tau_a}$ can be considered a delay element of the 1st order. The time constant τ_a can be determined in one of two alternative ways:

a) Measuring L_a and R_a ;

b) Applying a reduced voltage step in the armature circuit at the moment that the rotor of the motor is blocked.

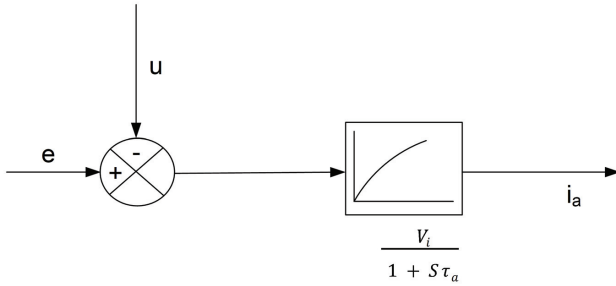


Figure A.8 – Block Diagram of the DC Motor Armature Circuit

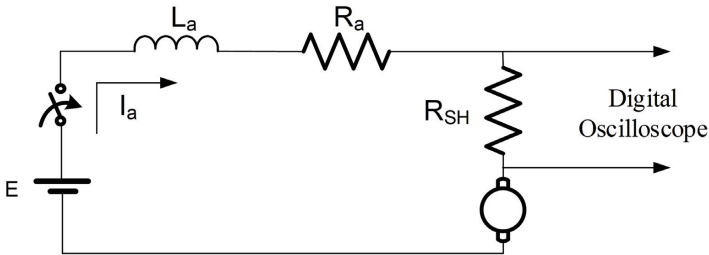


Figure A.9 – Reduced Voltage step Applied to the Armature Circuit

Figure A.9 shows the reduced voltage step applied to the armature circuit.

The current i_a is captured through an oscillograph or digital oscilloscope (voltage drop in the R_{SH} (*Shunt resistor*)). The shunt resistor R_{SH} can be replaced by a current Hall sensor, which is an usual alternative. Figure A.10 shows the expected time transient response.

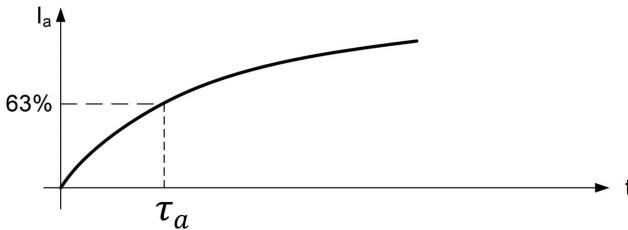


Figure A.10 – Current Response for a Voltage step Applied to the Armature Circuit

Marking up to 63% of the regime value and checking the corresponding time on

the horizontal axis that corresponds to a time constant τ_a .

$$i_a = \frac{e - u}{1 + s\tau_a} V_i \quad (\text{A.18})$$

An interpretation of the constant V_i is given in A.18. The V_i is a multiplicative factor when the motor has the rotor locked and with rated voltage applied to the armature.

$$I_{AK} = \frac{E_N}{R_a} \quad (\text{A.19})$$

$$\frac{I_{AK}}{I_N} = \frac{E_N}{R_a I_N} \quad (\text{A.20})$$

Comparing (A.19) and (A.17) results in:

$$I_{AK} = V_i I_N \quad (\text{A.21})$$

Thus, the V_i factor can be interpreted as the multiplicative factor of the rated current to get a I_{AK} (*Locked rotor current*), when nominal voltage is applied to the armature circuit (starting current in pu).

Figure A.11 shows the schematic diagram of the separated excitation DC motor with rated flux and considering the normalized magnitudes (pu) in lower case letters.

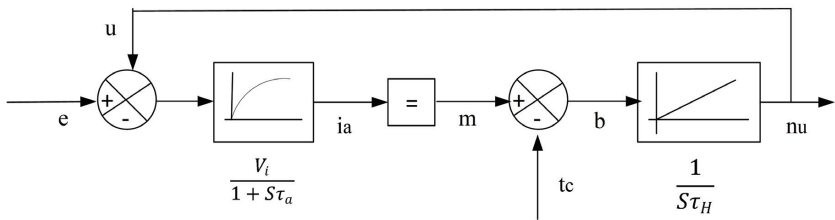


Figure A.11 – Schematic Block Diagram of the Independent Excitation DC Motor

A.4.4 Complete Block Diagram with Regulators, Filters and Transducers

Figure A.12 shows the complete block diagram of the controlled drive.

where:

τ_{gs1} (*Filter time constant of the reference channel of the speed loop*)

τ_{gs2} (*Filter time constant of the reference channel of the current loop*)

V_{Rn} (*Gain of the speed regulator*)

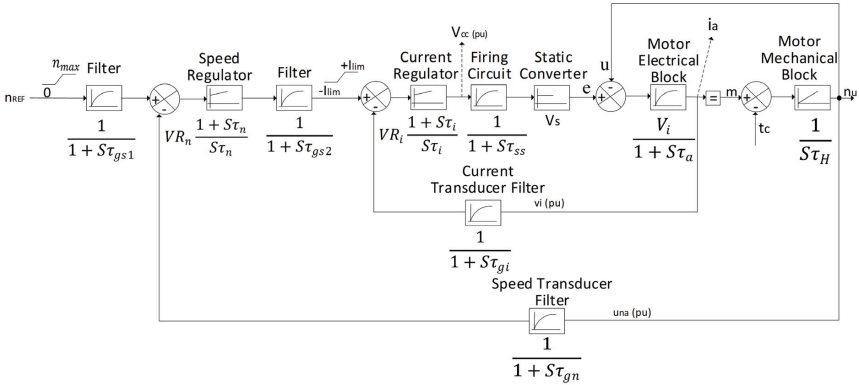


Figure A.12 – Complete Block Diagram of Controlled Drive

- V_{Ri} (Gain of the current regulator)
- τ_n (Time constant of the speed regulator)
- τ_i (Current regulator time constant)
- τ_{gn} (Filter time constant of the speed transducer)
- τ_{gi} (Filter time constant of the current transducer)
- τ_{ss} (Firing circuit time constant)
- V_s (Gain of the static converter)
- τ_a Inductor circuit or armature time constant
- V_i (Gain of machine electric part)
- V_{cc} Control voltage of thyristor firing circuit
- i_a Armature current in pu
- t_c (Load torque in pu)
- n_u (Speed in pu)
- n_{REF} (Reference speed)

The regulators shown in Fig. A.12 were considered as PI (proportional integral) and their parameters will be determined by the design procedure in this work.

A.5 Current Regulator and Filters Project of DC Machine (practical case)

In this appendix will be described the current control loop with current regulators and filters parameters project [37].

Figure A.13 shows the current regulation loop and Table A.1 shows the DC motor data.

The current transducer is a diode bridge connected between a resistor and the

Table A.1 – DC Motor Data

Power (kW)	Rated current (A)	Rated speed (rpm)	No load speed (rpm)	Voltage (V)	Armature resistance (Ω)	Armature inductance (mH)	Accel. ¹ time constant T_H (s)	Rated torque Nm	J inertial moment ($kg.m^2$)
1.7	7.72	1500	1770	220 V	7.0	490	1.54	10.8	0.09

¹ accelerating

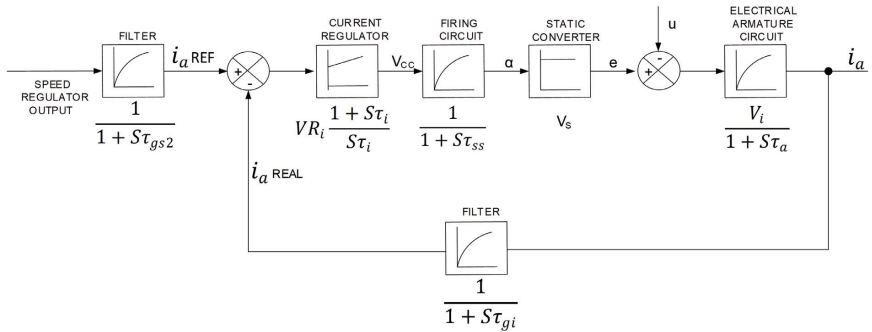


Figure A.13 – Current Regulation Loop

alternating current side. The diode bridge is fed by the *CT* (*Current transformer*)s secondary of 30/5 A. Figure A.14 shows the current transducer connected in a typical DCM driven circuit.

where:

L_d (*Smoothing reactor inductance*)

L_s (*Separated field inductance*)

The v_i (*Signal from the current transducer*) has a 1/6 cycle ripple wave. Thus, the filter time constant of the current transducer is:

$$\tau_{gi} \leq \frac{1}{2} \frac{\text{period}}{\text{number of pulses}} \text{(s)} \tag{A.22}$$

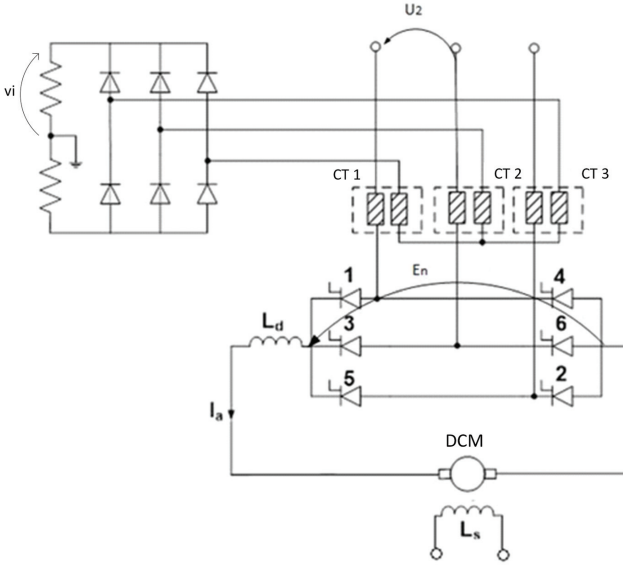


Figure A.14 – Current Transducer

$$\tau_{gi} \leq \frac{1}{2} \times \frac{16.7 \times 10^{-3}}{6} \quad (s) \quad \therefore \tau_{gi} \leq 1.39 \text{ ms}$$

For 60 Hz, a period of 16.7 ms and a six-pulse bridge, the filter time constant of the current transducer is then adopted as:

$$\tau_{gi} \leq 1.39 \text{ ms} \tag{A.23}$$

The firing circuit cannot instantly respond to the change in the firing angle α . This time constant can vary in the range of zero to one sixth of a cycle. Thus, the time constant of the firing circuit $\tau_{ss} = 2.5 \text{ ms}$ is defined.

From the armature resistance R_a and armature inductance L_a , the inductor circuit time constant τ_a was obtained measuring L_a and R_a and calculated as demonstrated below.

$$\tau_a = \frac{L_a}{R_a} = \frac{490 \times 10^{-3}}{7} \tag{A.24}$$

$$\tau_a = \frac{L_a}{R_a} = 70 \text{ ms} \tag{A.25}$$

This constant τ_a was calculated considering the total inductance L_a in series with the armature circuit, which corresponds to the inductance of the machine added to the inductance of the external smoothing reactor.

Considering E_N equal to the rated voltage at the rectifier bridge output, the V_i (motor current amplification factor) is:

$$V_i = \frac{E_n}{R_a \times I_a} = \frac{220}{7 \times 7.72} = 4.07 \quad (\text{A.26})$$

The gain of the converter V_s is obtained as follow, considering that the overlapping effect is neglected. E (*DC supply voltage*) is given by equation:

$$E = 1.35 \times U_2 \times \cos\alpha \quad (\text{A.27})$$

U_2 (*AC supply voltage*) is applied on the converter bridge:

$$\frac{dE}{d\alpha} = -1.35 \times U_2 \times \sin\alpha \quad (\text{A.28})$$

Multiplying part by part by $\frac{\pi}{E_N}$ results in:

$$\frac{d(\frac{E}{E_N})}{d(\frac{\alpha}{\pi})} = -1.35 \times \frac{U_2}{E_N} \times \pi \times \sin\alpha \quad (\text{A.29})$$

In order to define U_2 , the *AC* supply voltage applied on the converter bridge and neglecting the overlap angle μ , the following equation is used:

As $E_n = 220V$ and considering the firing angle $\alpha = 30^\circ$

$$220 = 1.35 \times U_2 \times \cos(30^\circ) \therefore U_2 = 188 V \quad (\text{A.30})$$

Then, considering α_u equal to $\alpha_u = \frac{\alpha}{\pi}$ and substituting Equation A.30 in A.29, results in:

$$\frac{d_e}{d\alpha_u} = -1.35 \times \frac{188}{220} \times \pi \sin\alpha \therefore \frac{d_e}{d\alpha_u} = -1.15\pi \sin\alpha \quad (\text{A.31})$$

resulting in:

$$V_S = \left| \frac{d_e}{d\alpha_u} \right| = 1.15 \times \pi \times \sin\alpha$$

When $\alpha = 90^\circ$, the maximum gain is:

$$V_{S1} = \frac{d_e}{d\alpha_u} = 1.15 \times \pi \quad \therefore V_{S1} = 3.61 \quad (\text{A.32})$$

For $\alpha = 30^\circ$, the gain is given by:

$$V_{S2} = \frac{d_e}{d\alpha_u} = 1.15 \times \pi \times 0.5 \quad \therefore V_{S2} = 1.80 \quad (\text{A.33})$$

The average gain of static converter V_s can be determined as:

$$V_S = \frac{V_{S1} + V_{S2}}{2} = 2.71 \quad (\text{A.34})$$

The current regulation system gain is then obtained:

$$V_{sia} = V_s \times Vi = 2.71 \times 4.07 = 11.03 \quad (\text{A.35})$$

The sum of the small-time constants α is:

$$\sigma = \tau_{ss} + \tau_{gi} = 2.5 + 1.39 \quad \therefore \sigma = 3.89 \quad (\text{A.36})$$

Then:

$$\frac{\tau_a}{4\sigma} = \frac{70}{4 \times 3.89} = 4.50 > 1 \quad (\text{A.37})$$

According to Table A.3 from [4], the regulator type PI should be adopted.

According to Table A.4 of the same referenced book, the gain and the time constant of the regulator V_{Ri} can be obtained:

$$V_{Ri} = \frac{\tau_a}{2 \times V_{sia} \times \sigma} = \frac{70}{2 \times 11.03 \times 3.89} = 0.8 \quad (\text{A.38})$$

Then, the current regulator time constant τ_i is:

$$\tau_i = 4 \times \sigma \times \frac{\tau_a}{\tau_a + 3 \times \sigma} = 4 \times 3.89 \times \frac{70}{70 + 3 \times 3.89} = 13.34ms \quad (\text{A.39})$$

The time constant value of the reference channel filter [ms] is:

$$\tau_{gs2} = 4 \times \sigma \times (1 - e^{-(\frac{\tau_a}{4 \times \sigma} - 1)}) \quad (\text{A.40})$$

$$\tau_{gs2} = 4 \times 3.89 \times (1 - e^{-(\frac{70}{4 \times 3.89} - 1)}) = 15.09ms \quad (\text{A.41})$$

Capacitors Calculus

- Reference value filter:

$$C_s = \frac{R_{S1} + R_{S2}}{R_{S1} \times R_{S2}} * \tau_{gs2} \quad (\text{A.42})$$

$$C_s = \frac{22 + 22}{22 \times 22} \times 15.09 \mu F = 1.37 \mu F \quad (\text{A.43})$$

- Current transducer filter

$$C_i = \frac{R_{i1} + R_{i2}}{R_{i1} \times R_{i2}} * \tau_{gi} \quad (\text{A.44})$$

$$C_i = \frac{15 + 15}{15 \times 15} \times 1.39 \therefore C_i = 0.19 \mu F \quad (\text{A.45})$$

The closest and chosen capacitors values were $C_s = 1.22 \mu F$ and $C_i = 0.22 \mu F$ as shown in Fig. A.15.

A.5.1 Current Regulator Parameters

In summary, the current regulator parameters are shown in Table A.2:

Table A.2 – Current Regulator Parameters

Type	Gain (V_{Ri})	Time Constant (τ_i)	Reference channel Filter time constant (τ_{gs2})	Feedback channel filter time constant (τ_{gi})
PI	0.8	13.34	15.09	1.39

A.5.2 Current Regulator Arrangement

Figure A.15 shows the current regulator. Its inner current loop structure was proposed by [4].

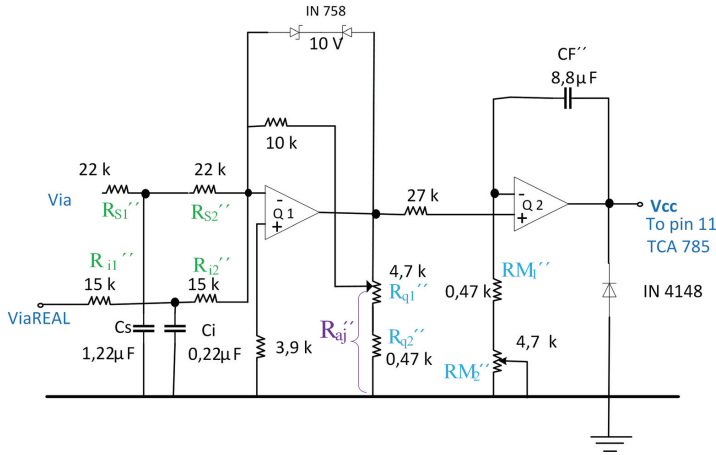


Figure A.15 – Implementation of Current Regulator

A.5.2.1 Calculus of RM_2'' and R_{q1}''

In order to make the adjustment of RM_2'' (*Integral branch adjustment resistor of current regulator*) and R_{q1}'' (*Proportional branch adjustment resistor of current regulator*), the specific values of each one of these resistors will be calculated.

RM_2'' was obtained as:

$$\tau_n = (RM_1'' + RM_2'') \times CF'' \quad (\text{A.46})$$

$$RM_1'' + RM_2'' = \frac{\tau_i}{CF''} = \left(\frac{13.34 \times 10^{-3}}{8.8 \times 10^{-6}} \right) = 1.52 \text{ k}\Omega \quad (\text{A.47})$$

$$RM_2'' = \frac{\tau_i}{CF''} - RM_1'' = 1520 - 470 = 1.05 \text{ k}\Omega \quad (\text{A.48})$$

The R_{aj}'' (*adjustment resistance of current regulator*) was calculated as:

$$R_{aj}'' = \frac{(R_F'' \times (R_{q1}'' + R_{q2}''))}{(V_{Ri} \times (R_{i1}'' + R_{i2}''))} \quad (\text{A.49})$$

$$R_{aj}'' = \frac{(10 \times (4.7 + 0.47))}{(0.8 \times (15 + 15))} \times 10^3 \quad (\text{A.50})$$

$$R_{aj}'' = 2.15 \text{ k}\Omega \quad (\text{A.51})$$

Then, as R''_{q2} (*Proportional branch steady resistor of current regulator*)=470 Ω

$$R''_{q1} + R''_{q2} = 2150 \Omega \quad (\text{A.52})$$

$$R''_{q1} = 2150 - 470 \Omega \quad (\text{A.53})$$

$$R''_{q1} = 1.68 \text{ k}\Omega \quad (\text{A.54})$$

Adopting the V_{Ri} as the variable in evidence, it will be possible to find the V_{Ri} limits by just changing R''_{aj} as follows.

Equation A.49 and isolating the variable V_{Ri} , it results in:

$$V_{Ri} = \frac{(R''_F \times (R''_{q1} + R''_{q2}))}{(R''_{aj} \times (R''_{i1} + R''_{i2}))} \quad (\text{A.55})$$

For the minimum R''_{aj} =0.47 k Ω , the maximum V_{Ri} is:

$$V_{Ri}max = \frac{(10 \times (4.7 + 0.47))}{(0.47 \times (15 + 15))} = 3.6 \quad (\text{A.56})$$

For the maximum R''_{aj} = 4.8 k Ω , the minimum V_{Ri} is:

$$V_{Ri}min = \frac{(10 \times (5.17 + 0.47))}{(4.8 \times (15 + 15))} = 0.33 \quad (\text{A.57})$$

Thus, as the defined resistors, the V_{Ri} can vary from 0.33 to 3.6.

The current regulator data are given in Table A.3.

Table A.3 – Complementary Current Regulator Data

Optimized R''_{aj}	R''_{q1}	RM''_2	Optimized gain (V_{Ri})	Minimum gain ($V_{Ri}min$)	Maximum gain ($V_{Ri}max$)
2.15 k Ω	1.68 k Ω	1.05 k Ω	0.8	0.33	3.6

A.6 Speed Regulators and Filters Project of DC machine (practical case) Project

In order to define the parameters of speed filters and regulators [36, 37, 35], the current loop will be replaced by a first order delayed block whose equivalent time constant is τ_e (*Equivalent time constant*) as in [4]:

$$\tau_e = 2 \times \sigma + \frac{1}{2} \times \tau_{gs2} \quad (\text{A.58})$$

$$\tau_e = 2 \times 3.89 + \frac{1}{2} \times 15.09 \approx 15 \text{ ms} \quad (\text{A.59})$$

In that way, the speed block diagram can be represented as in Figure A.16, [38]:

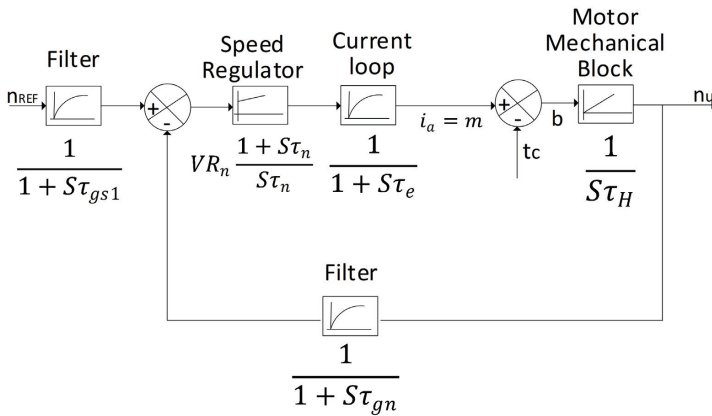


Figure A.16 – Speed Regulation Loop

The speed transducer filter time constant is $\tau_{gn} = 100$ ms.

The speed loop has the following time constants:

τ_H (accelerating time constant) = 1.54 s

τ_e (equivalent time constant of stabilization loop) = 15 ms

τ_{gn} (speed transducer filter time constant) = 100 ms

The small-time constants τ_e and τ_{gn} will be replaced by representative time constant σ' as follows:

$$\sigma' = \tau_e + \tau_{gn} \quad (\text{A.60})$$

$$\sigma' = 15 + 100 = 115 \text{ ms} \quad (\text{A.61})$$

As the division $\frac{\tau_H}{4 \times \sigma'} = \frac{1.54}{4 \times 0.115} = 3.34 > 1$, then, in accordance with Table 6.3 from [4], a proportional-integral regulator (PI) should be used.

From Table 6.4 from [4], the optimized gain and time constant of the regulator are:

$$V_{RN} = \frac{\tau_H}{2 \times \sigma'} = \frac{1.54}{2 \times 0.115} = 6.7 \quad (\text{A.62})$$

$$\tau_n = 4 \times \sigma' = 460 \text{ ms} \quad (\text{A.63})$$

The speed transducer is a tachogenerator coupled with the DC motor shaft. The filter was used to reduce the high wave that was part of the tachogenerator output voltage. The considered time constant was:

$$\tau_{gn} = 100 \text{ ms} \quad (\text{A.64})$$

The reference channel filter has the following time constant:

$$\tau_{gs1} = 4 \times \sigma' \times (1 - e^{-(\frac{\tau_H}{4 \times \sigma'})}) = 416 \text{ ms} \quad (\text{A.65})$$

A.6.1 Capacitors calculus

Adopting the resistances $R'_{s1} = R'_{s2} = 100 \text{ k } \Omega$ as part of the reference value filter and $R'_{i1} = R'_{i2} = 100 \text{ k } \Omega$ as part of the speed transducer filter, it results in:

- Reference value filter capacitor:

$$C_n = \frac{R'_{s1} + R'_{s2}}{R'_{s1} \times R'_{s2}} * \tau_{gs1} = 8.32 \text{ } \mu F \quad (\text{A.66})$$

The closest capacitor value was got by four capacitors $2.2 \text{ } \mu F$ in parallel, resulting in $8.8 \text{ } \mu F$.

- Speed transducer filter capacitor:

$$C_L = \frac{R'_{i1} + R'_{i2}}{R'_{i1} \times R'_{i2}} * \tau_{gn} = 2.2 \text{ } \mu F \quad (\text{A.67})$$

A.6.2 Speed Regulator Parameters

In summary, the speed regulator parameters are shown in Table A.4.

Table A.4 – Speed Regulator Parameters

Type	Gain (V_{RN})	Time Constant (τ_n)	Reference channel Filter time constant (τ_{gs1})	Speed transducer filter time constant (τ_{gn})
PI	6.7	460	416	100

Figure A.17 shows the speed regulator. This speed regulator structure was proposed by [4]

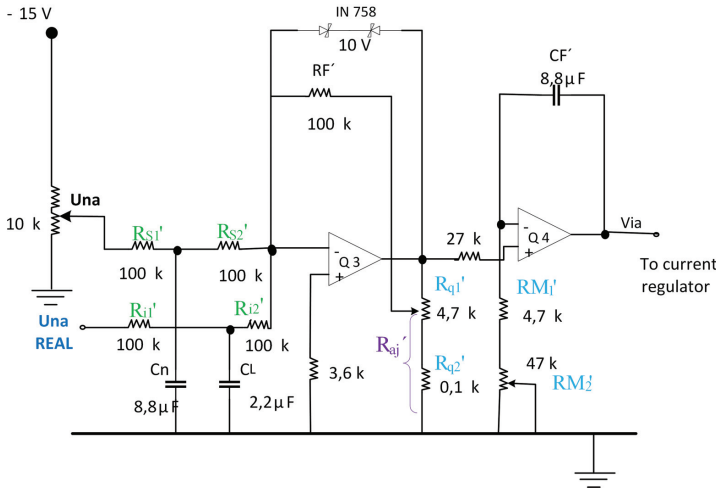


Figure A.17 – Implementation of Speed Regulator

A.6.2.1 Calculus of RM'_2 and R'_{q1}

In order to do the adjustment of RM'_2 (*Integral branch adjustment resistor of speed regulator*) and R'_{q1} (*Proportional branch adjustment resistor of speed regulator*), the specific values for each of these resistors will be calculated.

RM'_2 was obtained as follow:

$$\tau_n = (RM'_1 + RM'_2) \times CF'$$

$$(RM'_1 + RM'_2) = \frac{\tau_n}{CF'} = \frac{460 \times 10^{-3}}{8.8 \times 10^{-6}} = 52.27 \text{ k}\Omega \quad (\text{A.68})$$

$$RM'_2 = \frac{\tau_n}{CF'} - RM'_1 = 52.27 - 4.7 = 47.57 \text{ k}\Omega \quad (\text{A.69})$$

Note: The RM'_2 was adjusted in 47.0 k Ω , the maximum value available.

Follow the calculus used to calculate the adjustment resistance R'_{aj} (*adjustment resistance of speed regulator*) and R'_{q1} :

$$R'_{aj} = \frac{(R_F \times (R'_{q1} + R'_{q2}))}{(V_{RN} \times (R'_{i1} + R'_{i2}))} \quad (\text{A.70})$$

$$R'_{aj} = \frac{(100 \times (4.7 + 0.10))}{(6.7 \times (100 + 100))} \times 10^3 = 358.2 \Omega \quad (\text{A.71})$$

Then, as R'_{q2} (*Proportional branch steady resistor of speed regulator*)=100.0 Ω , the adjusted R'_{q1} is

$$R'_{q1} = 358.2 - 100 \Omega \quad (\text{A.72})$$

$$R'_{q1} = 258.2 \Omega \quad (\text{A.73})$$

Adopting the variable V_{Rn} as not defined, it will be possible to find the V_{Rn} limits by changing of the R'_{aj} as follow:

Using Equation A.70 and isolating the variable V_{Rn} results in:

$$V_{Rn} = \frac{(R_F \times (R'_{q1} + R'_{q2}))}{(R'_{aj} \times (R'_{i1} + R'_{i2}))} \quad (\text{A.74})$$

For the minimum R'_{aj} =0.10 k Ω , the V_{Rn} max is:

$$V_{Rn}max = \frac{(100 \times (4.7 + 0.10))}{(0.10 \times (100 + 100))} = 24 \quad (\text{A.75})$$

For the maximum R'_{aj} =4.8 k Ω , the V_{Rn} min is:

$$V_{Rn}min = \frac{(100 \times (4.7 + 0.10))}{(4.8 \times (100 + 100))} = 0.5 \quad (\text{A.76})$$

Thus, as the defined resistors for the controller, the V_{Rn} can vary from 0.5 to 24.

The R'_{aj} was empirically defined as R'_{aj} =600.0 Ω , which resulted in V_{Rn1} equal to:

$$V_{Rn1} = \frac{(100 \times (4.7 + 0.10))}{(0.6 \times (100 + 100))} = 4.0 \quad (\text{A.77})$$

Then, instead of considering the optimized value $V_{Rn} = 6.7$, (A.62), $V_{Rn1}=4.0$ was considered for this practical experiment and the results are shown below.

The speed regulator data follow in Table A.5.

Table A.5 – Speed Regulator Parameters

Optimized R'_{aj}	R'_{q1}	RM'_2	Optimized gain V_{Rn}	Minimum gain (V_{Rnmin})	Maximum gain (V_{Rnmax})
358.2 Ω	258.2 Ω	47.57 k Ω	6.7	0.5	24

A.6.3 General Arrangement

Figure A.18 shows the general diagram including all the module interconnections [36], [37].

Notes:

1- The P1 value (the maximum speed adjustment) was empirically adjusted as shown in Fig. A.18.

2- By means of P2 shown in Fig. A.18; increasing the gain of Q6, the limit current of main circuit is decreased; in other way, when the gain is decreased, the limit current is increased, see the block diagram in Fig. A.12.

A.7 Results

Although the optimized gain V_{Rn} of 6.7 has been calculated, the gain was empirically adjusted to 4.0 with the R'_{aj} equal to 600 Ω .

The motor speed and current waveforms for the gain of 4.0 are shown in Fig. A.19 at the moment when the motor is driven by the control system from its rest position. The gain was empirically adjusted to 4.0 with the R'_{aj} equal to 600 Ω , which resulted in a satisfactory dynamic response to the current and speed startup transitory, as shown in Fig. A.19, (yellow curve: current and blue curve: speed).

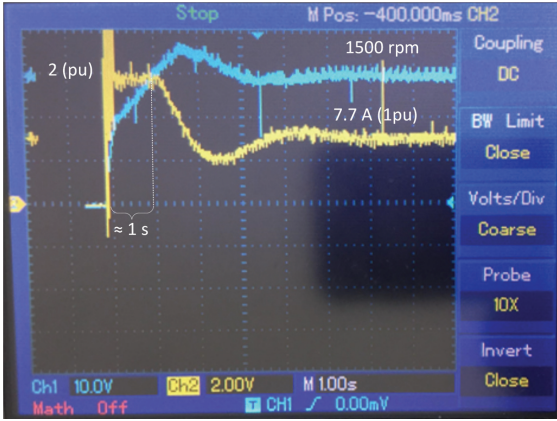


Figure A.19 – Speed and Current Waveforms

Variables:

T_{fr} : Friction torque

T_m (Motor torque)

T_n (Motor rated torque)

T_c : Load torque

J : Inertial moment

N_n : Rated speed

n : Speed

t : Time

I_n (Rated Current)

Note: The motor data are in Table A.1. The balance equation (Newton's second law) of the system is:

$$T_m - T_{fr} - T_C = J \times \frac{d_n}{d_t} \quad (\text{A.78})$$

Considerations:

$T_m = 2 \times T_n$ (the limit torque was adjusted by the regulator system by the limit current).

Torque = $k \times \phi \times I$, considering $I_{limit} = 2 \times I_n$.

T_c and T_{fr} depend on the speed n . This affirmation was demonstrated in Fig. A.20 and below:

When the *DCM* is coupled with an *SG* that feeds a bank of resistors, it is known that T_{fr} is proportional to the speed n . The load torque T_c is also approximately propor-

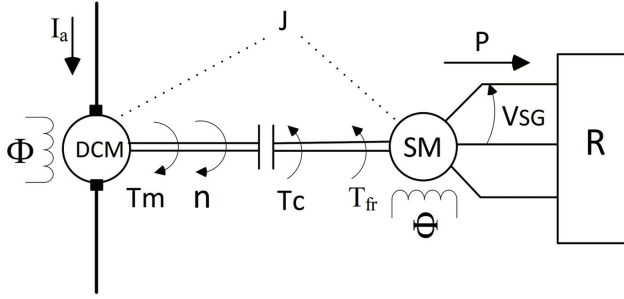


Figure A.20 – DCM coupled with SG and a Resistive Load

tional to the speed n , as demonstrated below:

$$P = \frac{V_{SG}^2}{R} \quad (\text{A.79})$$

and as $V_{SG} = k \times n \times \phi$ and as $\phi = \text{constant}$, then $k' = k \times \phi$, therefore,

$$V_{SG} = k' \times n \quad (\text{A.80})$$

Substituting (A.80) into (A.79) gives:

$$P = \frac{k'^2 \times n^2}{R} \therefore P = k'' \times n^2 \quad (\text{A.81})$$

Note: k'' is the proportionality constant 2.

Considering the steady state conditions, T_m is equal to T_c , that result in:

$$T_c = \frac{P_{mec}}{n} \quad (\text{A.82})$$

Note: As P_{mec} (*Mechanical power*) is equal to $\frac{P_{elec}}{\eta}$, the η was considered constant in an average value.

Substituting Equation (A.81) into Equation (A.82), the result is:

$$T_c = \frac{k''' \times n^2}{n} \therefore \quad (\text{A.83})$$

$$T_c = k''' \times n \text{ (end of demonstration)} \quad (\text{A.84})$$

Note: k''' is the proportionality constant 3.

In order to find the motor acceleration time, considering the system configuration shown in Fig. A.17, the following calculation is used.

Substituting $T_m=2 \times T_n$ into Equation (A.78) results in:

$$2 \times T_n - T_{fr} - T_c = J \times \frac{d_n}{d_t} \quad (\text{A.85})$$

As the magnetic field ϕ is constant, then $T_{fr}+T_c=(k_1+k_2) \times n$, or, in summary:

$$T_{fr} + T_c = k'''' \times n \quad (\text{A.86})$$

Note: k'''' is the proportionality constant 4.

Substituting Equation (A.86) into Equation (A.85) gives:

$$2 \times T_n - k'''' \times n = J \times \frac{d_n}{d_t} \quad (\text{A.87})$$

From Table A.1, $T_n=10.8$ Nm.

$$J \times \frac{d_n}{d_t} + k'''' \times n = 2 \times 10.8 \quad (\text{A.88})$$

$$\frac{d_n}{d_t} + \frac{k''''}{J} \times n = \frac{21.6}{J} \quad (\text{A.89})$$

For k'''' definition, the motor speed is in rated speed as described below:

$$T_n = k'''' \times \frac{2 \times \pi}{60} \times 1500 \quad (\text{A.90})$$

$$k'''' = \frac{60 \times 10.8}{2 \times \pi \times 1500} \therefore \quad (\text{A.91})$$

$$k'''' = \frac{64.8}{300 \times \pi} = 0.069 \frac{Nm}{\frac{rad}{s}} \quad (\text{A.92})$$

Getting J of motor plus load from Table A.1 and substituting k'''' from (A.92) into Equation (A.89) gives:

$$\frac{d_n}{d_t} + \frac{0.069}{0.09} \times n = \frac{21.6}{0.09} \quad (\text{A.93})$$

Linear differential equation:

$$\frac{d_n}{d_t} + 0.77 \times n = 240 \quad (\text{A.94})$$

Considering [39], the solution for (A.94) is:

$$n = e^{-\int P dt} \times \left[\int Q \times e^{\int P dt} dt + C \right] \quad (\text{A.95})$$

Considering [39] and Equation (A.94), P= 0.77 and Q= 240, then:

$$n = e^{-\int 0.77 dt} \times \left[\int 240 \times e^{\int 0.77 dt} dt + C \right] \quad (\text{A.96})$$

$$n = e^{-0.77t} \times \left[\int 240 \times e^{0.77t} dt + C \right] \quad (\text{A.97})$$

$$n = e^{-0.77t} \times \left[\int \frac{240 \times e^{0.77t}}{0.77} dt + C \right] \quad (\text{A.98})$$

$$n = e^{-0.77t} \times \left[311.68 \times e^{0.77t} + C \right] \quad (\text{A.99})$$

In order to find the constant C, the boundary condition is used:

$$Fort = 0, n = 0 \quad (\text{A.100})$$

Substituting (A.100) into (A.99) gives:

$$0 = 1 \times [311.68 + C] \quad (\text{A.101})$$

$$C = -311.68 \quad (\text{A.102})$$

Substituting (A.102) into (A.99) gives:

$$n = e^{-0.77t} \times [311.68 \times e^{0.77t} - 311.68] \frac{rad}{s} \quad (\text{A.103})$$

Converting $\frac{rad}{s}$ to *rpm* results in:

$$n = e^{-0.77t} \times [311.68 \times e^{0.77t} - 311.68] \times \frac{60}{2 \times \pi} rpm \quad (\text{A.104})$$

$$n = 2976.32e^{-0.77t} \times [e^{0.77t} - 1] rpm \quad (\text{A.105})$$

For n=1500 rpm, it gives:

$$1500 = 2976.32e^{-0.77t} \times [e^{0.77t} - 1] \quad (\text{A.106})$$

$$1500 = 2976.32 \times [1 - e^{-0.77t}] \quad (\text{A.107})$$

Solving the equation (A.107) by the iterative method results in:

$$t = 0.91s \quad (\text{A.108})$$

APPENDIX B – Analogical Control Board (Firing Circuit)

B.1 Introduction

This appendix presents the concepts of operation and functioning of firing circuit to control the three-phase thyristor bridge firing angle using the integrated circuit TCA 785 and other components, The TCA 785 was developed by ICOTRON-SIEMENS. This firing circuit was implemented and tested in the Laboratory of research development of electrical didactic laboratory of Federal University of Itajubá [40], [41], [3].

This electronic circuit generates all the logic of the command signals that will control the thyristors operation. The aim of the device is to drive the thyristors by using the necessary gate current.

This firing circuit was developed to control the firing angle of thyristors, transistors, and TRIACs continually in the 0° to 180° range. It has a large number of configurations and few external components.

In the first part of this appendix is shown the firing circuit logic and, in the second part, the functions are shown. The most contribution of this appendix is the presentation of a complete firing circuit with all details that becomes possible an easy implementation.

This kind of control board is used in the primary machine of the synchronous generator in order to control the primary machine speed that drives the *SG*.

Figure B.1 shows the basic organization of the control circuit in block diagram.

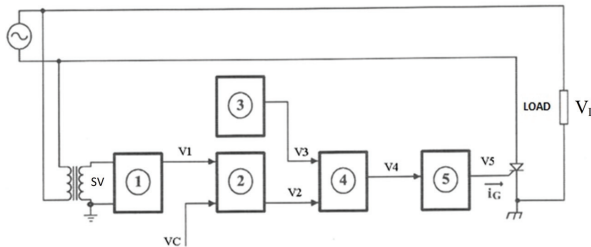


Figure B.1 – Basic Organization of Control Circuit.

Legend

1: Function of synchronism and sawtooth wave generation

- 2: Function of comparing
 - 3: Oscillator
 - 4: Logical block E
 - 5: Amplification, isolating and attack
- SV (Synchronous voltage)*
V1 (Sawtooth voltage)
VC (Control voltage)
V3 (Rectangular wave)
V2 (Rectangular pulse)
V4 (Rectangular pulses train)
V5 (Amplified rectangular pulses train)
IG (Gate current)
VL (Load voltage)

The thyristor bridge is composed of control and power circuits and between them there is an isolation which should be kept, mainly, between the load and the electrical grid. In order to achieve this goal of isolation, the stages of Figure B.1 are coupled by a pulse transformer or by optocouplers (stage 3). For this purpose, an optic coupler TIL 111 (stage 3) produced by Texas Instruments was used.

Besides the optic coupler, independent voltage sources are necessary to supply energy to the stage 4 in order to have an isolation more efficient. In order to reduce the number of components, a TCA 785 and simple rectangular pulses can be used, instead of the rectangular pulses train applied in thyristors. Therefore, this can be achieved using a TCA 785 for stages 1 and 2 and the 555 device set as monostable for stages 3 and 4.

Figure B.2 shows the block diagram of the control circuit using the integrated circuits TCA 785 and 555.

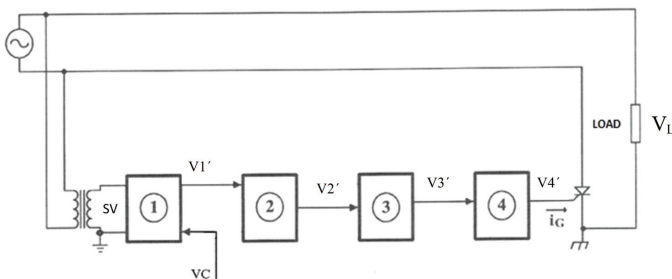


Figure B.2 – Blocks Diagram of Control Circuit using the TCA 785 and 555.

Legend:

- 1: TCA 785

2: Monostable 555

3: Optic coupler TIL 111

4: Amplification, isolating and attack

SV: Synchronous voltage

V1' (*Rectangular pulse*)

V2' (*Wider Rectangular pulse*), *V3'* (*Wider Rectangular pulse*) and *V4'* (*Wider Rectangular pulse*)

VL: Load voltage

B.2 Stage Descriptions

This section will show the main characteristics of the integrated circuit TCA 785 and its functions.

B.2.1 Pulse generation by TCA 785

The main TCA 785 function is to control the firing angle of thyristors, TRIACs and transistors continually in the range from 0° to 180° . Its configuration options enable a simplified selection of external devices for connections and disconnections. This keeps the final circuit simpler and smaller than other available options.

B.2.2 Integrated Circuit Characteristics

The main characteristics of this integrated circuit are:

- Internal required current: 5 mA;
- Digital logic is highly immune to interference;
- Two main outputs with 55 mA current and two other outputs with open collector pins rated to 1.5 mA current;
- Three TCA 785 are needed for a three-phase system;
- The period of the output pulse is defined by the external capacitor;
- The output voltage is adjusted at 3.1 V;
- Simultaneous inhibition of all outputs is possible;
- One output is for TRIACs control.

Figures B.3 and B.4 [1] show the internal diagram and signals in the TCA 785 outputs.

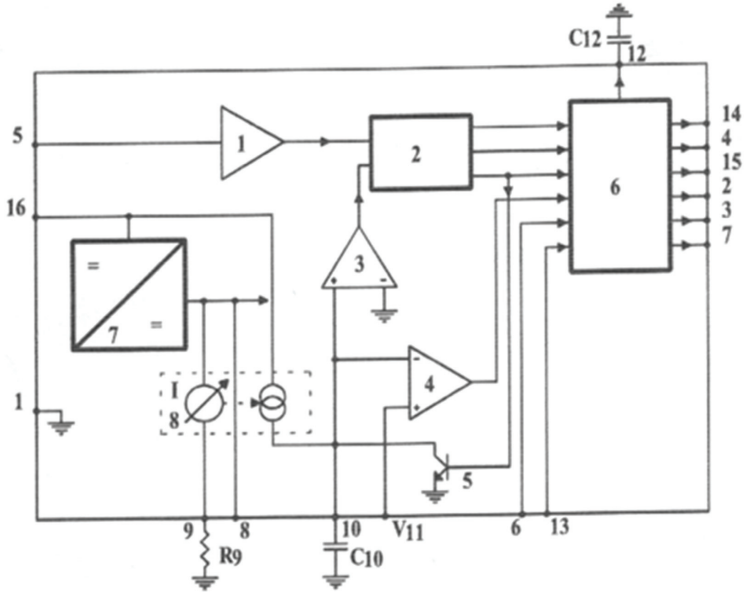


Figure B.3 – Internal Diagram of TCA 785.

Legend:

- 1: Zero detection
- 2: Synchronism memory
- 3: C10 discharge monitoring
- 4: Control comparator
- 5: Synchronizing voltage
- 6: Logical unit
- 7: Voltage internal regulator (3.1 V)
- 8: Steady current source

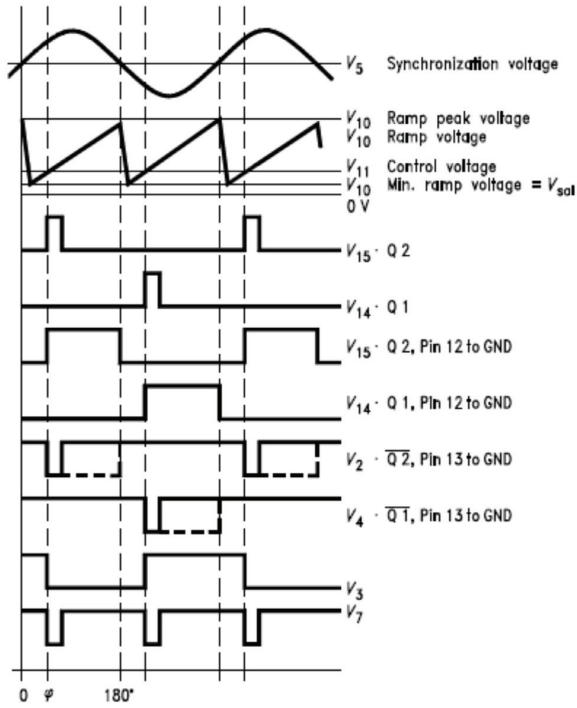


Figure B.4 – Waveforms Diagram for TCA 785. [1]

Figure B.5 shows the TCA 785 pins and wrapping.

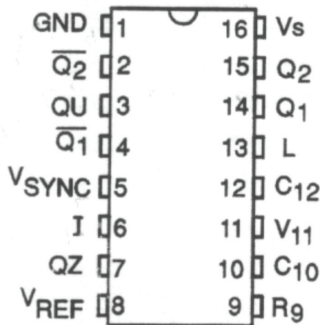


Figure B.5 – TCA 785 Wrapping and Pins

The pins and their functions are as follows:

- 01 Ground
- 02 Pin 15 complementary output with open collector
- 03 Positive pulse output with open collector
- 04 Pin 14 complementary output with open collector
- 05 Synchronism input (antiparallel diodes)
- 06 Inhibits all outputs when they are grounded
- 07 Open collector output to activate TRIACs
- 08 Steady supply 3.1 V
- 09 Potentiometer to ramp adjustment ($20 < R9 < 500k\Omega$)
- 10 Capacitor to generate the ramp ($C10 \leq 0.5\mu F$)
- 11 Controls voltage input (DC)
- 12 Controls the output pulse width of 14 and 15
- 13 Controls the output pulse width of 02 and 04
- 14 Positive pulse output in the positive half wave
- 15 Positive pulse output in the negative half wave
- 16 DC supply; it is not guaranteed for stabilization

B.3 Operation of TCA 785

The integrated circuit (IC) feed is done by pin 16 referenced to the ground terminal (pin 1) with a voltage range between 8 V and 18 V. Internally, the IC is fed by a regulated voltage of 3.1 V, regardless of the possible changes in its external feed. The synchronism is obtained by a zero detector (pin 5), which is connected to a synchronism transformer. The ramp generator, whose control is located in the logical unit, consists of a steady current source that charges an external capacitor C10. The charge current is set by an external resistance R9 in order to adjust the ramp amplitude, which goes to zero whenever the synchronism voltage exceeds zero. Then, the group R9 and C10 determine the ramp inclination.

The control comparator compares the ramp voltage and control voltage and when they are equal to each other, the comparator sends pulses to the output through the logical unit. Then, positive pulses appear in the positive half-wave in the synchronism

voltage V15 in pin 15. In addition, positive pulses appear in the negative half-wave in the synchronism voltage V14 in pin 14. V14 and V15 are 180° delayed between themselves. The widths of these pulses are determined by external capacitor C12 connected between pin 12 and the ground pin, as shown in Table 3.1. Their amplitudes are equal to the supplied voltage in pin 16. The pin outputs 14 and 15 have complementary outputs that are respectively in pins 2 and 4. These pins 2 and 4 are an open collector transistor that requires an external resistor connected between pins 2 and 16 in the first case, and between pins 4 and 16 for the second case. The maximum resistor current is 5 mA. The width of the pulses can be controlled by the resistor connected between pins 13 and 16. Pin 6 causes an inhibition of all TCA 785 outputs when it is grounded.

Table B.1 – Pulse width from pins 14 and 15 related to capacitor C12 values, [3]

C12 [pF]	100	220	330	680	1000
Pulses width [ms]	0.080	0.130	0.200	0.370	0.550

To avoid any interference including radio frequencies, it is recommended to install ceramic capacitors at pins 8, 11 and 16, which are rated as follows: $C8 = 10 \text{ nF}$, $C11 = 100 \text{ nF}$ and $C16 = 10 \text{ }\mu\text{F} + 10 \text{ nF}$

B.4 Equations

(a) Charge current of capacitor C10:

$$I_{10} = \frac{V_{ref} \times K}{R9} \quad (\text{B.1})$$

(b) Ramp voltage

$$V_{10} = \frac{V_{ref} \times K \times \Delta t}{R9 \times C10} \quad (\text{B.2})$$

(c) Starting point

$$tz = \frac{R9 \times C10}{V_{ref} \times K} \times V_{11} \quad (\text{B.3})$$

(d) Pulse width

$$T_P = 30\mu s, \text{ without } C12 \quad (\text{B.4})$$

$$T_P \approx \frac{430 \mu s}{nF} \text{ with } C12 \quad (\text{B.5})$$

where:

$$V_{ref} = V_8 = 3.1 V$$

$$K = 1.25$$

$$C_{10} \leq 0.5 \mu F$$

$$25 k\Omega < R_9 < 500 k\Omega$$

B.5 The Pulse Enlargement Stage using the Integrated Circuit 555

The integrated circuit 555 was developed as a unit that has various aims, and is able to operate in large ranges, either monostable or stable.

In Figure B.6, the 555 is operating as monostable, which results in larger pulses than the pulses received in its input. The 555 then causes an enlargement of the TCA 785 pulse that was received in its input. It is possible to adjust the output pulse width from the 555 through the 50 kΩ potentiometer connected between the source VCC and pin 6 of the 555.

Figures B.6 and B.7 show the 555 operating as monostable and monostable with an adjustable width output pulse.

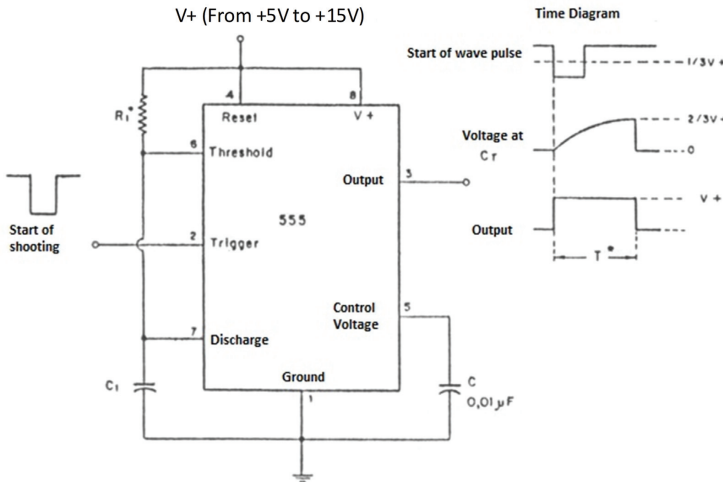


Figure B.6 – CI 555 as Monostable

Note:

The 555 in Figure B.6 is set as: $T = 1.1 \times R_1 \times C_1$

R_1 : Range from 10 kΩ to 14 MΩ

C1: Range from 100 pF to 1000 μ F

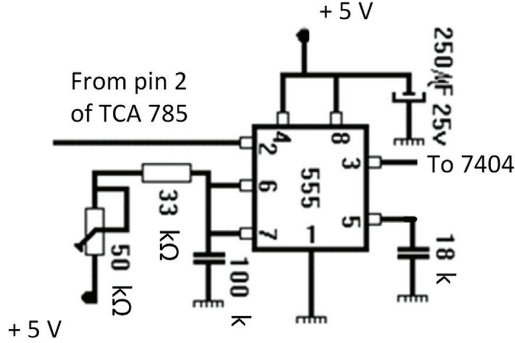


Figure B.7 – Monostable with Adjustable output Pulse Width.

B.6 Coupling Stage with TIL111

The goal of this stage is the pulse transmission to the next stage and, at the same time, to supply electrical insulation between the high and low power circuits. The TIL111 is an optocoupler that has an infra-red LED between pins 1 and 2 and a photo transistor NPN in pins 4, 5 and 6.

Figure B.8 shows the internal diagram of the TIL111.

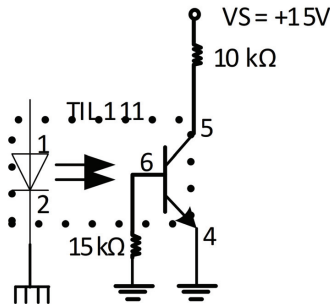


Figure B.8 – Internal Diagram of TIL111.

The diode and the photo transistor of the TIL111 should be fed by independent voltage sources (5V and ground 1, +15V and ground 2).

B.7 Attack Stage

This last circuit stage is in charge of supplying current increment to the TIL111 output pulse, which is necessary so that the gate firing can be done and the conduction current occurs. Thus, the transistor PNP BC558 operates as a switch. As shown in Figure B.9, the transistor PNP BD136 operates as a switch which supplies the current and voltage to the gate. This transistor is assisted by a capacitor “SPEED UP” that is responsible for accelerating the transistor switching. The gate thyristor current is also assisted by another “SPEED UP” and this gate current is adjusted by a 200 Ω potentiometer. The gate current is coupled to the thyristor and flows through a diode so that negative voltage does not reach the gate. In summary, the general characteristics are:

- To amplify the control signals from the signal stages;
- To have current source characteristics instead of voltage source;
- To avoid negative voltage appearing on the gate cathode junction.

Figure B.9 shows the attack stage circuit.

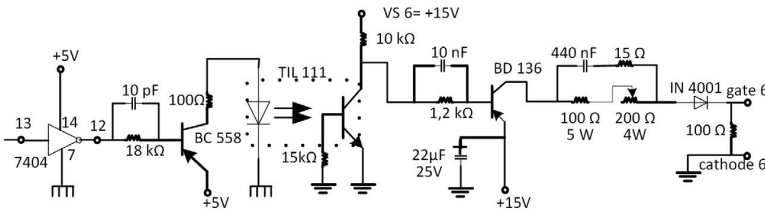


Figure B.9 – Attack stage circuit.

B.8 Control Voltage

As shown in Figure B.10 and B.12, this stage supplies the control voltage to the three TCA 785 devices, which are part of the firing control circuit. This stage is basically composed of an operational amplifier 741 that is configured as a voltage follower, which means that it is not an inverter amplifier with gain 1. Potentiometers P1 and P2 define the maximum (180°) and minimum (0°) adjustments to the conduction angle. Potentiometer P3 defines the conduction angle, which is an adjustable value in the range between potentiometers P1 and P2.

Figure B.10 shows the control voltage circuit with the CI 741.

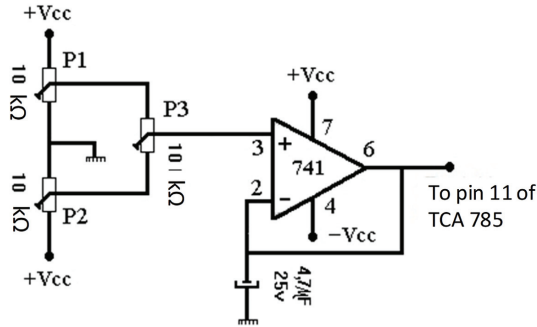


Figure B.10 – Control Voltage Circuit.

B.9 General Overview

Figure B.11 shows the block diagram.

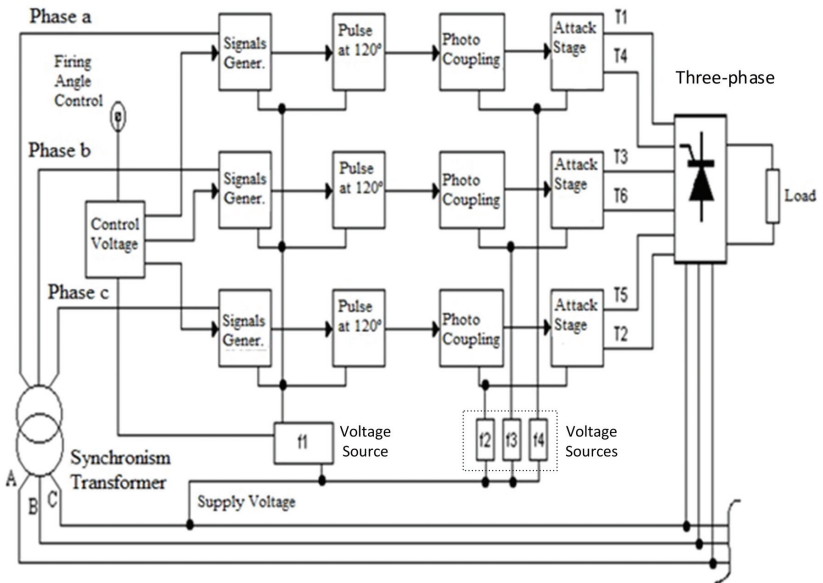


Figure B.11 – Block Diagram of Complete Control Circuit

Figure B.12 shows the electrical diagram of the firing circuit of the thyristor bridge [42], [43], [44]. Figure B.13 also shows the electrical diagrams used for the 6 voltage sources that are shown in Figure B.12.

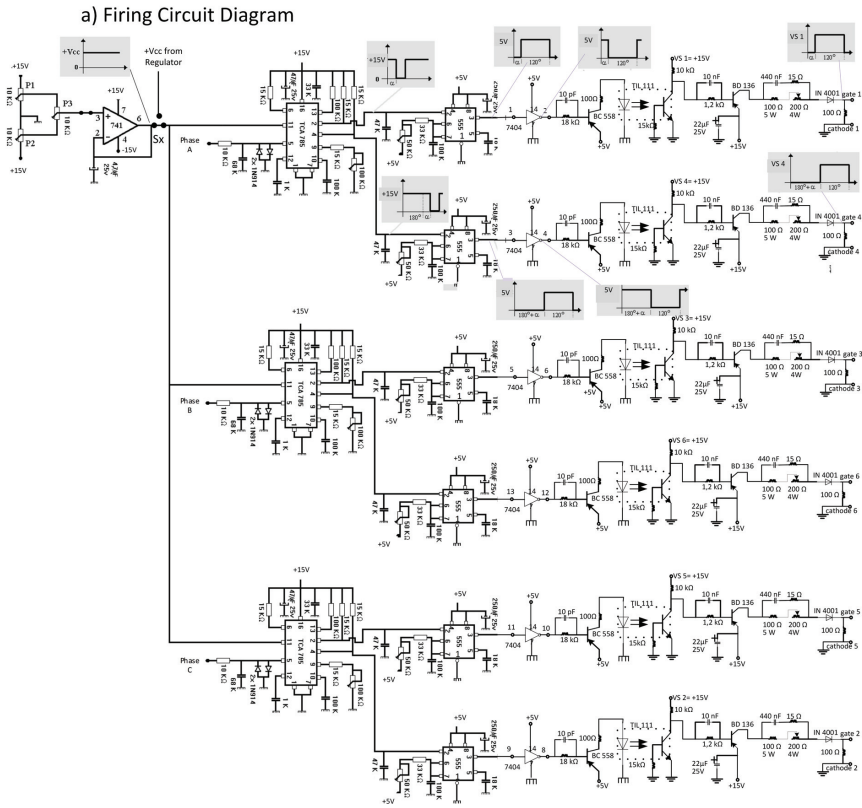


Figure B.12 – Firing Circuit Diagram

b) Voltage Sources (VSs)

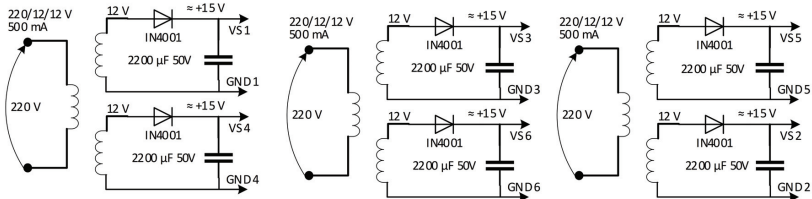


Figure B.13 – Voltage Sources for Firing Circuit Diagram

Notes:

1. A switch S_x was installed to select the operation to either the manual or automatic

position between pin 3 of buffer 741 and potentiometers P1 and P3. Sx is in the manual position as demonstrated in Figure B.12. When Sx is in the automatic position, the signal comes from the regulator output instead of potentiometers P1 and P3.

2. P1 serves to adjust the maximum alpha conduction angle and P2 serves to adjust the minimum alpha conduction angle.
3. The integrated circuit TCA 785 is a current version of TCA 780. Both have the same functions and pins.

B.10 Conclusion

This appendix presented the concepts of operation and functioning of firing circuit to control the three-phase thyristor bridge firing angle using the integrated circuit TCA 785.

This electronic circuit generates all the logic of the command signals that will control the thyristors operation. The aim of the device is to drive the thyristors by using the necessary gate current.

This firing circuit was developed to control the firing angle of thyristors, transistors, and TRIACs continually in the 0° to 180° range. It has a large number of configurations and few external components as demonstrated in this appendix.

The firing circuit logic and functioning algorithm were shown, as well as, the firing circuit and parts of this firing circuit. The most contribution of this appendix is the presentation of complete firing circuit tested and implemented in the Laboratory of research development of electrical didactic laboratory of Federal University of Itajubá with all details that becomes possible a new assembly that can be done for anyone using these same components.

APPENDIX C – Voltage Regulators and Filters Project to Synchronous Machine

C.1 Introduction

Generator frequency and voltage regulation means to enable the generator to respond the load disturbances and electrical system variation in a way that the system frequency and voltage can be maintained constant and within the acceptable limits.

This chapter will show a new technique named symmetrical optimization to carry out adjustments of the voltage regulator parameters as shown in [45]. This new technique has already been applied in the speed regulator of a *DCM*. Otherwise, there is nothing about it in the scientific community related to use this technique over generator voltage regulator. Then, this one is the original contribution of this appendix.

This appendix presents theory concepts and practical experiment about the development of analogical automatic voltage regulator applied on the *SG* terminals, which operates in an isolated electric system. Moreover, this kind of voltage regulator and its parameters, such as gain and regulator time constant will be defined and adjusted by this cited technique [4, 45].

The methodology shows here serves to establish the first approximation of the voltage regulator parameters for *SG* voltage regulator, such as gain and regulator time constant. The final adjustments are always done experimentally (fine adjustment at the workbench).

The voltage regulator used in chapters 1 and 2 are digital ones, otherwise, these can be replaced by analogical ones as those described here and in appendix G.

C.2 Calculus of Generator Field Resistance and Inductance

Figure C.1 shows the auxiliary circuit mounted in the laboratory to determine the generator field resistance and τ' (*Generator field time constant*). As shown in Figure C.1, dividing the V_{fd} (*Generator field terminal voltage*), by the I_{cc} (*Generator field circuit current*), the R_{fdmed} (*Measured field electrical resistance*) is given below:

$$R_{fdmed} = \frac{116.3V}{0.42A} \approx 277 \Omega \quad (C.1)$$

As additional information and to calculate the reference temperature resistance,

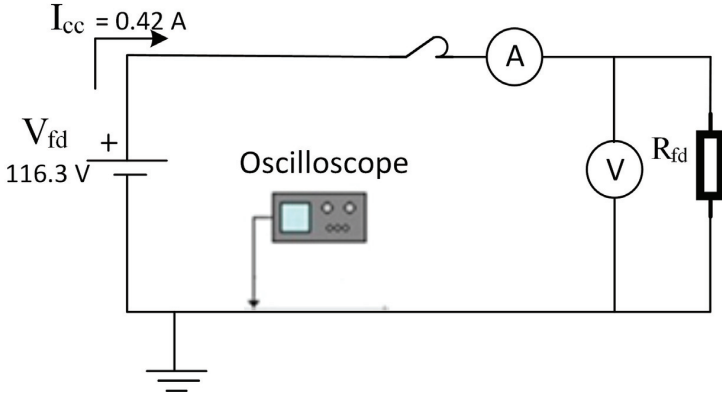


Figure C.1 – Auxiliary Circuit Mounted in the Laboratory

[46], to $40\text{ }^{\circ}\text{C}$, Θ_{ref} , for the temperature rise test [47, 48], the equation indicated in C.2 is used:

$$R_{fdref} = R_{fdmed} \times \frac{234.5 + \Theta_{ref}}{234.5 + \Theta_{med}} \quad (\text{C.2})$$

considering:

R_{fdmed} : Measured field electrical resistance

Θ_{ref} : Reference temperature resistance

Θ_{med} : Measured winding temperature

The $277\ \Omega$ resistance measured during the experiment was obtained for $\Theta_{med} = 22.0\text{ }^{\circ}\text{C}$. Otherwise, the reference field resistance for $40\text{ }^{\circ}\text{C}$ is calculated in Equation C.3:

$$R_{fdref} = 277 \times \frac{234.5 + 40.0}{234.5 + 22.0} = 296.4\ \Omega \quad (\text{C.3})$$

Note: The field winding is made of copper.

Figure C.2 shows the current I_{cc} during the field energization transitory.

From Figure C.2, it is found $\tau' = 160\text{ ms}$, that corresponds to time interval to current I_{cc} , reaches 63 % of steady state current, that is equal to 0.42 A. Once the field resistance and the generator time constant have been defined by Equation C.4, the field inductance is calculated:

$$\tau' = \frac{L_{fd}}{R_{fd}} \quad (\text{C.4})$$

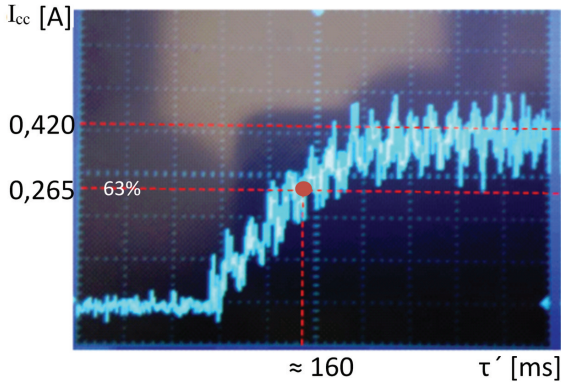


Figure C.2 – Generator Time Constant Determination

Thus, it can be seen that:

$$L_{fd} = \tau' \times R_{fd} = 160.0 \times 10^{-3} \times 277 = 44.3 \text{ H} \quad (\text{C.5})$$

The generator field circuit parameters are shown in Table C.1.

Table C.1 – Excitation Parameters of Salient Poles Synchronous Generator

Generator field resistance	$R_{fd} = 277 \Omega$
Generator field inductance	$L_{fd} = 44.3 \text{ H}$

C.3 Voltage Regulators and Filters Project

C.3.1 Introduction

The generator system regulator compares a reference voltage and an output generator voltage; this difference results in control of the synchronous generator excitation voltage to increase or decrease the excitation current in accordance with the desired output voltage V_{ref} (*Reference Voltage*). In this way, the generator output voltage tends to stay within a predefined voltage range under rated load variations.

Figure C.3 shows a simplified block diagram of the voltage regulation.

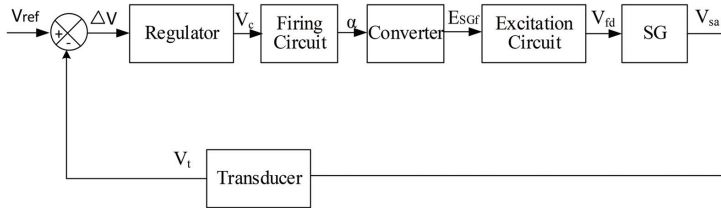


Figure C.3 – Simplified Block Diagram of Voltage Regulation

Legend:

V_C : Control voltage;

V_{fd} : Generator field voltage;

V_{sa} (*Generator output voltage*)

V_i (*Transducer output voltage*)

V_{ref} : Reference voltage;

ΔV : Voltage error signal;

SG : Synchronous generator;

E_{SGf} (*Synchronous generator field terminal voltage*)

α : Firing angle.

Note 1: For $E_{SGf} = V_{fd}$, The voltage drop in the cables and connections in the circuit between the field thyristorized converter bridge output and the machine field terminals is neglected;

Note 2: V_{fd} produces field excitation current and by means of this one the armature voltage, V_{sa} , is induced.

C.3.2 Voltage Regulator Optimization

In the proposed scheme, the full wave three-phase rectifier with thyristor (Graetz) shown in Figure C.4 will be responsible for synchronous generator excitation control.

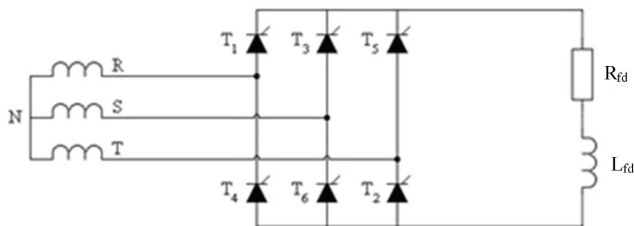


Figure C.4 – Full Wave Three-phase Rectifier with thyristor [2]

Legend

R_{fd} (*Field resistor*)

L_{fd} (Field inductor)

The thyristor circuit within this topology does not react immediately to variation of the firing angle, whereas after the commutation moment, the pair of thyristors starts conduction just after the conduction of previous couple of thyristors. In general, a typical reaction time value τ_{ss} (firing circuit time constant) [49] is:

$$\tau_{ss} = 1.5 \text{ ms}$$

The feedback channel filter time constant, τ_{gi} , reduces the ripple due to the function of the transducer diodes bridge. This time constant filters the proportional signal so that the interference can be minimized. In this work τ_{gi} , the feedback channel filter time constant, is as shown below [49]:

$$\tau_{gi} = 1.5 \text{ ms}$$

The voltage regulator is responsible for dynamic characteristic compensation of the voltage control loop as shown in Figure C.5:

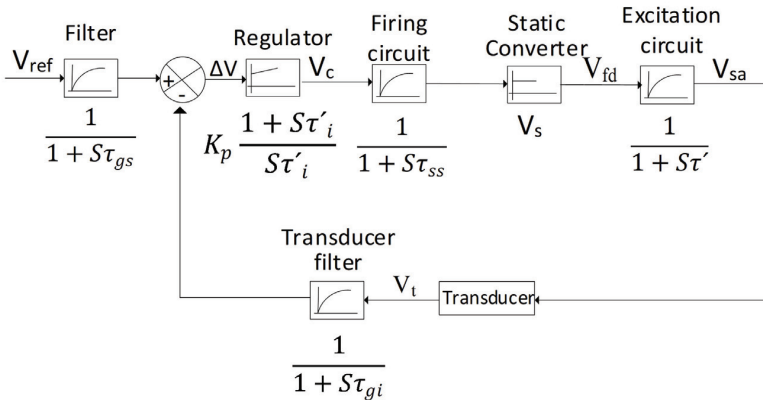


Figure C.5 – Full Blocks Diagram of Voltage Regulation System

Legend:

- τ' : Generator field time constant
- τ'_i (Regulator time constant)
- τ_{gi} : Feedback channel filter time constant
- τ_{gs} (Smoothing time constant)
- τ_{ss} : Firing circuit time constant
- V_s : Gain of static converter

After the filtered reference signal, not considering the regulator and transducer

blocks, if the time constant is more than the sum of the rest of the first order delays (whose blocks have the first-degree polynomial in the denominator), this is termed as a large time constant. The rest of them are called small time constants. The sum of small time constant σ is:

$$\sigma = \tau_{ss} + \tau_{gi} = 3.0 \text{ ms} \quad (\text{C.6})$$

The resulting value from the ratio between the generator field time constant, τ' and four times the sum of the small time constants, σ is:

$$\frac{\tau'}{4 \times \sigma} = \frac{160 \times 10^{-3}}{4 \times 3.0 \times 10^{-3}} = 13.3 \quad (\text{C.7})$$

This relation is shown in Figure C.6.

Table C.2 summarizes the time constants of the controlled system [4]:

Table C.2 – Excitation Parameters of Salient Poles Synchronous Generator

Generator field time constant	Large	$\tau' = 160.0 \text{ ms}$
Firing circuit time constant	Small	$\tau_{ss} = 1.5 \text{ ms}$
Time constant of feedback channel filter	Small	$\tau_{gi} = 1.5 \text{ ms}$

The smoothing time constant, τ_{gs} , which minimizes the overshoot from the step signal in the loop entry, is:

$$\tau_{gs} = 4 \times \sigma \times \left(1 - e^{-\left(\frac{\tau'}{4\sigma} - 1\right)} \right) \quad (\text{C.8})$$

Substituting the corresponding values in Equation C.8 results in:

$$\tau_{gs} = 4 \times 3.0 \times \left(1 - e^{-\left(\frac{160 \times 10^{-3}}{4 \times 3.0 \times 10^{-3}} - 1\right)} \right) = 12 \text{ ms} \quad (\text{C.9})$$

The smoothing time constant τ_{gs} and the resulting value from the ratio between the large and small time constants define the point P shown in Figure C.6 [4]:

According to Table 6.3 from [4], the PI regulator should be chosen as shown in Table C.3.

Table C.3 – Excitation Parameters of Salient Poles Synchronous Generator

Type of Regulator	Optimization Method	
PI	$\frac{\tau'}{4\sigma} > 1$	Symmetrical optimization (SO)

When the ratio $\frac{\tau'}{4\sigma}$ is bigger than 6, this is much greater than 1, ($\gg 1$). Then, the regulator to be chosen would be the P regulator as [4], however, this regulator introduces

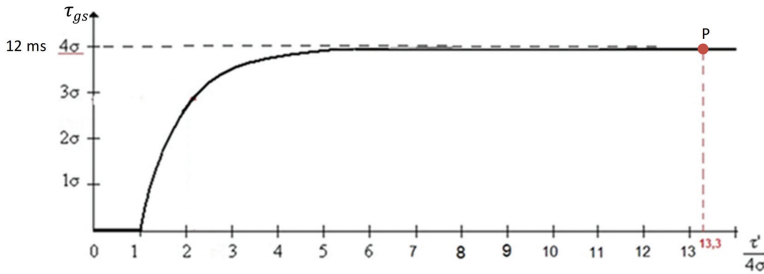


Figure C.6 – Value of τ_{gs} and Relation between the large and the Small Time Constants

an error in the steady state response, that result in an undesirable condition. Therefore, the result of ratio $\frac{\tau'}{4\sigma}$ was considered only greater than 1, it means > 1 . For that reason, the *PI (Proportional-integral regulator)*(proportional-integral) regulator and symmetrical optimization (*SO*) method were chosen.

The PI regulator adds the pole in the origin, which results in zero error in steady state mode. The PI regulator has a proportional part whose response is instantaneous and an integral part whose response is delayed. Then, the PI regulator was considered the better regulator for this system.

This *PI* regulator is defined by the following transfer function $F(s)$:

$$F(s) = K_p \times \frac{1 + s\tau'_i}{s\tau'_i} \quad (\text{C.10})$$

Legend:

K_p (*Voltage regulator gain*)

τ'_i : Regulator time constant

The *PI* regulator or *PI* controller is widely used in electrical drives and it has a phase delay compensation, which results in better transient responses and a small precision variation in steady state. It may, thus, be used to minimize the error in steady state.

After the stage of choosing the controller type and the optimization method to be used, the final definition of the controller can be obtained by adjusting the regulator parameters and applying the selected method.

Otherwise, in order to initialize the regulator optimization, it will be necessary to use the Graetz bridge with thyristors that was presented in Figure C.4. Considering the topology of this bridge, the synchronous generator field terminal voltage, E_{SGf} , is

calculated by Equation (C.11):

$$E_{SGf} = 1.35 \times E_{pp} \times \cos\alpha \quad (\text{C.11})$$

Developing the expression above:

$$\frac{E_{SGf}}{E_N} = 1.35 \times \frac{E_{pp}}{E_N} \times \left[\cos\left(\frac{\alpha}{\pi}\right) \times \pi \right] \quad (\text{C.12})$$

E_N : Rated voltage across SG field terminals.

and deriving Equation C.11 against the variable $\frac{\alpha}{\pi}$, we obtain the following:

$$\frac{d\left(\frac{E_{SGf}}{E_N}\right)}{d\left(\frac{\alpha}{\pi}\right)} = -1.35 \times \pi \times \frac{E_{pp}}{E_N} \times \left[\sin\left(\frac{\alpha}{\pi}\right) \times \pi \right] \quad (\text{C.13})$$

Defining $e = \frac{E_{SGf}}{E_N}$ and $\alpha_u = \frac{\alpha}{\pi}$ (firing angle, in pu) results in:

$$\frac{de}{d\alpha_u} = 1.35 \times \pi \times \frac{E_{pp}}{E_N} \times [\sin(\alpha)] \quad (\text{C.14})$$

From control theory, the converter gain V_s is presented as a variation modulus between output variation and input variation:

$$V_s = \left| \frac{de}{d\alpha_u} \right| \quad (\text{C.15})$$

Adopting Equation (C.15), Equation (C.14) can be rewritten as:

$$V_s = 1.35 \times \pi \times \frac{E_{pp}}{E_N} \times [\sin(\alpha)] \quad (\text{C.16})$$

The rectifier circuit presented in Figure C.7 has a voltmeter connected to the bridge output terminals in order to measure the voltage, and an amperemeter in series with the positive terminal and with the field generator resistor to measure the I_{exc} (*excitation current*):

From 113.08 V applied across bridge by varivolt, the measured parameters during the tests were:

- $I_{exc} \approx 0.35$ A - rated excitation current;
- E_{pp} (*Phase-phase voltage*) (ERS, EST, ETR) = 113.08 V phase-phase voltage at the voltage variator output;

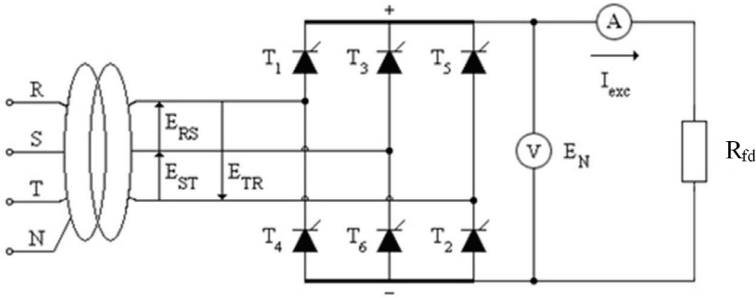


Figure C.7 – Graetz Bridge with Thyristor and 220 V Grid Voltage

- $E_N = 103.74$ V - rated voltage at rectifier bridge output.

Substituting the measured parameters in Equation (C.16) gives:

$$V_s = \left| -1.35 \times \pi \times \frac{113.08}{103.74} \times \sin\alpha \right|$$

The convertor gain V_s is then:

$$V_s = 4.64 \times \sin\alpha \tag{C.17}$$

In this kind of control, the α range consists of angles between 30° and 90° , the lower limit is defined by reasons of drive safety, and the upper limit is defined by reasons of continuity of work. Therefore, converter gain is not dimensional and, in general, it is obtained at an intermediate α value. Thus, the defined value of α was 60° that result in V_s equal to:

$$V_s = 4.64 \times \sin 60^\circ = 4.02$$

In this way, the converter gain will be applied to the voltage regulator gain calculation as shown in Table C.4:

Table C.4 – Regulator Parameters Adjustments and Optimization [4].

Symmetrical optimization	Regulator parameter adjustments	
		τ'_i
Symmetrical functions	$\frac{4\sigma\tau'}{\tau'+3\sigma}$	$\frac{\tau'}{2V_s\sigma}$

Table C.5 – Optimized Voltage Regulator Parameters

Parameters	Proportional-Integral
Voltage regulator optimized gain	$K_p = 6.63$
Regulator time constant	$\tau'_i = 7.7 \text{ ms}$

Referring to Table C.4, the regulator gain K_p can be calculated as the following equation:

$$K_p = \frac{\tau'}{2 \times V_s \times \sigma} \quad (\text{C.18})$$

$$K_p = \frac{160 \times 10^{-3}}{2 \times 4.02 \times 3.0 \times 10^{-3}} = 6.63$$

Referring again to Table C.4, the voltage regulator time constant, τ'_i , is calculated as in the following equation:

$$\tau'_i = \frac{4 \times \sigma \times \tau'}{\tau' + 3 \times \sigma} \quad (\text{C.19})$$

$$\tau'_i = \frac{4 \times 3.0 \times 160}{160 + 3 \times 3.0} \times 10^{-3} = 7.7 \text{ ms}$$

Table C.5 summarizes the classification and optimization parameters needed for the voltage regulator implementation at the workbench.

Considering these results, R_{q1} (*Proportional branch adjustment resistor of voltage regulator*) and RM_2 (*Integral branch adjustment resistor of voltage regulator*) adjustments will be calculated over the voltage regulators implemented in the laboratory, as shown in Figure C.8.

Note: This cited methodology was developed to analogical regulators. Otherwise, the digital regulators, MP 410T produced by Semikron have parameters adjusted manually, by the use of control keys. In other words, electronic board MP 410T does not require the resistor adjustments R_{q1} and RM_2 as shown in this cited methodology of this appendix.

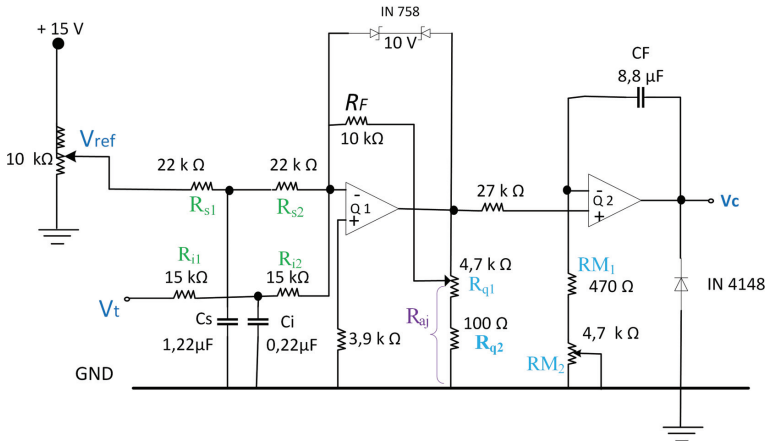


Figure C.8 – Voltage regulator

C.3.3 Practical Implementation of Voltage Regulator

The regulator implementation uses the parameters previously calculated as [4]. Thus, to calculate the R_{q1} and RM_2 (*adjustable resistor of integral branch*) adjustments, the parameters previously calculated should be considered, such as gain K_p and time constant τ'_i . Figure C.9 shows the voltage regulator topology that was implemented in the laboratory with the passive filter “T” in the reference channel (blue line) to minimize the maximum peak.

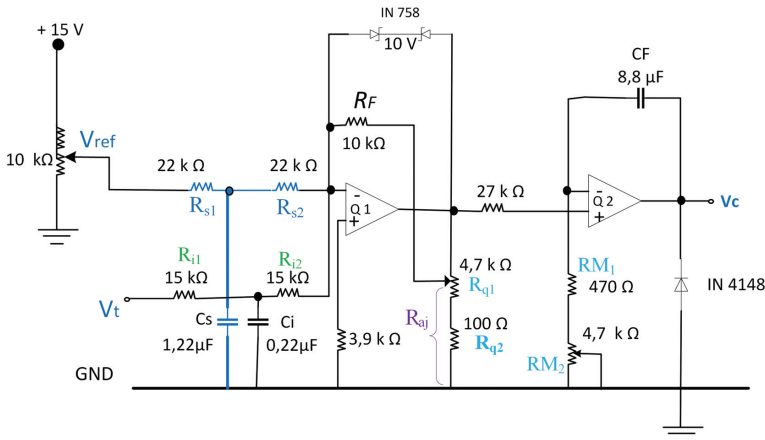


Figure C.9 – Voltage Regulator Topology with “T” Filter in the Reference Channel

With the topology indicated in Figure C.9 [49], it becomes easier to calculate the

regulator gain, K_p . Thus:

$$K_p = \frac{R_F}{a \times (R_{i1} + R_{i2})} \quad (\text{C.20})$$

Isolating the variable a gives:

$$a = \frac{R_F}{K_p \times (R_{i1} + R_{i2})} \quad (\text{C.21})$$

The resistor value to the gain adjustment can be expressed as R_{tp} (*total resistor value of proportional branch*), $R_{tp} = R_{q1} + R_{q2} = 4.8 \text{ k}\Omega$. This means:

$$R_{aj} = a \times R_{tp} \quad (\text{C.22})$$

Again, isolating the variable a gives:

$$a = \frac{R_{aj}}{R_{tp}} \quad (\text{C.23})$$

Matching Equations C.23 and C.21 and isolating R_{aj} (*adjustment resistance of voltage regulator*) gives:

$$\frac{R_{aj}}{R_{tp}} = \frac{R_F}{K_p \times (R_{i1} + R_{i2})} \quad (\text{C.24})$$

$$R_{aj} = \frac{R_F \times R_{tp}}{K_p \times (R_{i1} + R_{i2})} \quad (\text{C.25})$$

$$R_{aj} = \frac{R_F \times (R_{q1} + R_{q2})}{K_p \times (R_{i1} + R_{i2})} \quad (\text{C.26})$$

Substituting the values in Equation C.26 gives:

$$R_{aj} = \frac{10 \times (4.7 + 0.10)}{6.63 \times (15 + 15)} = 241.3 \Omega \quad (\text{C.27})$$

Adopting the gain K_p as not defined, it is possible to find the limits of K_p by changing R_{aj} as follows:

Based on Equation C.26 and isolating the variable K_p results in:

$$K_p = \frac{R_F \times (R_{q1} + R_{q2})}{R_{aj} \times (R_{i1} + R_{i2})} \quad (\text{C.28})$$

For $R_{aj}=0.10k\Omega$, the minimum R_{aj} value, the K_{pmax} (*maximum regulator gain*) is:

$$K_{pmax} = \frac{10 \times (4.7 + 0.10)}{0, 10 \times (15 + 15)} = 16 \quad (C.29)$$

For $R_{aj}=4.8k\Omega$, the maximum R_{aj} value, the K_{pmin} (*minimum regulator gain*) is:

$$K_{pmin} = \frac{10 \times (4.7 + 0.10)}{4.8 \times (15 + 15)} = 0.33 \quad (C.30)$$

Then, as the defined resistors for the controller, K_p can vary from 0.33 to 16.

Adjustment of the time constant causes more stabilization over the output reaction values. Thus, in this way, the regulator time constant τ'_i is:

$$\tau'_i = R_{ti} \times C_F \quad (C.31)$$

$$R_{ti} = \frac{\tau'_i}{C_F} \quad (C.32)$$

Where, R_{ti} (*total resistor value of integral branch*), $R_{ti} = RM1$ (*integral branch steady resistor of voltage regulator*) + $\beta RM2$, and then:

$$\beta RM2 = R_{ti} - RM1 \quad (C.33)$$

Substituting Equation C.32 in Equation C.33 gives:

$$\beta RM2 = \frac{\tau'_i}{C_F} - RM1 \quad (C.34)$$

Then, the adjusted resistor is:

$$\beta RM2 = \frac{7.7 \times 10^{-3}}{8.8 \times 10^{-6}} - 0.47 \times 10^3 = 405 \Omega \quad (C.35)$$

C.4 Results

The adjustments of R_{aj} and $\beta RM2$ are shown in Figure C.10.

Table C.6 shows the values of the gains and adjustments implemented during the voltage regulator implementation stage.

Then, the full implementation of the voltage regulator for the synchronous generator is shown in Figure C.11 [45]:

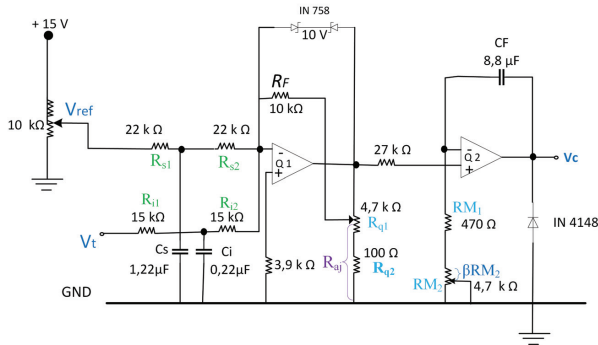


Figure C.10 – Voltage Regulator Topology

Table C.6 – Voltage Regulator Adjustments

Gain adjustment resistor	$R_{aj} = 241.3 \Omega$
Adjusted time constant resistor	$\beta RM2 = 405 \Omega$
Voltage regulator optimized gain	K_p (regulator gain) = 6.63
Maximum regulator gain	$K_{pmax} = 16$
Minimum regulator gain	$K_{pmin} = 0.33$
Regulator time constant	$\tau'_i = 7.7$ ms

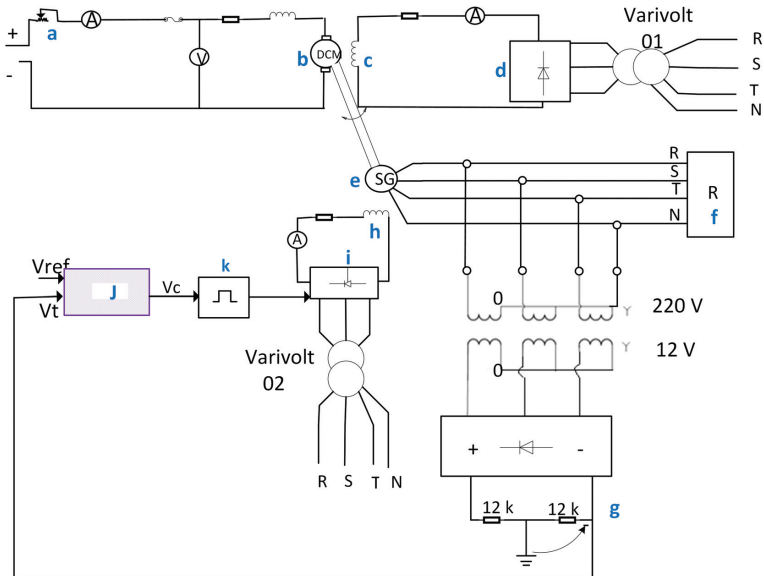


Figure C.11 – Voltage Regulator System for Synchronous Machine

Legend:

a	Rheostat	f	Three-phase load
b	DC motor armature	g	Voltage transducer
c	DC motor field	h	Synchronous generator field
d	Diodes bridge	i	Thyristors bridge
e	Synchronous generator	j	Voltage regulator
		k	Firing Circuit

C.5 Conclusion

This appendix presented theory concepts and practical experiment mounted in laboratory about the development of an analogical automatic voltage regulator applied on the *SG* terminals, which operates in an isolated electric system. Moreover, the kind of voltage regulator was defined and its parameters as gain and regulator time constant were estimated or calculated using the symmetrical optimization technique [4, 45].

APPENDIX D – Four-quadrant Regenerative Driven System for DC Machine applying Speed Reversion using either Armature Current Reversion or Field Current Reversion

D.1 Introduction

A regenerative driven system for DC machines in four quadrants was implemented in the laboratory of research development of electrical didactic laboratory of Federal University of Itajubá, [26]. The speed reversion was done using two distinct methods: the first consisted of armature DC current inversion through the use of two converters, whereas, the second, consisted of inversion of the field current through the use of one converter. The results of both methods are presented, discussed and compared. The symmetrical optimization method [4] was chosen to adjust the regulator parameters.

The controlled drive system for DC machines is widely used in industry, [35, 36, 49, 26]. Speed reversion is needed in many industrial processes. In order to achieve this aim, this work will present the use of the two cited methods to return regenerative energy to the grid during the braking process [26, 38].

D.2 Block Diagram of Controlled Drive System for use in DC Machine

Figure D.1 shows the full block diagram of the DC machine:

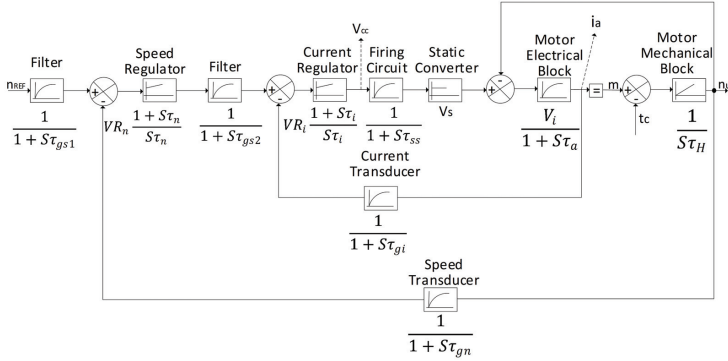


Figure D.1 – Full Blocks Diagram of DC Machine

Legend:

τ_{gs1} Filter time constant of the reference channel of the speed loop

τ_{gs2} Filter time constant of the reference channel of the current loop

V_{Rn} Gain of the speed regulator

V_{Ri} Gain of the current regulator

τ_n Time constant of the speed regulator

τ_i Current regulator time constant

τ_{gn} Filter time constant of the speed transducer

τ_{gi} Filter time constant of the current transducer

τ_{ss} Time constant of the firing circuit

V_s Gain of the static converter

τ_a Armature circuit time constant

V_i Gain of machine electric part

V_{cc} Control voltage of thyristor firing system

Note: Figure D.1 shows the PI regulators of DC machine. The motor regulator parameters were obtained by the symmetrical optimization method [4].

D.3 Laboratory Implementation

In order to implement the system in the laboratory, the following data plates were shown in D.1 to D.3 [38].

Note: All these values were obtained as described in [38] and in appendix A.

Table D.1 – Motor Data

Power	Current	Rated speed	No load speed	Rated voltage	Armature resistance (ΣRa)
1.7 kW	7.72 A	1500 rpm	1770 rpm	220 V	7.0 Ω

Table D.2 – Speed Regulator Parameters

Type	Gain (V_{Rn})	Time constant (τ_n)	Reference channel filter time constant (τ_{gs1})	Speed transducer filter time constant (τ_{gn})
PI	6.7	460 ms	416 ms	100 ms

Table D.3 – Current Regulator Parameters

Type	Gain (V_{Ri})	Time constant (τ_i)	Reference value filter (τ_{gs2})	Feedback current filter (τ_{gi})
PI	0.8	13.34 ms	15.43 ms	1.39 ms

D.4 Full Hardware of Implemented Drive System

Figure D.2 shows the implemented drive system and Figure D.3 shows the full hardware of the control system [4], including the control switches.

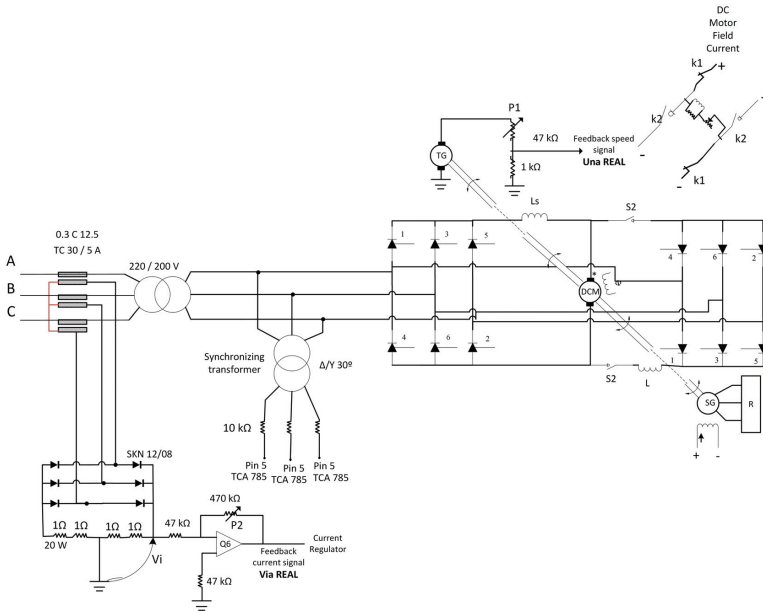


Figure D.2 – Implemented Drive System

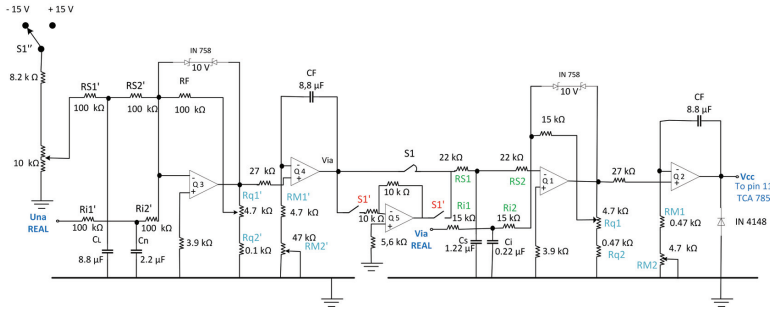


Figure D.3 – Control Circuit

D.5 Speed Inversion by Armature Current Inversion

Considering the diagram shown in Figure D.4, after the switch S1'' turns from negative to positive, the operations occur as shown in quadrants I, II and III. When the switch S1'' turns from positive to negative, the operations occur as shown in quadrants III, IV and I.

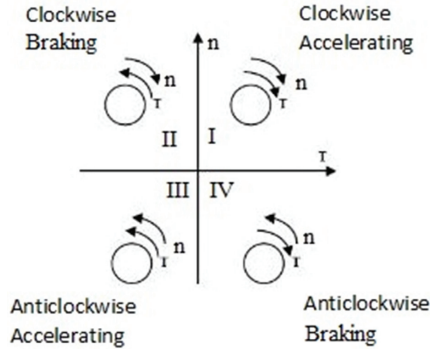


Figure D.4 – Conjugate (t) versus Speed (n) Diagram

In order to clarify Figure D.2, the switch S2 is closed and then converter I and converter II are running one at a time. This system is known as a dual converter, without circulation current.

In this way, if converter I is running, the switch S1 shown in Figure D.3 is close and switches S1' are open. On the contrary, if converter II is running, the switches S1' are closed and S1 is open. The switch S1'' enables the speed inversion. The switch S1'' will promote the blockage of the converter pulses I and unblock the converter pulses II as shown in Figure D.5. There is a period of about some milliseconds in which both converters are blocked and, thus, they are not running. Figure D.5 shows this sequence:

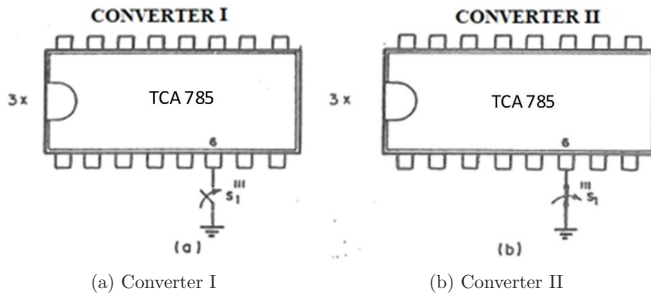


Figure D.5 – Closing of Converters I and II

The commutation switch concentrates the switches S_1 , S_1' , S_1'' and S_1''' , which are shown in Table D.4 with their operations and interlocks. This kind of switch as shown in Figure D.6 is composed of 2 switches per disc that totalling 6 switches. Thus, it is possible to configure many different combinations among them. Table D.4 shows the open and closed combinations of these switches.

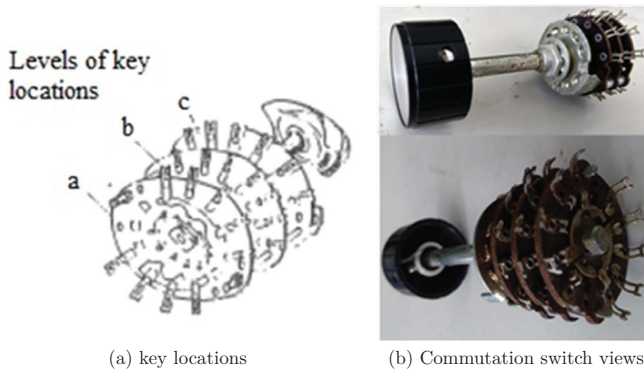


Figure D.6 – Commutation Switch S_1

The bridge firing system was implemented using 3 integrated circuit TCA 785 devices for each converter bridge. Then, when S_1''' is closed, pin 6 is connected to earth and then bridge I is blocked. In reference to converter II, this is turned on because S_1''' from Figure D.5b is opening, contrary S_1''' from Figure D.5a. During commutation between two switches S_1''' from converters I and II, there is a short period of about 50 ms in which these two switches are kept closed. For this reason, both converters are kept blocked in this period until the total extinction of bridge current that is under operation. The other bridge will just be in operation after the current extinction. The dual converters under

study are rated to run without circulation current. Figure D.6 shows the commutation switch used in the circuit.

In addition, Table D.4 below shows the switch behaviour when $S1''$ changes its current state.

Table D.4 – Cause and Effect Matrix

$S1$	$S1'$	$S1''$	$S1'''$ Converter I	$S1'''$ Converter II
open	closed	$S1''$ changes from -15V to +15V	closed	open
closed	open	$S1''$ changes from +15V to -15V	open	closed

D.6 Rotation Inversion using the Field Current Inversion

In this case, it is necessary to use only a converter of Figure D.2 and the switches shown in Figure D.2 and Figure D.7. If switch $k1$ is closed, $k2$ is open, so the field current is running in a specific direction. On contrary, if switch $k2$ is closed and $k1$ is open, then the field current is appearing in another direction. Figure D.7 shows the control circuit.

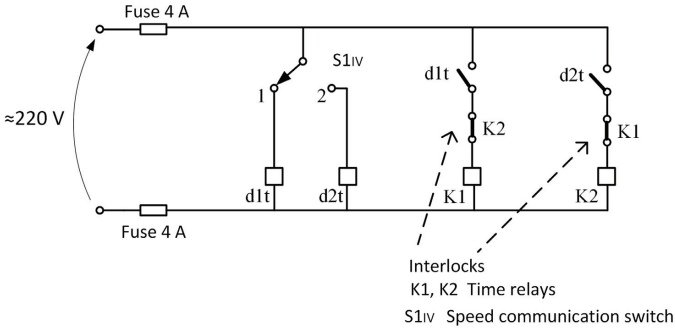


Figure D.7 – Control Circuit

When the commutation switch $S1^{IV}$ is in position 1, $k1$ is energized. If $S1^{IV}$ is in position 2 and then there occurs a delay monitored by the time relay corresponding to approximately 100 ms, this results in contactor $k1$ being turned off and contactor $k2$ turned on. That minimum time is necessary so that stored energy in the field can be discharged. With this aim, the resistance equivalent to 700Ω was inserted in parallel to the motor field circuit as shown in Figure D.8.

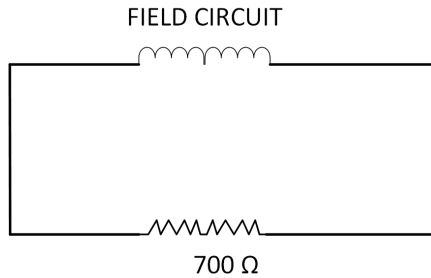


Figure D.8 – Resistance to Energy Dissipation in Machine Field Circuit

D.7 Results

Figure D.9 shows the speed inversion process in the dual converter (armature current inversion). Figure D.10 shows the cited process related to field current inversion. In Figure D.10, the friction process is used to stop the machine. In this case, the time required is longer than the case in which the regenerative braking occur.

It is also noted that for the braking due to armature current inversion, the period of time required for braking and rotation inversion (quadrants I and II) is different from the period of time corresponding to braking and rotation inversion of the motor in opposite speed direction (quadrants III and IV in Figure D.4. This phenomenon is due to summing or subtracting between the main flux and armature reaction flux. In this way, the resulting flux is bigger in one case than in the other. As the limited current was kept practically constant for both cases, the braking's resulting conjugate was different, which resulted in different rotation inversion periods in these two cases.

In the rotation inversion case using the field current, this cited phenomenon was not observed, which means that the braking and inverted direction acceleration periods are practically equal for both directions.

D.8 Conclusion

Both of the methods using speed regenerative reversion described in this work have good results. The method that uses field current inversion has a major advantage due to the fact that it uses only one converter. In cases where a high speed is not required to start the braking process, this is the recommended method. There is a new dual converters method in which the change of converters is faster than seen in this work because it can accept circulation current. Implementation of this new method is foreseen as future work.

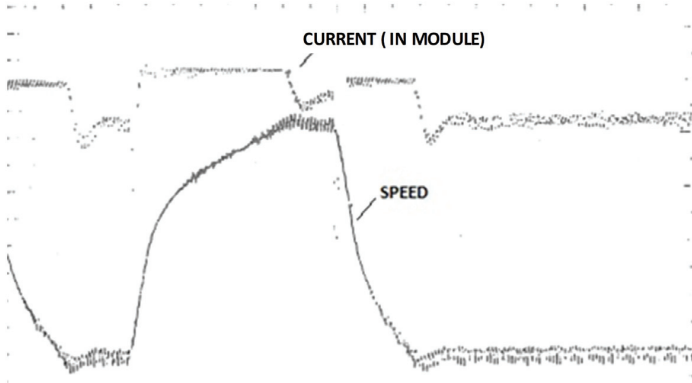


Figure D.9 – Rotation Inversion using the Armature Current Inversion

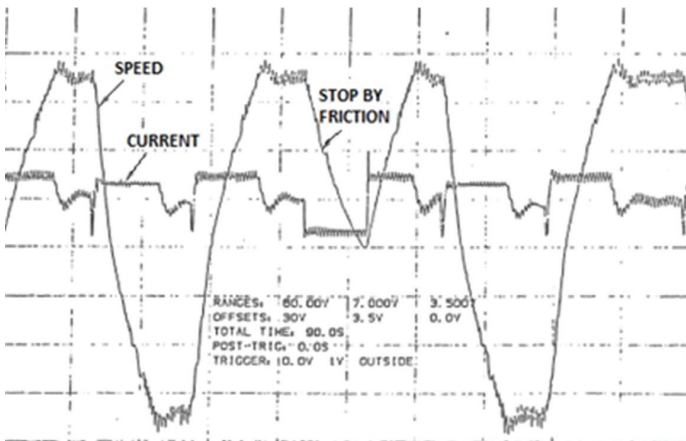


Figure D.10 – Rotation Inversion using the Field Current Inversion

APPENDIX E – Induction Motor Parameters

The follow calculus was developed as [33] to find the induction motor parameters.

E.1 No Load and Locked Rotor Tests

The Figure E.1 shows the circuit implemented in laboratory to no load test and locked rotor test. The temperature during the test was $26^{\circ}C$.

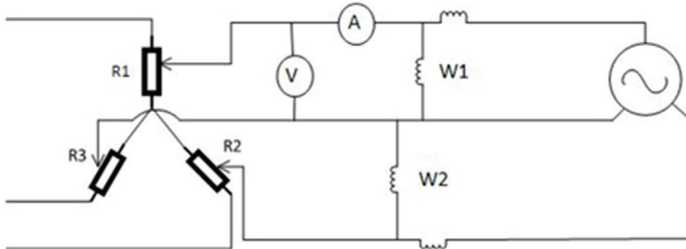


Figure E.1 – No load test and locked rotor test circuit

The Figure E.2 shows the induction motor *IM* equivalent circuit.

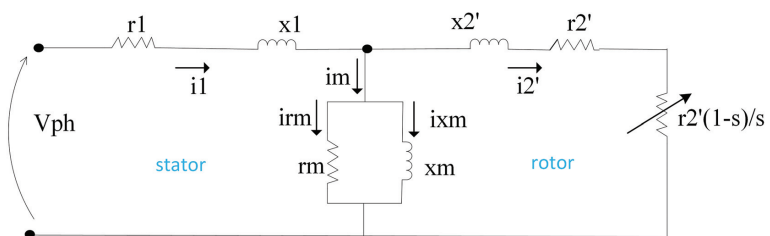


Figure E.2 – Induction Motor Equivalent Circuit

Note: $V_{ph} = V_{phase}$

E.1.1 No Load Test

In this section will be presented the no load test and locked rotor test to calculus the IM parameters such as impedances, currents, losses and efficiency

The Table E.1 presented the no load test measurements.

Table E.1 – No load Test

Vapplied (V)	W1 (W)	W2 (W)	A(A)	W1+W2(W)
240	-120.0	+220.0	1.50	100.0
220	-100.0	+170.0	1.35	70.0
200	-70.0	+130.0	1.15	60.0
180	-60.0	+110.0	1.00	50.0
160	-40.0	+80.0	0.90	40.0
140	-30.0	+60.0	0.75	30.0
120	-20.0	+45.0	0.65	25.0
100	-15.0	+30.0	0.55	15.0
80	-10.0	+20.0	0.50	10.0
60	-4.0	+12.5	0.25	8.5
40	0.0	+5.0	0.15	5.0

Figure E.3 shows the curve of voltage applied and power measured by watt-meter (W1) and (W2). Note that the cross of curve and vertical axe result in estimated P_{av} (*attrition and ventilation losses*). In this case P_{av} is 3 W as demonstrated in the Figure E.3.

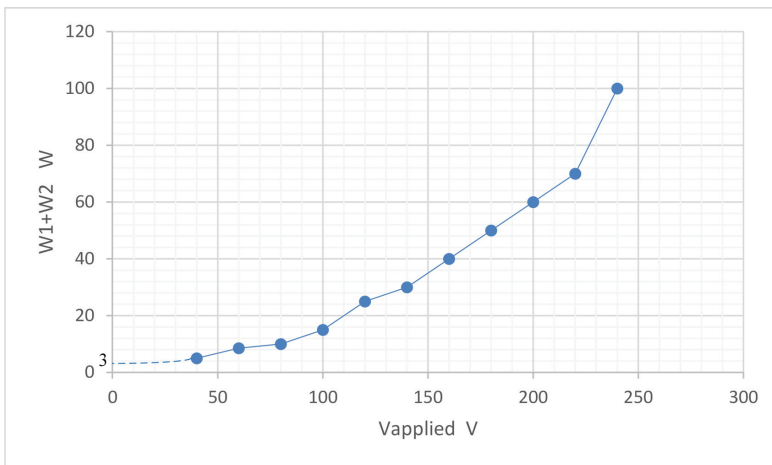


Figure E.3 – Results of no-Load Test: W1+W2 vs Voltage Applied

- Magnetization Current

Note:

I_m (*Magnetization Current*)

$I_m = 1.35$ A as shown in Table E.1.

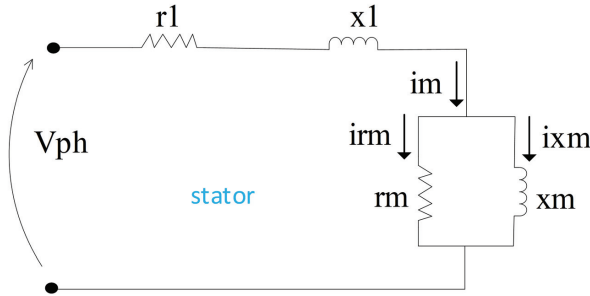


Figure E.4 – Equivalent Circuit – No-Load Test

E.1.2 Locked Rotor Test

The Table E.2 shows the locked rotor test measurements.

Table E.2 – Current Regulator Parameters

W1 (W)	W2 (W)	V (V)	In (A)	W1+W2 (W)
20	65	39.34	1.80	85

- I_n

$$I_n = \frac{P}{\sqrt{3} \times V_{pp} \times \cos\phi \times \eta} \quad (\text{E.1})$$

$$I_n = \frac{370}{\sqrt{3} \times 220 \times 0.71 \times 0.76} \quad (\text{E.2})$$

Note:

η : motor efficiency

Figure E.5 shows the induction motor IM equivalent circuit during locked rotor test

E.2 Stator and Rotor Parameters

Legend:

R_m (Motor Average Measured Resistance)

R_y (Phase resistance in star connection)

R_d (Phase resistance in delta connection)

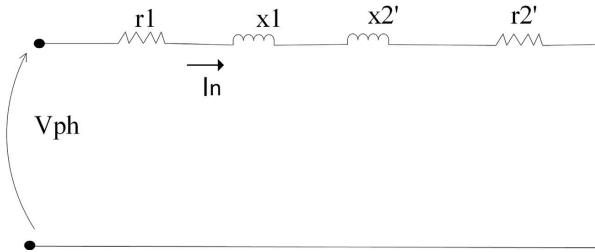


Figure E.5 – Equivalent Circuit Locked Rotor Test

Table E.3 – Average Resistance

$R_{AA'}$	$R_{BB'}$	$R_{CC'}$
10.03	10.30	10.16

$$R_m = \frac{10.03 + 10.3 + 10.16}{3} = 10.16 \Omega \tag{E.3}$$

- r_1 (Stator winding resistance) Calculus

Follow the calculus memory of stator winding resistor r_1 .

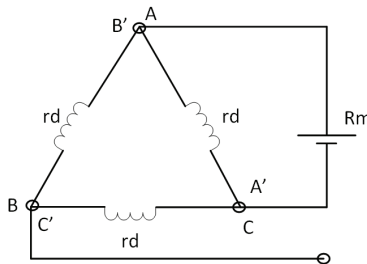


Figure E.6 – IM Winding Connection

$$R_m = \frac{rd \times 2rd}{3rd} \tag{E.4}$$

$$R_m = \frac{2}{3}rd \tag{E.5}$$

$$rd = \frac{3}{2}R_m \tag{E.6}$$

$$\text{As } ry = \frac{1}{3}rd \quad (\text{E.7})$$

And putting (E.6) into (E.7), it has

$$ry = \frac{R_m}{2} = \frac{10.16}{2}$$

$$ry = r1 = 5.08 \Omega \quad (\text{E.8})$$

- r_2' (*Rotor winding resistance referred to stator winding*) Calculus

From Table E.2, $W1+W2=85$ W

$$W1 + W2 = 3 \times (r1 + r2') \times in^2 \quad (\text{E.9})$$

$$\frac{85}{3 \times 1.8^2} = 5.08 + r2'$$

$$r2' = 3.66 \Omega \quad (\text{E.10})$$

- Q (*Reactive power*)

$$Q = \sqrt{3} \times (W2 - W1) \quad (\text{E.11})$$

From Table E.2, $W2-W1=45$

$$Q = \sqrt{3} \times (65 - 20) = 77.94 \text{ Var} \quad (\text{E.12})$$

$$Q = 3 \times (x1 + x2') \times In^2 \quad (\text{E.13})$$

- x_1 (*Stator winding reactance*) and x_2' (*Rotor winding reactance referred to stator winding*)

doing (E.13) and (E.2) in (E.14)

$$77.94 = 3 \times (x1 + x2') \times 1.8^2 \quad (\text{E.14})$$

$$(x1 + x2') = 8.01 \Omega \quad (\text{E.15})$$

$$\begin{bmatrix} x1 \mapsto x2' \\ r1 \mapsto r2' \end{bmatrix} \quad (\text{E.16})$$

doing (E.8) and (E.10) in (E.16)

$$\begin{bmatrix} x1 \mapsto x2' \\ 5.08 \mapsto 3.66 \end{bmatrix}$$

$$x1 = \frac{r1 \times x2'}{r2} \quad (\text{E.17})$$

$$x1 = \frac{5.08 \times x2'}{3.66} \quad (\text{E.18})$$

From (E.15) and (E.18), result in

$$5.08 \times x2' + x2' \times 3.66 = 29.32 \quad (\text{E.19})$$

$$x2' \times 8.74 = 29.32 \quad (\text{E.20})$$

$$x2' = 3.35 \Omega \quad (\text{E.21})$$

doing (E.21) in (E.18), result in

$$x1 = \frac{5.08 \times 3.35}{3.66} \quad (\text{E.22})$$

$$x1 = 4.65 \Omega \quad (\text{E.23})$$

E.3 Power and Losses Calculus

The P_{av} was defined in Figure E.3 and consist in 3 W. P_{nl} (*No load losses*) is obtained from no load test for 220 V, it resulted in 70 W ($W1 + W2$).

- $P_{jstator}$ (*No load stator Joules Losses*)

$$P_{jstator}26^\circ = 3 \times r1 \times im^2 \quad (E.24)$$

$$P_{jstator}26^\circ = 3 \times 5.08 \times 1.35^2 \quad (E.25)$$

$$P_{jstator}26^\circ = 27.77 \text{ W} \quad (E.26)$$

- P_{hf} (*hysteresis and Foucault losses*)

$$P_{hf} = (W1 + W2) - 3 \times r1 \times im^2 - P_{av} \quad (E.27)$$

$$P_{hf} = 70 - 3 \times 5.08 \times 1.35^2 - 3 \quad (E.28)$$

$$P_{hf} = 39.23 \text{ W} \quad (E.29)$$

E.3.1 No Load Reactive Power

$$Q_0 = \sqrt{3} \times (W2 - W1) \quad (E.30)$$

From Table E.1, $W2 - W1 = 270 \text{ W}$

$$Q_0 = \sqrt{3} \times 270 \text{ Var}$$

$$Q_0 = 467.65 \text{ Var} \quad (E.31)$$

E.3.2 Magnetization Branch

- Q_m (*No load Reactive Power in Magnetization Branch*)

$$Q_m = Q_0 - 3 \times x1 \times I_0^2 \quad (E.32)$$

$$Q_m = 467.65 - 3 \times 4.65 \times 1.35^2 \quad (E.33)$$

$$Q_m = 442.23 \text{ Var} \quad (E.34)$$

- Θ_0 (*Magnetization Branch Power Factor Angle*)

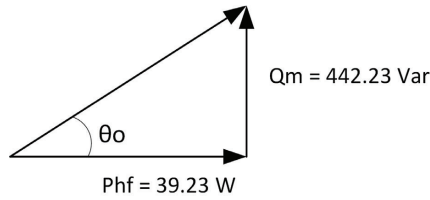


Figure E.7 – Magnetization branch power factor

$$\Theta_0 = \arctan \frac{442.23}{39.23} \quad (\text{E.35})$$

$$\Theta_0 = 84.93^\circ \quad (\text{E.36})$$

- I_{rm} (*Magnetization branch current across resistance*)

$$I_{rm} = I_m \times \cos \Theta_0 \quad (\text{E.37})$$

$$I_{rm} = 1.35 \times \cos 84.93 \quad (\text{E.38})$$

$$I_{rm} = 0.1193 \text{ A} \quad (\text{E.39})$$

- I_{xm} (*Magnetization branch current across inductor*)

$$I_{xm} = I_m \times \sin \Theta_0 \quad (\text{E.40})$$

$$I_{xm} = 1.35 \times \sin 84.93 \quad (\text{E.41})$$

$$I_{xm} = 1.34 \text{ A} \quad (\text{E.42})$$

- r_m (*Magnetization branch resistance*)

$$r_m = \frac{P_{hf}}{3 \times I_{rm}^2} \tag{E.43}$$

$$r_m = \frac{39.23}{3 \times 0.1193^2} \tag{E.44}$$

$$r_m = 918.79 \ \Omega \tag{E.45}$$

- x_m (Magnetization branch reactance)

$$x_m = \frac{Q_m}{3 \times I_{xm}^2} \tag{E.46}$$

$$x_m = \frac{442.23}{3 \times 1.34^2} \tag{E.47}$$

$$x_m = 82.10 \ \Omega \tag{E.48}$$

E.4 Parameters of Induction Motor

Figure E.8 shows all *IM* parameters calculated as resistors, reactance and currents as data obtained during experiment, without temperature correction because the motor operated no load.

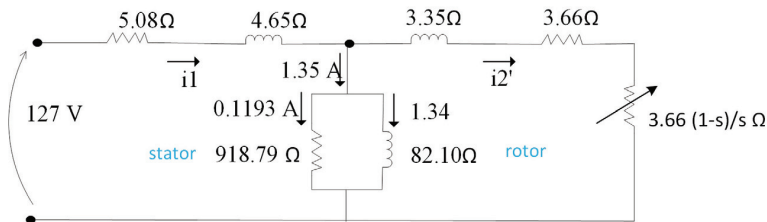


Figure E.8 – Parameters of Induction Motor

E.5 Induction Motor Efficiency

It will be calculated the temperature correction factor, corrected resistances to 40 °C, corrected winding losses, P_{win} (Winding losses) 40°C, and total losses, P_{tl} (Total losses), before induction motor efficiency calculus.

E.5.1 Temperature Correction Factor and Resistance Correction

The temperature correction factor is used in order to attend the IEC standard, [47, 48], that requires the resistances correction to lead to the starting reference resistance for the temperature rise tests, [48].

- K_t (*Temperature correction factor for 40 degree C*)

$$K_t 40^\circ C = \frac{234.5 + 40}{234.5 + 26} \quad (\text{E.49})$$

$$K_t 40^\circ C = 1.054 \text{ for } r_1 \text{ and } r'_2 \quad (\text{E.50})$$

- r_{140C} (*Corrected stator winding resistance for 40 degree C*)

$$r_1 40^\circ C = r_1 26^\circ \times 1.054 \quad (\text{E.51})$$

$$r_1 40^\circ C = 5.08 \times 1.054 \quad (\text{E.52})$$

$$r_1 40^\circ C = 5.35 \Omega \quad (\text{E.53})$$

- r'_{240C} (*Corrected rotor winding resistance referred to stator for 40 degree C*)

$$r'_2 40^\circ C = r_2 26^\circ \times 1.054 \quad (\text{E.54})$$

$$r'_2 40^\circ C = 3.66 \times 1.054 \quad (\text{E.55})$$

$$r'_2 40^\circ C = 3.86 \Omega \quad (\text{E.56})$$

E.6 Corrected Winding Losses for 40 °C and Total Losses

- P_{win40C} (*Corrected winding losses for 40 degree C*)

The P_{win} measured in locked rotor test, Table E.2, need to be corrected for 40 °C. Follow the corrected winding losses for 40 °C.

$$P_{win} 40^{\circ}C = K_t \times P_{win} 26^{\circ}C \quad (E.57)$$

$$P_{win} 40^{\circ}C = 1.054 \times 85 W \quad (E.58)$$

$$P_{win} 40^{\circ}C = 89.59 W \quad (E.59)$$

- P_{tl} (Total losses)

The P_{tl} calculus:

$$P_{tl} = P_{hf} + P_{av} + P_{win} 40^{\circ}C \quad (E.60)$$

$$P_{tl} = 39.23 W + 3 W + 89.59 W \quad (E.61)$$

$$P_{tl} = 131.82 W \quad (E.62)$$

E.7 Motor Efficiency Estimate

- P_{out} (Motor output power)
- P_{in} (Motor input power)

Note: (Motor data plate is shown in Table 1.8)

$$\eta = \frac{P_{out}}{P_{in}} \quad (E.63)$$

$$P_{in} = P_{out} + P_{tl} \quad (E.64)$$

$$P_{in} = 370 + 131.82 W \quad (E.65)$$

$$P_{in} = 501.82 W \quad (E.66)$$

$$\eta = \frac{370}{501.82} \quad (\text{E.67})$$

$$\eta = 73.73 \% \quad (\text{E.68})$$

E.8 Induction Motor Currents

Follow the calculus of $I dw_{MT}$ and $I w_{MT}$. These values are shown in Table 1.10 for all scenarios tested.

- $I dw_{MT}$

$$Q = \sqrt{3} \times 220 \times I dw_{MT} = \sqrt{3} \times (W2 - W1) \quad (\text{E.69})$$

$$Q = \sqrt{3} \times 220 \times I dw_{MT} = 467.65 \quad (\text{E.70})$$

$$I dw_{MT} = 1.23 \text{ A} ** \quad (\text{E.71})$$

Note **: The difference between $I dw_{MT}$ and I_{xm} is perfectly acceptable. The difference close to 0.1 A between expected and found values is due to small measurements errors and instruments precision and accuracy errors. It does not affect the presented modelling. Therefore, the results and modelling continue valid.

- $I w_{MT}$

$$P = (W1 + W2) = 70.0 \text{ W} \quad (\text{E.72})$$

$$Q = \sqrt{3} \times (W2 - W1) = 467.6 \text{ W} \quad (\text{E.73})$$

$$S = \sqrt{70.0^2 + 467.6^2} = 472.86 \text{ VA} \quad (\text{E.74})$$

$$\cos\phi = \frac{P}{S} = \frac{70}{472.86} \quad (\text{E.75})$$

$$\cos\phi = 0.148 \quad (\text{E.76})$$

$$I_{w_{MT}} = I_0 \times \cos\phi = 1.35 \times 0.148 \quad (\text{E.77})$$

$$I_{w_{MT}} = 0.20 \text{ A} \quad (\text{E.78})$$

In Figure E.9 is shown the resistor banks current and the no load *IM* current.

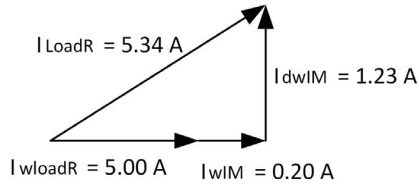


Figure E.9 – Resistors bank and IM currents in scenarios C as Table 1.10

APPENDIX F – Solving Equations with Matlab

F.1 Introduction

This appendix demonstrates how the equations indicated in chapter 1 are solved. There will be presented the Matlab code for equation solution used in two typical schemes mounted in laboratory. The first one is focused on electrical system scheme mounted in laboratory for feeding three resistor banks as shown in Figure 1.11. The second is focused on the scheme for feeding three resistor banks and an induction motor together as shown in figure 1.12. In the equation system, there are four known variables and four unknown variables that will be found.

F.2 Equations

F.2.1 Electrical system feeding three resistor banks

Based on Figure 1.11, the equations below are formulated to calculate the currents Iw_{SG} , Ic_1 , Iw_{IG} , Ic_2 .

$$I_{SG}^2 = Iw_{SG}^2 + I_{c1}^2 \quad (F.1)$$

$$I_{IG}^2 = Iw_{IG}^2 + I_{c2}^2 \quad (F.2)$$

$$I_c = I_{c1} + I_{c2} \quad (F.3)$$

$$Iw_{loadR} = Iw_{SG} + Iw_{IG} \quad (F.4)$$

F.2.2 Electrical system feeding three resistor banks and an induction motor

Based on Figure 1.12, the equations below are formulated to calculate the currents Iw_{SG} , Ic_1 , Iw_{IG} , Ic_2 . The currents Iw_{MT} and Ic_{MT} are given values and these were calculated as appendix E.

$$I_{SG}^2 = Iw_{SG}^2 + I_{c1}^2 \quad (F.5)$$

$$I_{IG}^2 = Iw_{IG}^2 + I_{c2}^2 \quad (\text{F.6})$$

$$I_c - I_{dwMT} = I_{c1} + I_{c2} \quad (\text{F.7})$$

$$Iw_{loadR} + Iw_{MT} = Iw_{SG} + Iw_{IG} \quad (\text{F.8})$$

F.2.3 Power and Efficiencies

From the results of previous equations, the power of PSG , PIG , P_{DCMSG} , P_{DCMIG} and the efficiencies η_{group} , η_{SG} , η_{IG} were calculated as equations below.

$$P_{SG} = \sqrt{3} \times V_{SG} \times Iw_{SG} \quad (\text{F.9})$$

$$P_{IG} = \sqrt{3} \times V_{IG} \times Iw_{IG} \quad (\text{F.10})$$

$$P_{DCMSG} = Va_{DCMSG} \times Ia_{DCMSG} \quad (\text{F.11})$$

$$P_{DCMIG} = Va_{DCMIG} \times Ia_{DCMIG} \quad (\text{F.12})$$

$$\eta_{group\%} = \frac{P_{SG} + P_{IG}}{P_{DCMSG} + P_{DCMIG}} \times 100 \quad (\text{F.13})$$

$$\eta_{SG\%} = \frac{P_{SG}}{P_{DCMSG}} \times 100 \quad (\text{F.14})$$

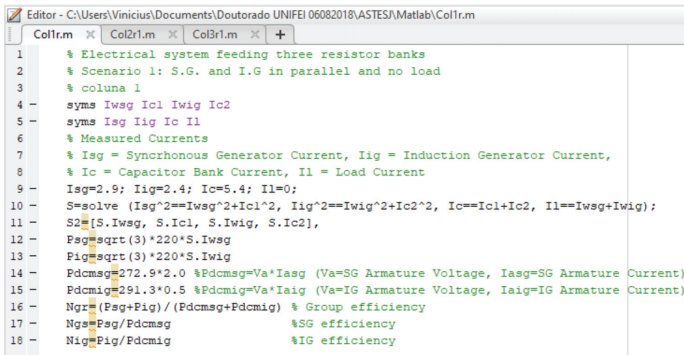
$$\eta_{IG\%} = \frac{P_{IG}}{P_{DCMIG}} \times 100 \quad (\text{F.15})$$

F.3 Matlab Code

F.3.1 Electrical system feeding three resistor banks

This section shows the Matlab code used to solve the equations formulated for each scenario. Not make sense to show all scenarios because it would be repetitive and not effective. Then, in order to obtain the results, the new entering data Iw_{SG} , I_{c1} , Iw_{IG} , I_{c2} from Table 1.9 should be inserted in line 9 of Matlab code, Figures F.1, F.2 or F.3, this code should be run and the viable result should be considered.

- Scenario 1B as Table 1.9, column 1.



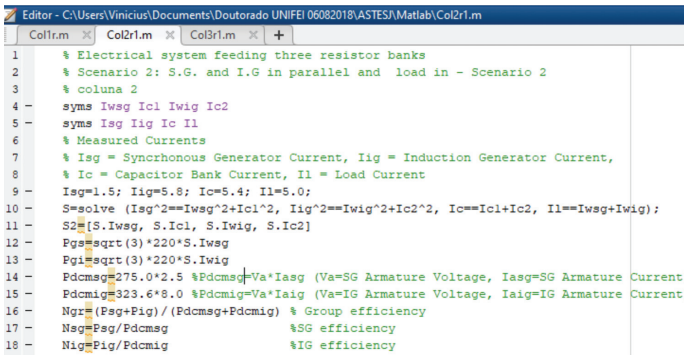
```

1 % Electrical system feeding three resistor banks
2 % Scenario 1: S.G. and I.G in parallel and no load
3 % coluna 1
4 - syms Iwsg Icl Iwig Ic2
5 - syms Isg Iig Ic Il
6 % Measured Currents
7 % Isg = Synchronous Generator Current, Iig = Induction Generator Current,
8 % Ic = Capacitor Bank Current, Il = Load Current
9 - Isg=2.9; Iig=2.4; Ic=5.4; Il=0;
10 - S=solve (Isg^2==Iwsg^2+Icl^2, Iig^2==Iwig^2+Ic2^2, Ic==Icl+Ic2, Il==Iwsg+Iwig);
11 - S2=[S.Iwsg, S.Icl, S.Iwig, S.Ic2];
12 - Psg=sqrt(3)*220*S.Iwsg
13 - Pig=sqrt(3)*220*S.Iwig
14 - Pdcmsg=272.9*2.0 %Pdcmsg=Va*Iasg (Va=SG Armature Voltage, Iasg=SG Armature Current)
15 - Pdcmig=291.3*0.5 %Pdcmig=Va*Iaig (Va=IG Armature Voltage, Iaig=IG Armature Current)
16 - Ngr=(Psg+Pig)/(Pdcmsg+Pdcmig) % Group efficiency
17 - Ngs=Psg/Pdcmsg %SG efficiency
18 - Nig=Pig/Pdcmig %IG efficiency

```

Figure F.1 – Scenario 1B

- Scenario 2B as Table 1.9, column 2.



```

1 % Electrical system feeding three resistor banks
2 % Scenario 2: S.G. and I.G in parallel and load in - Scenario 2
3 % coluna 2
4 - syms Iwsg Icl Iwig Ic2
5 - syms Isg Iig Ic Il
6 % Measured Currents
7 % Isg = Synchronous Generator Current, Iig = Induction Generator Current,
8 % Ic = Capacitor Bank Current, Il = Load Current
9 - Isg=1.5; Iig=5.8; Ic=5.4; Il=5.0;
10 - S=solve (Isg^2==Iwsg^2+Icl^2, Iig^2==Iwig^2+Ic2^2, Ic==Icl+Ic2, Il==Iwsg+Iwig);
11 - S2=[S.Iwsg, S.Icl, S.Iwig, S.Ic2];
12 - Psg=sqrt(3)*220*S.Iwsg
13 - Pig=sqrt(3)*220*S.Iwig
14 - Pdcmsg=275.0*2.5 %Pdcmsg=Va*Iasg (Va=SG Armature Voltage, Iasg=SG Armature Current)
15 - Pdcmig=323.6*8.0 %Pdcmig=Va*Iaig (Va=IG Armature Voltage, Iaig=IG Armature Current)
16 - Ngr=(Psg+Pig)/(Pdcmsg+Pdcmig) % Group efficiency
17 - Ngs=Psg/Pdcmsg %SG efficiency
18 - Nig=Pig/Pdcmig %IG efficiency

```

Figure F.2 – Scenario 2B

- Scenario 3B as Table 1.9, column 3.

F.3.2 Electrical system feeding three resistor banks and an induction motor

This section will show the Matlab code used to solve the equations formulated for each scenario. Not make sense to show all scenarios because it would be repetitive and not effective. Then, in order to obtain the new results, the new entering data Iw_{SG} , Ic_1 , Iw_{IG} , Ic_2 from Table 1.10 should be inserted in line 9 of Matlab code, Figures F.1, F.2 or F.3, this code should be run and the viable result should be considered.

- Scenario 1C as Table 1.10, column 1.

```

Editor - C:\Users\Vinicius\Documents\Doutorado UNIFEI 06082018\ASTES\Matlab\Col3r1.m
Col1r1.m x Col2r1.m x Col3r1.m x +
1 % Electrical system feeding three resistor banks
2 % Scenario 3: S.G. and I.G in parallel and load in - Scenario 3
3 % coluna 3
4 syms Iwsg Icl Iwig Ic2
5 syms Isg Iig Ic Il
6 % Measured Currents
7 % Isg = Synchronous Generator Current, Iig = Induction Generator Current,
8 % Ic = Capacitor Bank Current, Il = Load Current
9 Isg=2.0; Iig=5.1; Ic=5.4; Il=5.0;
10 S=solve (Isq^2==Iwsg^2+Icl^2, Iig^2==Iwig^2+Ic2^2, Ic==Icl+Ic2, Il==Iwsg+Iwig);
11 S2=[S.Iwsg, S.Icl, S.Iwig, S.Ic2],
12 Psg=sqrt(3)*220*S.Iwsg
13 Pgi=sqrt(3)*220*S.Iwig
14 Pdcmsg=276.2*3.8 %Pdcmsg=Va*Iasg (Va=SG Armature Voltage, Iasg=SG Armature Current)
15 Pdcmig=316.7*7.0 %Pdcmig=Va*Iaig (Va=IG Armature Voltage, Iaig=IG Armature Current)
16 Ngr=(Psg+Pig)/(Pdcmsg+Pdcmig) % Group efficiency
17 Nsg=Psg/Pdcmsg %SG efficiency
18 Nig=Pig/Pdcmig %IG efficiency

```

Figure F.3 – Scenario 3B

```

Editor - C:\Users\Vinicius\Documents\Doutorado UNIFEI 06082018\ASTES\Matlab\Mot Res\Col1mrr1.m
Col1mrr1.m x Col2mrr1.m x +
1 % Electrical system feeding three resistor banks and an induction motor together
2 % Scenario 1: S.G. and I.G in parallel and no load - Scenario 1
3 % coluna 1
4 syms Iwsg Icl Iwig Ic2
5 syms Isg Iig Ic Il
6 % Measured Currents
7 % Isg = Synchronous Generator Current, Iig = Induction Generator Current,
8 % Ic = Capacitor Bank Current, Il or (IloadR) = Load Current
9 Isg=2.8; Iig=2.3; Ic=5.4; Il=0; Idwmt=1.22; Iwmt=0.184;
10 S=solve (Isq^2==Iwsg^2+Icl^2, Iig^2==Iwig^2+Ic2^2, Ic=Idwmt==Icl+Ic2, Il+Iwmt==Iwsg+Iwig);
11 S2=[S.Iwsg, S.Icl, S.Iwig, S.Ic2],
12 Psg=sqrt(3)*220*S.Iwsg
13 Pgi=sqrt(3)*220*S.Iwig
14 Pdcmsg=278.9*2.0 %Pdcmsg=Va*Iasg (Va=SG Armature Voltage, Iasg=SG Armature Current)
15 Pdcmig=288.9*1.0 %Pdcmig=Va*Iaig (Va=IG Armature Voltage, Iaig=IG Armature Current)
16 Ngr=(Psg+Pig)/(Pdcmsg+Pdcmig) % Group efficiency
17 Nsg=Psg/Pdcmsg %SG efficiency
18 Nig=Pig/Pdcmig %IG efficiency

```

Figure F.4 – Scenario 1C

- Scenario 2C as Table 1.10, column 2.

```

Editor - C:\Users\Vinicius\Documents\Doutorado UNIFEI 06082018\ASTES\Matlab\Mot Res\Col2mrr1.m
Col1mrr1.m x Col2mrr1.m x +
1 % Electrical system feeding three resistor banks and an induction motor together
2 % Scenario: S.G. and I.G in parallel and load in - Scenario 2
3 % coluna 2
4 syms Iwsg Icl Iwig Ic2
5 syms Isg Iig Ic Il
6 % Measured Currents
7 % Isg = Synchronous Generator Current, Iig = Induction Generator Current,
8 % Ic = Capacitor Bank Current, Il or (IloadR) = Load Current
9 Isg=0.7; Iig=6.0; Ic=5.4; Il=5.0; Idwmt=1.23; Iwmt=0.2;
10 S=solve (Isq^2==Iwsg^2+Icl^2, Iig^2==Iwig^2+Ic2^2, Ic=Idwmt==Icl+Ic2, Il+Iwmt==Iwsg+Iwig);
11 S2=[S.Iwsg, S.Icl, S.Iwig, S.Ic2],
12 Psg=sqrt(3)*220*S.Iwsg
13 Pgi=sqrt(3)*220*S.Iwig
14 Pdcmsg=277*2.9 %Pdcmsg=Va*Iasg (Va=SG Armature Voltage, Iasg=SG Armature Current)
15 Pdcmig=330*8.0 %Pdcmig=Va*Iaig (Va=IG Armature Voltage, Iaig=IG Armature Current)
16 Ngr=(Psg+Pig)/(Pdcmsg+Pdcmig) % Group efficiency
17 Nsg=Psg/Pdcmsg %SG efficiency
18 Nig=Pig/Pdcmig %IG efficiency

```

Figure F.5 – Scenario 2C

- Scenario 3C as Table 1.10, column 3.

```

Editor - C:\Users\Vincius\Documents\Doutorado UNIFEI 06082018\ASTES\Matlab\Mot Res\Col3mrr1.m
Col1mrr1.m x Col2mrr1.m x Col3mrr1.m x +
1 % Electrical system feeding three resistor banks and an induction motor together
2 % Scenario 3: S.G. and I.G in parallel and load in - Scenario 3
3 % coluna 3
4 - syms Iwsg Icl Iwig Ic2
5 - syms Isg Iig Ic Il
6 % Measured Currents
7 % Isg = Synchronous Generator Current, Iig = Induction Generator Current,
8 % Ic = Capacitor Bank Current, Il or (IloadR) = Load Current
9 - Isg=1.6; Iig=5.0; Ic=5.4; Il=5.0; Idwmt=1.23; Iwmt=0.2;
10 - S=solve (Isg^2==Iwsg^2+Icl^2, Iig^2==Iwig^2+Ic2^2, Ic-Idwmt==Icl+Ic2, Il+Iwmt==Iwsg+Iwig);
11 - S2=[S.Iwsg, S.Icl, S.Iwig, S.Ic2],
12 - Psg=sqrt(3)*220*S.Iwsg
13 - Pig=sqrt(3)*220*S.Iwig
14 - Pdcmsg=277.5*4.0 %Pdcmsg=Va*Iasg (Va=SG Armature Voltage, Iasg=SG Armature Current)
15 - Pdcmig=318*7.0 %Pdcmig=Va*Iaig (Va=IG Armature Voltage, Iaig=IG Armature Current)
16 - Ngr=(Psg+Pig)/(Pdcmsg+Pdcmig) % Group efficiency
17 - Nsg=Psg/Pdcmsg %SG efficiency
18 - Nig=Pig/Pdcmig %IG efficiency

```

Figure F.6 – Scenario 3C

APPENDIX G – PI Regulator Gain Correction

G.1 Introduction

This appendix demonstrates how the gains shown in appendixes A and C are calculated with more accuracy. This content aims to detail and validate the methodology shown in cited appendixes, which was implemented in [34]. The speed and current regulators used in chapters 1 and 2 are digital ones, otherwise, these can be replaced by analogical ones as those described here and in appendixes A and C with the same functionality.

G.2 Calculations

Follow below the Figure G.1 that shows the main variables to calculate the PI regulator gain with more accuracy.

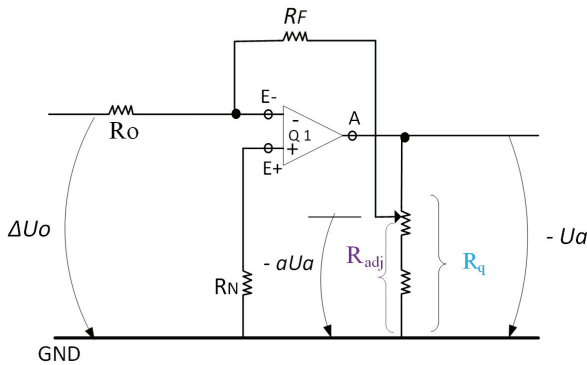


Figure G.1 – Proportional device with adjustable gain

The gain was calculated as being:

$$V_{Ra} = \frac{V_{Ro}}{a} \quad (G.1)$$

and adopting V_{Ro} (*Regulator original gain*):

$$V_{Ro} = \frac{R_F}{R_o} \quad (\text{G.2})$$

and

$$a = \frac{R_{adj}}{R_q} \quad (\text{G.3})$$

Considering the R_{adj} (*adjustment resistance of regulator*), this equation G.3 is validated when the resistance R_q is so lower than resistance R_F .

In order to calculate the accurate gain, the resistance R_{adj} is in parallel with the resistance R_F , whereas the left terminal is connected in negative operational amplifier inlet that is a virtual ground.

Then, the circuit to determination of variable a is shown in figure G.2

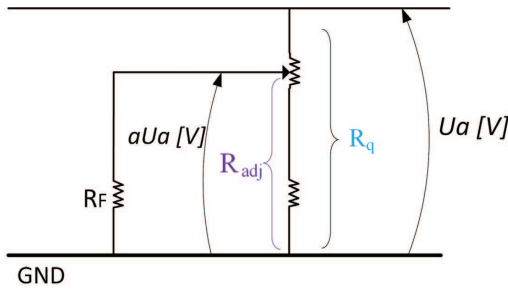


Figure G.2 – Circuit to determination of variable a

$\therefore R_{equ}$ (*Equivalent resistance*) is:

$$R_{equ} = \frac{R_F \times R_{adj}}{R_F + R_{adj}} \quad (\text{G.4})$$

That is demonstrated by the following Figure G.3.

Being R_{tot} (*Total resistance*) is shown in G.5:

$$R_{tot} = R_q - R_{adj} + R_{equ} \quad (\text{G.5})$$

Based on Figure G.3, the following equation G.6 is valid:

$$R_q - R_{adj} = (1 - a) \times R_{tot} \quad (\text{G.6})$$

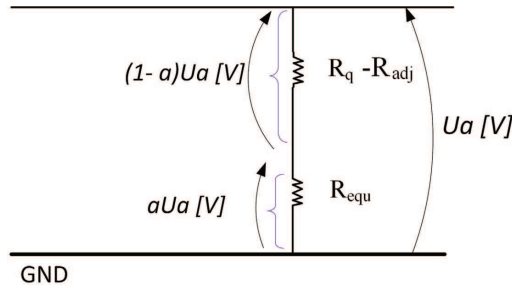


Figure G.3 – Simplified circuit

Then, the V_{Ra} (*Total regulator gain*) is given by equation G.7 [4]:

$$V_{Ra} = \frac{1}{a} \times V_{Ro} \times \left[1 + (a - a^2) \times \frac{R_q}{R_F} \right] \quad (\text{G.7})$$

The first stage is the calculation of a factor from equation G.7 and through by replacement of a value in equation G.6, that is used to determinate R_{adj} in all following calculations. results in more accurate.

G.3 Current regulator adjustment resistance calculation

Follow the current regulator calculations.

As appendix A and equation G.2, the incoming values are: $V_{Ri} = 0.8$ and V''_{Ro} (*Current regulator original gain*) = $\frac{10}{30} = 0.33$

As equation G.7, the a calculation is:

$$0.80 \times a = 0.33 \times \left[1 + (a - a^2) \times \frac{5.17}{10} \right] \quad (\text{G.8})$$

$$a^2 + 3.69a - 1.934 = 0 \quad (\text{G.9})$$

Solving the equation G.9, gives:

$$a = 0.465 \quad (\text{G.10})$$

R''_{aje} (*Accurate adjustment resistance of current regulator*) calculation is given by the equation G.11, that results from G.6:

$$R''_{aje}{}^2 + 16.322R''_{aje} - 51.7 = 0 \quad (\text{G.11})$$

$$\therefore R''_{aje} = 2.716 \text{ k}\Omega \quad (\text{G.12})$$

As the resulting value from equation A.51 using the approximated value method is the $R''_{aj}=2.15 \text{ k}\Omega$, it means that the $R''_{aje} = 2.716 \text{ k}\Omega$, which was calculated by this more accurate method, is so close.

G.4 Speed regulator adjustment resistance calculation

Follow the speed regulator calculations.

As appendix A and equation G.2, the incoming values are: $V_{Rn} = 6.7$ and V'_{Ro}
(*Speed regulator original gain*) = $\frac{100}{200} = 0.5$

As equation G.7, the a calculation is:

$$6.7 = \frac{1}{a} \times 0.5 \times \left[1 + (a - a^2) \times \frac{4.8}{100} \right] \quad (\text{G.13})$$

$$6.7 \times a = 0.5 \times \left[\frac{100 + (a - a^2) \times 4.8}{100} \right] \quad (\text{G.14})$$

Solving the equation G.14, gives:

$$a^2 + 278.167a - 20.833 = 0 \quad (\text{G.15})$$

Solving the equation G.15, gives:

$$a = 0.07486 \quad (\text{G.16})$$

The R'_{aje} (*Accurate adjustment resistance of speed regulator*) calculation is given by the equation G.17, that results from G.6:

$$R'_{aje}{}^2 + 1328.53R'_{aje} - 480 = 0 \quad (\text{G.17})$$

$$\therefore R'_{aje} = 0.3612 \text{ k}\Omega \quad (\text{G.18})$$

As the resulting value from equation A.71 using the approximated value method is the $R'_{aj}=358.2 \Omega$, it means that the R'_{aje} value, which was calculated by this more accurate method, R'_{aje} (*Accurate adjustment resistance of voltage regulator*) = 361.2Ω , is so close.

G.5 Voltage regulator adjustment resistance calculation

Follow the speed regulator calculations.

As Figure C.8, appendix A and equation G.2, the incoming values are: K_{pe} (*Accurate voltage regulator gain*) = 6.63 and K_{Po} (*Voltage regulator original gain*) = $\frac{10}{30} = 0.33$

As equation G.7, the a calculation is:

$$6.63 \times a = 0.33 \times \left[\frac{10 + (a - a^2) \times 4.8}{10} \right] \quad (\text{G.19})$$

Solving the equation G.19, gives:

$$a^2 + 40.856a - 2.083 = 0 \quad (\text{G.20})$$

Solving the equation G.20, gives:

$$a = 0.0509 \quad (\text{G.21})$$

The R_{aje} calculation is given by the equation G.22, that results from G.6:

$$R_{aje}^2 + 191.67R_{aje} - 48 = 0 \quad (\text{G.22})$$

$$\therefore R_{aje} = 0.25 \text{ k}\Omega \quad (\text{G.23})$$

As the resulting value from equation A.71 using the approximated value method is the $R_{aj}=241.3 \Omega$, it means that the $R_{aje} = 250.0 \Omega$, which was calculated by this more accurate method, is so close.

G.6 Gain Calculations

The adjustment resistances calculated in appendixes A and C by the rough calculation method result in $R''_{aje}=2.15 \text{ k}\Omega$ for current regulator; $R'_{aje}=358.2$ for speed regulator and $R_{aje}=241.3$ for voltage regulator.

Then, for these cited adjustment resistances, the respective gains will be calculated by the more accurate method as follow below.

G.6.1 Current Regulator Gain

Regarding to current regulator shown in Figure A.15, follow the calculations in order to obtain the accurate current regulator gain.

From the equation G.4, the R''_{eq} (*Current regulator equivalent resistance*) is:

$$R''_{eq} = \frac{2.15 \times 10}{2.15 + 10} = 1.77 \text{ k}\Omega \quad (\text{G.24})$$

From the equation G.3, the variable 'a' is:

$$a = \frac{1.77}{5.17} = 0.342 \quad (\text{G.25})$$

Then, as the equation G.7, the gain V_{Rie} (*Accurate current regulator gain*) is:

$$V_{Rie} = \frac{0.333}{0.342} \times \left[1 + (0.342 - 0.342^2) \times \frac{5.17}{10} \right] = 1.087 \quad (\text{G.26})$$

∴ This gain $V_{Rie} = 1.087$ is so close to $V_{Ri} = 0.80$ that was used the rough calculation method in appendix A.

G.6.2 Speed Regulator Gain

Regarding to speed regulator shown in Figure A.17, follow the calculations in order to obtain the accurate speed regulator gain.

From the equation G.4, the R'_{eq} (*Speed regulator equivalent resistance*) is:

$$R'_{eq} = \frac{0.3582 \times 100}{100.3582} = 0.3569 \text{ k}\Omega \quad (\text{G.27})$$

From the equation G.3, the variable 'a' is:

$$a = \frac{0.3569}{4.8} = 0.07435 \quad (\text{G.28})$$

Then, as the equation G.7, the gain V_{Rne} (*Accurate speed regulator gain*) is:

$$V_{Rne} = \frac{0.5}{0.07435} \times \left[1 + (0.07435 - 0.07435^2) \times \frac{4.8}{100} \right] = 6.7472 \quad (\text{G.29})$$

∴ This gain $V_{Rne} = 6.7472$ is so much close to $V_{Rn} = 6.7$ that was used the rough calculation method in appendix A.

G.6.3 Voltage Regulator Gain

Regarding to speed regulator shown in Figure C.8, follow the calculations in order to obtain the accurate speed regulator gain.

From the equation G.4, the R_{eq} (*Voltage regulator equivalent resistance*) is:

$$R_{eq} = \frac{0.2413 \times 10}{10.2413} = 0.2356 \text{ k}\Omega \quad (\text{G.30})$$

From the equation G.3, the variable "a" is:

$$a = \frac{0.2356}{4.8} = 0.04908 \quad (\text{G.31})$$

Then, as the equation G.7, the gain K_{pe} is:

$$K_{pe} = \frac{0.333}{0.04908} \times \left[1 + \left(0.04908 - 0.04908^2 \right) \times \frac{4.8}{10} \right] = 6.9368 \quad (\text{G.32})$$

∴ This gain $K_{pe} = 6.9368$ is so close to $K_p = 6.63$ that was used the rough calculation method in appendix C.

G.7 Key Topics

The speed and current PI regulators for general control applications are implemented in Laboratory of research development of electrical didactic laboratory of Federal University of Itajubá (UNIFEI) and these are located in wooden box shown in Figure 1.9.

The current regulator shows in appendix A and that regulator implemented in [34] have identical topology.

The speed regulator shows in appendix A and that regulator implemented in [34] are similar. The unique difference is that has a fixed resistance 470Ω located in R'_{q1} branch, [34], instead of 100Ω shows in appendix A methodology. Related to gain 6.7 calculated in appendix A by rough method, the speed regulator with fixed resistance 470Ω would not be viable, whereas the maximum gain, V_{Rn} , obtained through by this regulator would be a bit upper 5.55. For this reason, the speed regulator with fixed resistance of R'_{q1} branch was defined as 100Ω , that became possible to show all adjustment methodology for this regulator in appendixes A and in this appendix G.

Otherwise, for the experiments that use speed regulator whose gain is 4.0 as D and [26], the speed regulator with fixed resistance 470Ω is enough. The gain 4.0 is lower than maximum gain 5.55 cited in previous paragraph.

In order to support the experiments show in D and illustrate the concepts described here, the section G.8 will show the calculations to set the speed regulator with gain 4.0.

G.8 Speed Regulator with Gain 4.0

For the adjustment of speed Regulator with gain 4.0, it has:

G.8.1 Calculation of Division Constant "a"

From the equation G.7, the gain V_{Rme} is:

$$V_{Rme} = \frac{0.5}{a} \times \left[1 + (a - a^2) \times \frac{5.17}{100} \right] = 4.0 \quad (G.33)$$

Then,

$$800a = 100 + 5.17a - 5.17a^2 \quad (G.34)$$

$$\therefore a = 0.1257 \quad (G.35)$$

G.8.2 Adjustment Resistance Calculation

The R''_{aje} (*Accurate adjustment resistance of Appendix D speed regulator*) calculation is given by the equation G.36, that results from G.6:

$$R''_{aje}{}^2 + 790.37R''_{aje} - 517 = 0 \quad (G.36)$$

$$\therefore R''_{aje} = 0.6535 \text{ k}\Omega \quad (G.37)$$

G.8.3 Rough Calculation for Gain 4.0

The gain for resistance calculated by the rough method is as follow:

From the equation G.1, the variable 'a' is:

$$4.0 = \frac{0.5}{a} \therefore a = 0.125 \quad (G.38)$$

From the equation G.4, the R''_{eq} (*Speed regulator equivalent resistance for $Rq2'=646.25 \Omega$*) is calculated as follow:

$$Rq2' = 0.125 \times 5.17 = 0.64625 \text{ k}\Omega \quad (G.39)$$

$$Rq2' = 646.25 \Omega \quad (G.40)$$

Using the accurate method, it results in

$$R''_{eq} = \frac{0.64625 \times 100}{100.64625} = 0.6421 \text{ k}\Omega \quad (G.41)$$

$$a = \frac{0.6421}{5.17} = 0.1242 \quad (\text{G.42})$$

Then, the gain V_{Rne2} (*Accurate speed regulator gain for $Rq2'=646.25 \Omega$*) is:

$$V_{Rne2} = \frac{0.5}{0.1242} - \left[1 + (0.1242 - 0.1242^2) \times \frac{5.17}{100} \right] \quad (\text{G.43})$$

$$V_{Rne2} = \frac{0.5}{0.1242} \times 1.005624 \quad (\text{G.44})$$

$$V_{Rne2} = 4.048 \quad (\text{G.45})$$

Therefore, the V_{Rne2} is close to the adjusted gain 4.0.

Bibliography

- 1 ARCHIVE., D. *TCA 785 Application Notes – SIEMENS*. 2019. Disponível em: <<https://www.datasheetarchive.com/TCA%20785%20application%20note-datasheet.html>>. 7, 94, 95
- 2 MOHAN, N.; UNDELAND, T. M.; ROBBINS, W. P. *Power electronics: converters, applications, and design*. [S.l.]: John wiley & sons, 2003. 7, 107
- 3 LANDER, C. W. *Eletrônica industrial: teoria e aplicações*. [S.l.]: McGraw-Hill, 1988. 9, 91, 97
- 4 FRÖHR, F.; ORTTENBURGUER, F. Introduction to electronic control (in spanish). *Marcombo SA, Siemens Aktiengesellschaft*, 1986. 9, 20, 76, 77, 80, 81, 82, 104, 109, 112, 114, 118, 119, 120, 121, 147
- 5 HAQUE, M. Self-excited single-phase and three-phase induction generators in remote areas. In: IEEE. *2008 International Conference on Electrical and Computer Engineering*. [S.l.], 2008. p. 38–42. 20
- 6 IBRAHIM, K.; LEIDHOLD, R. Variable frequency converter based voltage and frequency regulation of induction generator for stand-alone system application. In: IEEE. *AFRICON 2015*. [S.l.], 2015. p. 1–5. 20
- 7 TOUTI, E. et al. Asynchronous generator model for autonomous operating mode. In: IEEE. *Proceedings of the International Conference on Electronics, Computers and Artificial Intelligence-ECAI 2013*. [S.l.], 2013. p. 1–6. 20
- 8 MACEDO, D. M. "The use of pumps operating as turbines and induction generators in electric power generation" (in portuguese). Master in Science Dissertation, Federal University of Itajubá, UNIFEI. 2004. 20, 23, 49
- 9 Braga, A. V. et al. Isolated induction generator in a rural brazilian area: Field performance tests, doi:10.1016/ j. renene. 2015.05.057. *Renewable Energy Journal*, 2015. 20
- 10 SIMÕES, M. G.; FARRET, F. A. *Renewable energy systems: design and analysis with induction generators*. [S.l.]: CRC press, 2004. 20
- 11 DEMETRIADES, G. M. The use of induction generators for small-scale hydroelectric schemes in remote areas. In: IEEE. *2000 10th Mediterranean Electrotechnical Conference. Information Technology and Electrotechnology for the Mediterranean Countries. Proceedings. MeleCon 2000 (Cat. No. 00CH37099)*. [S.l.], 2000. v. 3, p. 1055–1058. 20
- 12 LEE, C.-H.; WANG, L. A novel analysis of parallel operated self-excited induction generators. *IEEE Transactions on Energy Conversion*, IEEE, v. 13, n. 2, p. 117–123, 1998. 20
- 13 WANG, L.; LEE, C.-H. Dynamic analyses of parallel operated self-excited induction generators feeding an induction motor load. *IEEE Transactions on Energy Conversion*, IEEE, v. 14, n. 3, p. 479–485, 1999. 20

- 14 CHAKRABORTY, C. et al. Performance of parallel-operated self-excited induction generators with the variation of machine parameters. In: IEEE. *Proceedings of the IEEE 1999 International Conference on Power Electronics and Drive Systems. PEDS'99 (Cat. No. 99TH8475)*. [S.l.], 1999. v. 1, p. 86–91. 20
- 15 GAWANDE, S. et al. Synchronization of synchronous generator and induction generator for voltage & frequency stability using statcom. In: IEEE. *2010 3rd International Conference on Emerging Trends in Engineering and Technology*. [S.l.], 2010. p. 407–412. 20
- 16 ION, C.; MARINESCU, C. Control of parallel operating micro hydro power plants. In: IEEE. *2010 12th International Conference on Optimization of Electrical and Electronic Equipment*. [S.l.], 2010. p. 1204–1209. 20
- 17 REDDY, P. J.; SINGH, S. Voltage and frequency control of parallel operated synchronous and induction generators in micro hydro scheme. In: IEEE. *2014 International Conference on Computation of Power, Energy, Information and Communication (IC-CPEIC)*. [S.l.], 2014. p. 124–129. 20
- 18 VANCO, W. E. et al. Experimental analysis of a self-excited induction generators operating in parallel with synchronous generators applied to isolated load generation. *IEEE Latin America Transactions*, IEEE, v. 14, n. 4, p. 1730–1736, 2016. 20
- 19 MAGALHÃES, A. S. et al. Parallel operation repowering of synchronous and induction generator. In: IEEE. *2016 IEEE 16th International Conference on Environment and Electrical Engineering (EEEIC)*. [S.l.], 2016. p. 1–6. 20
- 20 MELLO, F. P. Induction generators with inherent var generation capabilities an alternative to synchronous generators. XIII Symposium of Specialists in Electric Operational Expansion Planning, Foz do Iguaçu, Brazil. 2014. 20, 23, 61
- 21 WIJAYA, F. D.; GAJAYANA, L. N.; WIJAYA, H. P. Parallel operation synchronous and induction generator on microgrid testbed. In: IEEE. *2017 9th International Conference on Information Technology and Electrical Engineering (ICITEE)*. [S.l.], 2017. p. 1–5. 20
- 22 GAWANDE, S.; PORATE, K. Review of parallel operation of synchronous generator and induction generator for stability. In: IEEE. *2009 Second International Conference on Emerging Trends in Engineering & Technology*. [S.l.], 2009. p. 716–721. 20
- 23 GÜLEN, S. C. *Gas Turbines for Electric Power Generation*. [S.l.]: Cambridge University Press, 2019. 21
- 24 FITZGERALD, A. E. et al. *Electric machinery*. [S.l.]: McGraw-Hill New York, 2003. v. 5. 21, 23, 49
- 25 SILVA, V. Z. Dynamic emulation and analysis of synchronous and induction generators in parallel operation mode in an isolated electric system. In: FEDERAL UNIVERSITY OF ITAJUBA, UNIFEL. [S.l.], 2020. p. 1–172. Doctorate thesis. 22
- 26 REZEK, Â. J. J. et al. A four quadrant regenerative dc drive by speed reversal using armature current inverting and by means of field current inverter - a comparative analysis (in portuguese). IEEE - INDUSCON/96, São Paulo-SP. INDUSCON/96 Annals. 1996. 22, 119, 151

- 27 REZEK, Â. J. J. Fundamentos básicos de máquinas elétricas: teoria e ensaios. *Synergia, Rio de Janeiro-RJ and ACTA, Itajubá-MG*, 2011. 22
- 28 SILVA, V. Z.; REZEK, Â. J. J.; CORRÊA, R. D. L. Analysis of synchronous and induction generators in parallel operation mode in an isolated electric system, doi: 10.1109/pedg.2017.7972459. In: IEEE. *2017 IEEE 8th International Symposium on Power Electronics for Distributed Generation Systems (PEDG)*. [S.l.], 2017. p. 1-8. 23, 34, 35, 42, 44, 46, 47, 48, 49, 60
- 29 SILVA, Â. J. J. R. V. Z.; CORRÊA, R. L. Analysis of synchronous and induction generators in parallel operation mode in an isolated electric system using a ballast load as a regulation system under transient conditions, doi: 10.22270/ijesar.v4i2.112. In: IJESAR. [S.l.], 2018. p. 22-37. 23
- 30 SILVA, V. Z.; REZEK, Â. J. J.; CORRÊA, R. D. L. Novel analysis of synchronous and induction generators in parallel operation mode in an isolated electric system, doi: 10.25046/aj020625. *ASTES journal*, 2017. 23
- 31 CHAPALLAZ, J.-M.; EICHENBERGER, P.; FISCHER, G. *Manual on pumps used as turbines*. [S.l.]: Vieweg Braunschweig, Germany, 1992. 31
- 32 SILVA, V. Z.; REZEK, Â. J. J.; CORRÊA, R. D. L. Transients analysis of synchronous and induction generators in parallel operation mode in an isolated electric system, doi:10.1109/cobep.2017.8257236. In: IEEE. *2017 Brazilian Power Electronics Conference (COBEP)*. [S.l.], 2017. 49
- 33 OLIVEIRA, J. C.; COGO, J. R.; ABREU, J. P. G. Transformadores, teoria e ensaios. editora edgard blücher ltda. *São Paulo, SP*, 1984. 50, 127
- 34 SILVA, V. Z.; JUNQUEIRA, R. A. J.; OGOULOLA, C. E. G. Alternatives to control the frequency increase in an electric system with synchronous and induction generators in parallel operation mode, doi: 10.1016/j.epsr.2019.106136. *Electric Power Systems Research*, Elsevier, v. 180, 2020. 59, 63, 145, 151
- 35 MORAES, G. G.; FERREIRA, D. C. G.; JÚNIOR, G. S. F. Speed control of dc machine (in portuguese). Electrical engineering final course report, Federal University of Itajuba. 2013. 63, 80, 119
- 36 REZEK, Â. J. J. et al. Modelling and implementation of a series dc motor drive system, doi: 105772/59814. <https://www.intechopen.com>. INTECH, 2015. 65, 80, 84, 119
- 37 REZEK, Â. J. J. Permanent and transitory state analysis of an ac/dc electrical energy conversion (in portuguese). Master in Science Dissertation, EFEI. 1986. 65, 72, 80, 84
- 38 REZEK, Â. J. J. et al. Project and simulation of a controlled drive system to direct current machines (in portuguese). Annals of II Internation Seminary of Electrical Motors and regulatory drives, II SIMEAR, Vol III pages 141-160 – EPUSP, ABINEE TEC/91. 1991. 80, 119, 120
- 39 SPIEGEL, M. R. Mathematical handbook of formulas and tables. McGraw-Hill, 1968. 89

- 40 MENDONÇA, G. R. S.; REZEK, Â. J. J. Electronic circuit to firing angle command of a three-phase thyristor bridge (in portuguese). Electrical engineering final course report, UNIFEI. 2002. 91
- 41 MALVINO, A. P.; BATES, D. J. *Eletrônica-Vol. 1-8ª Edição*. [S.l.]: McGraw Hill Brasil, 2016. v. 2. 91
- 42 GUIMARÃES, C. A. M. A point-on-wave switching system based on microcomputer (in portuguese). Master in Science Dissertation, UFSC, Florianópolis-SC, Brazil. 1986. 101
- 43 COGO, J. R. Project and implementation of dc transmission system simulator (in portuguese). EFEI/FINEP agreement. 1985. 101
- 44 PINHEIRO, C. A. M.; COGO, J. R. Firing circuit of thyristors in three-phase grid (in portuguese). EFEI. 1985. 101
- 45 CAMACHO, C. A. P.; REZEK, Â. J. J. Use of symmetrical optimization technique to voltage adjust applied on synchronous generator (in portuguese). Master dissertation, Federal University of Itajubá, UNIFEI. 2007. 104, 116, 118
- 46 ALMEIDA, A. T. L. d. Máquinas síncronas. *Grupo de Estudo em Manutenção Eletro-Eletrônica e Instalações, Universidade Federal de Itajubá*, 2000. 105
- 47 IEC (Ed.). *IEC 60034-2-1 Rotating electrical machines, Standard methods for determining losses and efficiency from tests*. 105, 136
- 48 IEC (Ed.). *IEC 60034-1 Rotating electrical machines, Rating and performance*. 105, 136
- 49 REZEK, Â. J. J. et al. The modulus optimum (mo) method applied to voltage regulation systems: modeling, tuning and implementation. In: *Proc. International Conference on Power System Transients, IPST*. [S.l.: s.n.], 2001. v. 1, p. 24-28. 108, 114, 119

**More
Books!** 



yes
I want morebooks!

Buy your books fast and straightforward online - at one of world's fastest growing online book stores! Environmentally sound due to Print-on-Demand technologies.

Buy your books online at
www.morebooks.shop

Kaufen Sie Ihre Bücher schnell und unkompliziert online – auf einer der am schnellsten wachsenden Buchhandelsplattformen weltweit! Dank Print-On-Demand umwelt- und ressourcenschonend produziert.

Bücher schneller online kaufen
www.morebooks.shop

KS OmniScriptum Publishing
Brivibas gatve 197
LV-1039 Riga, Latvia
Telefax: +371 686 20455

info@omniscryptum.com
www.omniscryptum.com

OMNIscriptum



